

**MASTER**

**Wind energy potential in passages between buildings**

Khayrullina, A.A.

*Award date:*  
2012

[Link to publication](#)

**Disclaimer**

This document contains a student thesis (bachelor's or master's), as authored by a student at Eindhoven University of Technology. Student theses are made available in the TU/e repository upon obtaining the required degree. The grade received is not published on the document as presented in the repository. The required complexity or quality of research of student theses may vary by program, and the required minimum study period may vary in duration.

**General rights**

Copyright and moral rights for the publications made accessible in the public portal are retained by the authors and/or other copyright owners and it is a condition of accessing publications that users recognise and abide by the legal requirements associated with these rights.

- Users may download and print one copy of any publication from the public portal for the purpose of private study or research.
- You may not further distribute the material or use it for any profit-making activity or commercial gain

**Department of the Built Environment**  
Building Physics and Services

Den Dolech 2, 5612 AZ Eindhoven  
P.O. Box 513, 5600 MB Eindhoven  
The Netherlands

**Author**  
Adelya Khayrullina

**Student number**  
0756401

**E-mail**  
a.khayrullina@student.tue.nl

**Date**  
18<sup>th</sup> June 2012

Final master project

# Wind energy potential in passages between buildings

A.A. Khayrullina

## Personal information and supervisory committee

### Personal information

**Document type:** Master project  
**Project title:** Wind energy potential in passages between buildings  
**Date:** 18<sup>th</sup> June 2012  
**Student name:** Adelya Khayrullina  
**E-mail address:** [a.khayrullina@student.tue.nl](mailto:a.khayrullina@student.tue.nl)  
**Student number:** 0756401

### Study program related information

**Master:** Architecture, Building & Planning (ABP)  
**Speciality:** Building Physics and Services

### Supervisory committee

**Chairman:** prof.dr.ir. B. Blocken  
**E-mail address:** [b.j.e.blocken@tue.nl](mailto:b.j.e.blocken@tue.nl)

**2<sup>nd</sup> daily supervisor:** ir. T.A.J. van Hooff  
**E-mail address:** [t.a.j.v.hooff@tue.nl](mailto:t.a.j.v.hooff@tue.nl)

**Extra TU/e supervisor:** dr.ir. R. Harwig  
**E-mail address:** [r.harwig@tue.nl](mailto:r.harwig@tue.nl)

## Preface

**Author**  
Adelya Khayrullina

This thesis is made as a completion of the master education in Building Physics and Services at Eindhoven University of Technology.

By this short paragraph, I would like to express my immense appreciation to:

- prof.dr.ir. Bert Blocken for his inspirational lectures, substantial support and provided opportunity to perform this study under his professional supervision;
- ir. Twan van Hooff for his valuable knowledge, the ability to answer any question and to provide proper advice during this study;
- dr.ir. Rick Harwig for sharing his inspiration in sustainable energy and expert view on the project;
- ing. Jan Diepens and Harrie Smulders for their support concerning the software and the operation of servers.

Finally, I would like to thank my boyfriend Guillaume, family and friends for their personal support and care.

Adelya Khayrullina

Eindhoven, June 2012

## Summary

**Author**  
Adelya Khayrullina

Nowadays rational energy usage is a world-wide issue. Professionals from different countries are involved in the process of searching solutions for energy-efficient buildings. Due to the depletion of fossil fuel fields and their destructive influence on the environment, such as extra green-house effect, smog and acid rain, more and more attention is paid to the development of sustainable and renewable energy resources in order to solve problems related to the energy supply and environmental ecology.

This project is focused on the evaluation of wind conditions in building passages to assess wind energy potential. The research objectives are as follows:

- investigate the influence of geometrical variables such as building height, length, depth and separation distance on the amplification of the wind speed in the middle of a passage over the building height;
- define an integral parameter reflecting the relation of building geometry to wind amplification;
- determine the expediency of integrating wind turbines in building passages.

The building set-up consists of two parallel rectangular building blocks positioned side by side with a passage in between. An amplification of the wind through the passage is expected due to the channelling effect and the extent of this amplification represents the important evaluation parameter within the current study.

The study consists of a combination of literature research and Computational Fluid Dynamics simulations.

It is concluded, that the distribution of wind amplification factor within the building passages can hardly be described by a function of the universal ratio  $w/S$ , where  $w$  – a passage width,  $S$  – the building influence scale factor. However, the range of  $w/S$  is specified where the highest values of wind amplification factor are reached. The significant influence of the aerodynamic roughness length and wind direction on wind speed distribution within the passages is revealed. In addition, the estimation of the annual energy output is provided for three wind turbines with different rated power installed in between buildings with three different passage widths.

## Table of contents

Title		
Wind energy potential in passages between buildings		
	<b>1</b>	<b>Introduction</b> <b>8</b>
	1.1	<b>Problem statement</b> <b>8</b>
	1.2	<b>Research objectives</b> <b>9</b>
	1.3	<b>Methodology</b> <b>9</b>
	1.4	<b>Previous studies</b> <b>10</b>
		<i>Summary</i> <b>11</b>
	<b>2</b>	<b>Theory</b> <b>12</b>
	2.1	<b>Wind flow in the built environment</b> <b>12</b>
	2.1.1	<i>Wind flow over a uniform surface</i> <b>12</b>
	2.1.2	<i>Wind flow around a building</i> <b>14</b>
	2.2	<b>Integration of wind turbines into the built environment</b> <b>16</b>
	2.2.1	<i>Types of wind turbines</i> <b>16</b>
	2.2.2	<i>Comparison between HAWT and VAWT</i> <b>17</b>
	2.2.3	<i>Several examples of wind turbines integrated into built environment</i> <b>18</b>
	2.2.4	<i>Points of attention</i> <b>21</b>
	2.3	<b>Principal methods to assess wind performance and energy production</b> <b>22</b>
	2.3.1	<i>Meteorological potential</i> <b>22</b>
	2.3.2	<i>Site potential</i> <b>22</b>
	2.3.3	<i>Technical potential and energy estimation</i> <b>23</b>
	2.4	<b>CFD simulation guidelines</b> <b>25</b>
	2.4.1	<i>Target variables</i> <b>25</b>
	2.4.2	<i>Approximate equations</i> <b>25</b>
	2.4.3	<i>Geometrical representation of the obstacles</i> <b>26</b>
	2.4.4	<i>Computational domain dimensions</i> <b>26</b>
	2.4.5	<i>Choice of boundary and initial conditions</i> <b>27</b>
	2.4.6	<i>Choice of computational grid</i> <b>28</b>
	2.4.7	<i>Choice of numerical approximations</i> <b>28</b>
	2.4.8	<i>Choice of iterative convergence criteria</i> <b>28</b>
		<i>Summary</i> <b>28</b>
	<b>3</b>	<b>Validation study</b> <b>29</b>
	3.1	<b>Stathopoulos &amp; Storms case</b> <b>30</b>
	3.1.1	<i>Case overview</i> <b>30</b>
	3.1.2	<i>Validation study overview</i> <b>30</b>
	3.1.3	<i>Results</i> <b>36</b>
	3.2	<b>Beranek &amp; Van Koten case</b> <b>38</b>
	3.2.1	<i>Case overview</i> <b>38</b>

3.2.2	<i>Validation study overview</i>	38
3.2.3	<i>Results</i>	42
	<b>Summary</b>	<b>44</b>
4	<b>Parametric study</b>	<b>45</b>
4.1	<b>Study outline</b>	<b>45</b>
4.1.1	<i>Studied configurations</i>	45
4.1.2	<i>Numerical simulation parameters</i>	46
4.2	<b>Calculation results</b>	<b>51</b>
4.2.1	<i>Wind amplification factor <math>K</math></i>	51
4.2.2	<i>Analysis of amplification factor <math>K</math> on a certain building geometry</i>	55
4.2.3	<i>Amplification factor <math>K_{60}</math></i>	56
4.2.4	<i>Influence of terrain roughness</i>	57
4.2.5	<i>Influence of wind direction</i>	59
	<b>Summary</b>	<b>61</b>
5	<b>Estimation of the wind energy potential</b>	<b>62</b>
5.1	<b>Estimation outline</b>	<b>62</b>
5.1.1	<i>Geometry of the buildings</i>	62
5.1.2	<i>Meteorological data</i>	62
5.1.3	<i>Applied wind turbines</i>	63
5.2	<b>Calculation</b>	<b>64</b>
5.2.1	<i>Calculation for the prevalent wind direction</i>	64
5.2.2	<i>Calculation for <math>30^\circ</math> wind direction</i>	65
5.2.3	<i>Calculation for <math>[-30^\circ]</math> wind direction</i>	67
5.2.4	<i>The annual power generation</i>	68
	<b>Summary</b>	<b>69</b>
6	<b>Discussion</b>	<b>70</b>
6.1	<b>Influence of building geometry on the wind amplification in the passage</b>	<b>70</b>
6.2	<b>Influence of terrain roughness on the wind distribution in the passage</b>	<b>71</b>
6.3	<b>Influence of wind direction on the amplification</b>	<b>71</b>
6.4	<b>Feasibility of wind turbines in built environment</b>	<b>71</b>
6.5	<b>Current limitations of the study</b>	<b>73</b>
6.6	<b>Recommendations for further research</b>	<b>74</b>
7	<b>Conclusions</b>	<b>75</b>
	<b>References</b>	<b>76</b>

---

<b>Appendices</b>	<b>82</b>
<b>Appendix A – Tracking iterations</b>	<b>83</b>
<b>Appendix B – Weibull parameters</b>	<b>84</b>
<b>Appendix C – Technical specifications of wind turbines</b>	<b>85</b>



# 1 Introduction

## 1.1 Problem statement

Development of a renewable energy policy has become a priority task among researchers and governors all over the world due to an increase in energy consumption, rise in prices for fossil fuels and electricity, global climate change, environmental disasters, etc. (IEA, 2011; European Commission, 2011; Eurostat, 2011a; Eurostat, 2011b; UNFCCC, 2011). Regarding ecological value and economical prospects, wind energy generation is considered to be one of the most attractive technologies due to its inexhaustible resource availability, the potential to reduce CO<sub>2</sub> emissions, and to moderate the cost of electricity and decrease the reliance on scarce and expensive fossil fuels (IEA Wind, 2011).

Concerning its availability, Europe represents an area with relatively high average wind speeds, especially in Denmark, The Netherlands and United Kingdom (more than 5-6 m/s at the height of 80 m) (EEA, 2010). As a matter of fact, the installed capacity for electricity generation in Europe from wind significantly rose from 6 GW to 64 GW in the period from 1998 till 2008 (Eurostat, 2011a) and met 5.3% of EU electricity demand in 2010 (EWEA, 2011). The share of total electricity production in the Netherlands in 2010 amounts to more than 4% and the optimistic target set for 2020 equals 25% (EWEA, 2011). In accordance with statistical data for 2010 stated in EWEA (2011) the electricity production by onshore wind installations in Europe equals 171.1 TWh against 10.6 TWh of offshore wind farms.

The higher inland capacity can be explained by the difficulties associated with the electricity transport for offshore wind. In addition, the costs of foundation and grid connection through submarine cables are currently significantly higher compared to underground cables. Moreover, offshore application of wind mills can cause interference with shipping routes and areas for military use, oil and gas exploration, and tourist zones as well as disruption of marine species and habitats. The alternative position for wind farms could be agricultural land due to the relatively few obstacles and, thus, low roughness and can be combined with agronomy (EEA, 2010). However, birds and bats collision, obstacles on their migration routes and, thus, degradation of population as well as visual impact require special attention. The mountains are another possible location but imply high investment, construction and maintenance costs due to extreme climate conditions characterised by low temperature, high humidity and variability of climate conditions. All aforementioned reasons point to the alternative possibility of wind turbine integration into the built environment, in the vicinity of electricity users.

The research presented in this report aims to study the possible generation of environmentally friendly and cost-effective electricity in the urban environment by using wind turbines.

## 1.2 Research objectives

The objectives of the current study are:

- to investigate the influence of geometrical variables such as building height, length, depth and separation distance on the amplification of the mean wind speed in the middle of the passage over the building height;
- to define a unified parameter reflecting the relation of building geometry to wind amplification;
- to determine the feasibility of integrating wind turbines in building passages.

## 1.3 Methodology

The study is conducted in several stages as follows: initial, core and concluding phases (Figure 1.1).

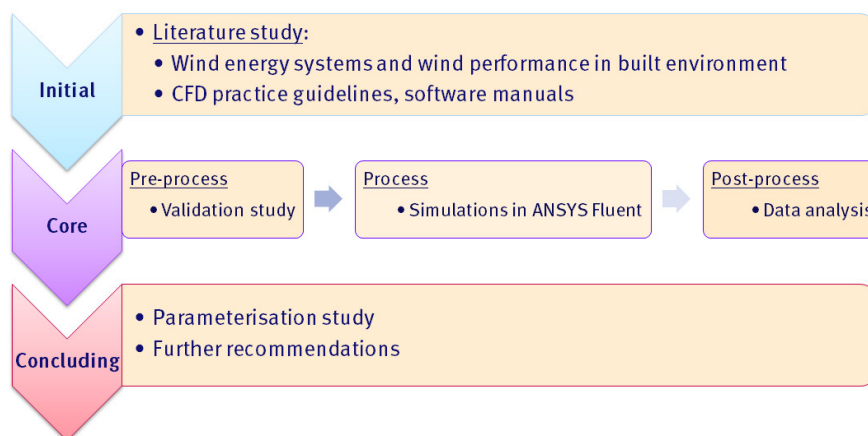


Figure 1.1 – Applied methodology

The initial phase consists of a literature study from which the research problem is identified and the practical application of wind energy systems integrated into the built environment is reviewed. Moreover, the guidelines for Computational Fluid Dynamics (CFD) as well as articles concerning research of the wind performance in urban environments and software tutorials are studied.

The core phase consists of three stages: pre-process (validation study, elaboration of computational models), process (simulations), analysis of data.

The parametric study is conducted by means of CFD. During data analysis the influence of geometrical parameters on the wind speed distribution in the middle of the passage are evaluated in order to define a unified parameter reflecting the relation of building geometry to wind velocity.

The concluding phase encloses the opinion on integration wind turbines in building passages as well as an analysis of limitations and assumptions of the performed study with certain recommendations for further research.

## 1.4 Previous studies

A number of studies have been performed in order to assess the feasibility of siting wind turbines in the built environment.

Campbell et al. (2001) focused on the development of techniques for integrating wind energy systems into urban areas. Their thorough approach included the balancing of aesthetic, aerodynamic, architectural, environmental and structural concerns. As a result, the authors suggested a method for predicting and assessing energy impacts caused by wind turbine integration, provided a classification of optimal building forms and developed several prototypes for structural systems for supporting turbines.

Dutton et al. (2005) reviewed different wind energy technologies and introduced their potential of electricity generation as well as disadvantages based on a comprehensive survey. The information about 41 different devices has been collected and summarised.

Lu et al. (2009) and Ayhan et al. (2012) investigated the wind conditions between two buildings and wind flow over the building roof in terms of building shape and its geometrical parameters by means of CFD. The studies revealed the concentration effect of buildings and possible enhancement of wind power utilisation by a factor up to 8. Abohela et al. (2011a) stated that a vaulted roof has an optimum shape for roof-mounted wind turbines and mentioned the requirement of positioning a wind turbine at a height equal to or more than 1.3 times the height of the building due to high turbulence intensities above the roof. More specific research in the field of roof-mounted wind turbines has been performed by Balduzzi et al. (2011). This study considers a Darrieus vertical axis wind turbine (VAWT) installed in a building rooftop as one of the most attractive solutions due to its low visual impact, the reduced acoustic emissions and better response to a turbulent and skewed oncoming flow. A wide-ranging analysis on different roof shapes showed a positive influence on the velocity increment for the sloping roof and a higher energy potential for wind turbines due to the skewed flow.

Abohela et al. (2011), Denoon et al. (2008) emphasised in their studies the significant role of the form of the building in harvesting wind power as well as the importance of a complete assessment of wind flow characteristics at the proposed site. The analysis of wind availability at certain locations and its power utility for electricity production have been extensively described in studies of Alnaser et al. (2000) and Glass et al. (2011).

The majority of studies regarding wind energy potential in the built environment concluded that wind energy could make a significant contribution to energy requirements for buildings.

The following algorithm can be suggested for assessment of the wind energy potential in the built environment:

- identification and assessment of urban locations for wind turbines, wind data analysis;

- performance study for a range of building forms by means of wind-tunnel testing on small-scale models and/or CFD simulations;
- evaluation of visual impact, noise and vibration emissions;
- consideration of safety measures.

## *Summary*

This Chapter introduces the topic, objectives and the methodology of the research. The overview of the related and relevant studies is included as well. The following Chapter provides the theory regarding urban wind flow, describes several examples of integrating wind turbines into the built environment and summarises the guidelines for conducting numerical simulations.

## 2 Theory

### 2.1 Wind flow in the built environment

#### 2.1.1 *Wind flow over a uniform surface*

Air pressure gradients due to differences in temperature as well as Coriolis force due to rotation of the Earth are causing wind formation in different scales: from sea breeze or valley winds to wind storms.

The atmospheric boundary layer (ABL) is the layer where wind is influenced by the Earth's roughness. Closer to the Earth's surface wind is decelerating by friction force and at the surface the wind is completely diminished. Its height is mainly determined by the temperature gradient in the lower atmosphere (stability) and the roughness of the surface (Figure 2.1). The ABL height can range from 50 m in stable conditions (e.g. night-time, when the Earth surface is cooling down) to 1 km in unstable conditions (e.g. day-time, when the surface is heating up; high cloud coverage and strong winds). In the lowest part of the ABL (10-20%), called atmospheric surface layer, the flow has a highly turbulent behaviour. The wind speed there depends on the underlying surface and decreases rapidly to zero at the surface (Verkaik, 2006).

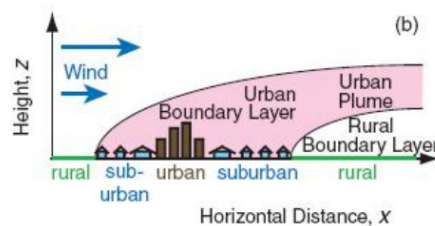


Figure 2.1 – Dependence of boundary layer height on surface roughness (Wallace & Hobbs, 2006)

The deceleration of the wind speed close to the surface is caused by the surface roughness which indicates vertical deviations of the real surface from an ideal plain. These deviations are induced by elements it contains such as buildings or vegetation. It determines the rate at which the wind speed decreases through the surface layer (serves as a momentum sink for the atmospheric flow) and also causes turbulence. Turbulence strongly enhances the vertical transport of heat, moisture, and other substances contained in the air from or to the surface of the Earth.

Roughness can be described by the aerodynamic roughness length  $y_0$  and the drag coefficient  $C_D$  (Wieringa, 1993). The value of  $C_D$  is dependent on reference height  $y$ , while  $y_0$  is height-independent for a certain height interval. That is why  $y_0$  is more preferred as a basic descriptive roughness parameter, while  $C_D$  can be considered for modelling purposes (Wieringa, 1992). Aerodynamic roughness length  $y_0$  defines the surface roughness observed by the flow. Among the smoothest surfaces are water, sand and snow ( $y_0 \approx 10^{-4}$  m); the surfaces with the highest aerodynamic roughness can be found in urban city centres ( $y_0 \approx 1-2$  m).

The drag coefficient quantifies the resistance of an object in a fluid environment (e.g., air) with the following equation:

$$C_D = (u_{ABL}^*/U)^2 \quad (2.1)$$

The wind velocity profile over a large, level surface of uniform roughness for thermally neutral stratification can be expressed by the following equation (log-law) mentioned by Richards & Hoxey (1993):

$$U(y) = \frac{u_{ABL}^*}{\kappa} \cdot \ln \left( \frac{y+y_0}{y_0} \right), \quad (2.2)$$

where  $U(y)$  is the mean wind speed at height  $y$ ,  $u_{ABL}^*$  is the friction velocity characterising velocity fluctuations in the turbulent boundary layer,  $\kappa$  – the von Kármán constant (equal to 0.42) and  $y_0$  – the aerodynamic roughness length.

The friction velocity is related to the shear stress at the surface  $\tau_0$  and can be expressed by the following equation:

$$u_{ABL}^* = \sqrt{\tau_0/\rho}, \quad (2.3)$$

where  $\rho$  is the air density.

One uses the log-law to determine the mean horizontal wind speed over irregular, rough surfaces (e.g. urban areas, farms, forests) above a certain height where individual roughness objects have no more impact on the flow and to describe the vertical wind speed profile shaped after undergoing a rough terrain with a fetch  $> 5$  km. This profile is generally applied as an inlet boundary condition for wind tunnel studies and computer simulations in that way considering the roughness conditions upwind of the model.

The mean wind speed profile can also be described by a power law approximation which describes measurements of wind speed as a function of height, averaged over periods of 10-60 min (Petersen et al., 1998):

$$\frac{U(y_1)}{U(y_2)} = \left( \frac{y_1}{y_2} \right)^\alpha, \quad (2.4)$$

where  $U(y_1)$  and  $U(y_2)$  are the wind speeds at heights  $y_1$  and  $y_2$  respectively;  $\alpha$  is the power law exponent.

The disadvantage of this approach is that  $\alpha$ , actually, varies with height and surface roughness change. Thus, power law has a limited use for neutrally-stable, equilibrium boundary layer over uniform terrain (Petersen et al., 1998).

In the science of fluid dynamics, atmospheric flows are described by Navier-Stokes equations known as the momentum equations and balancing the transport of fluid with source and sink terms due to pressure and viscosity. The continuity and energy equations refer to mass and energy conservation, respectively. The direct solution of these equations by CFD would require transcendent computational resources. Thus the set of equations has to be simplified to render it numerically solvable. The generally used method for the computation of turbulent flows in wind engineering is the Reynolds-Averaged Navier-Stokes (RANS) approach. Within this approach the equations are averaged in time over all the turbulent scales, to directly yield the statistically steady solution (Franke et al., 2004). The averaging leads to additional terms in the momentum

equation, so-called Reynolds stresses, accounting for fluctuating turbulent nature of the modelled atmospheric flow.

In order to describe Reynolds stresses as a function of the mean flow variables, a number of turbulence models can be used which can be generally categorised by two approaches. The first approach is based on the eddy viscosity assumption and models turbulent stresses as derivatives of the mean velocity. For this modelling approach additional equations are usually solved for turbulent kinetic energy  $k$  and the dissipation rate  $\varepsilon$ , or other equivalent quantities, such as  $\omega = k/\varepsilon$ . From these two quantities the turbulent or eddy viscosity is calculated. The second approach, known as Second Moment Closure (SMC) or Reynolds Stress Modelling (RSM), solves additional transport equations for each of the Reynolds stresses and the dissipation rate of the turbulent kinetic energy  $\varepsilon$ .

The  $k - \varepsilon$  model is widely used in the field of wind engineering. The turbulent kinetic energy  $k$  is a measure of the energy associated with the turbulent fluctuations in the flow per mass unit and dissipation rate  $\varepsilon$  is caused by work done by the smallest eddies in the flow against viscous stresses, which are defined as:

$$k = \frac{1}{2} \overline{u_i' u_i'}, \quad (2.5)$$

$$\varepsilon = \nu \overline{\frac{\partial u_i'}{\partial x_j} \frac{\partial u_i'}{\partial x_j}}, \quad (2.6)$$

where  $u_i'$  is a fluctuating velocity component,  $\nu$  is the kinematic viscosity.

Verified and validated two-equation turbulence models ( $k - \varepsilon$ ,  $k - \omega$ ,  $k - L$ ) provide reasonable results for many fluid flows and are widely used in CFD engineering (Letherman et al., 2000; Franke et al., 2004; Mochida & Lun, 2006; Zhai et al., 2007; Zhang et al., 2007).

### 2.1.2 *Wind flow around a building*

Figure 2.2 illustrates the wind-flow pattern around a single rectangular building. As the wind flow approaches the building, part of it flows around the building and part of the flow is deviated over the building (1). The maximum pressure at the windward facade appears at the stagnation point which is at approximately 70% of the building height. The flow from the stagnation point is divided upwards, sideways and downwards, representing lower pressure zones (2). The upward and sideward flows separate from the facade at the top and side edges. The air that is flowing downwards produces a standing vortex at ground level with the opposite direction to the approach flow (3). A stagnation point with low wind-speed values is created at the ground in front of the building, where both flows meet. The standing vortex flows around the building corners when the flow separates, resulting in corner streams with high wind speeds (4). Backflow or recirculation flow occurs at the leeward side of the building representing an underpressure zone and creating slow rotating vortices behind the building (5). A stagnation zone occurs at ground level where the flow directions are opposite and wind speeds are low (6). Beyond the stagnation zone, the flow follows its normal direction with low wind speeds.

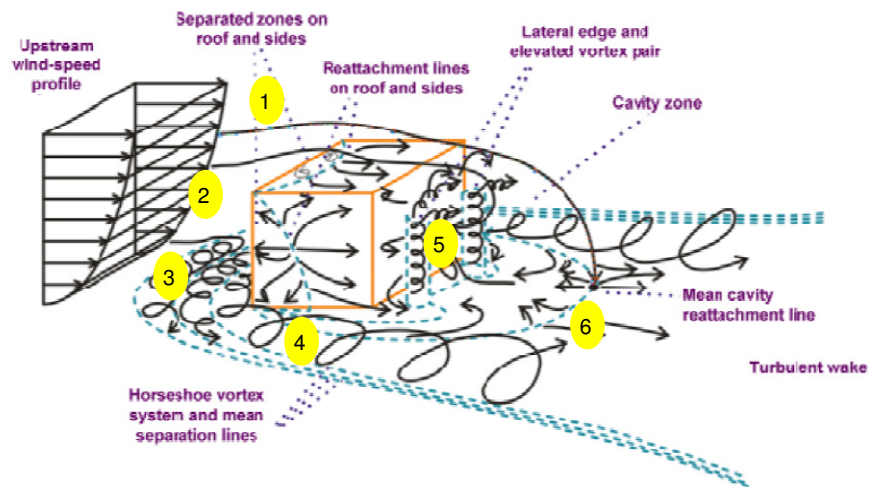


Figure 2.2 – Wind flow around a building (Blocken et al., 2011)



## 2.2 Integration of wind turbines into the built environment

Three ways of integrating wind turbines into the built environment are distinguished by Campbell et al. (2001) and by Aguiló & Wiltshire (2004):

- stand-alone wind turbines located on a free-standing tower away from the building itself;
- building mounted wind turbines installed on the building structure;
- building augmented wind turbines where the building geometry is shaped to concentrate the wind flow and direct it towards the wind turbines.

As for the wind turbine location in the built environment, high-rise buildings represent the largest potential due to increased wind speeds, proximity to electricity users, absence of constructional obstacles and minor visual impact (Müller et al., 2009).

### 2.2.1 Types of wind turbines

The following types of wind turbines are commonly applied in the built environment (Cace et al., 2007):

- horizontal axis wind turbine (HAWT);
- vertical axis wind turbine (VAWT);

HAWT represents the propeller-type rotor mounted on a horizontal axis that needs to be positioned into the wind direction by means of a tail or active yawing system (Figure 2.3).



Figure 2.3 – Several examples of HAWTs available on the market (Cace et al., 2007)

High sensitivity to changes in wind direction and turbulence have a negative effect on the performance due to the required repositioning of the turbine into the wind flow. The most favourable locations for HAWTs are open areas with smooth air flow and few obstacles. In case the wind turbine has a fastened axis as shown in Figure 2.4 and is thus able to catch wind from only one direction, it should be oriented into the prevailing wind direction.



Figure 2.4 – HAWT with a fastened axis “WindWall” (Cace et al., 2007)

Typically, a VAWT is only developed for urban deployment due to the absence of the requirement to be positioned into the wind direction (Figure 2.5). Despite the lower overall efficiency of these turbines in producing electricity comparing to HAWT, changes in wind direction have less negative effects on VAWT.

According to the principle used to capture the wind flow, VAWTs are originally categorised as Savonius or Darrieus types. For the Savonius type the rotation speed of the induced blades is always lower than the wind speed. The shape of the rotor of the Darrieus type, in contrast, allows the rotor to spin faster than the wind speed (Cace et al., 2007).



Figure 2.5 – Several examples of VAWTs available on the market (Cace et al., 2007)

### 2.2.2 Comparison between HAWT and VAWT

HAWTs might be considered as more conventional since they are currently more efficient in converting wind flow into electricity. However, for maximum efficiency HAWTs require low turbulent winds. Thus, for the built environment VAWTs, which harvest the turbulent wind flow coming from any direction and do not need to yaw into the direction of the wind, are theoretically superior to HAWTs (Cace et al., 2007).

### 2.2.3 *Several examples of wind turbines integrated into built environment*

The first commercial building with integrated large-scale wind turbines (29 meter in diameter) is the Bahrain World Trade Centre of which the construction was completed in 2008 (Figure 2.6).

It represents a twin skyscraper complex with a height of 140 m with three massive horizontal-axis turbines. Each turbine with 225 kW of installed power is arranged vertically along the facade at heights 60 m, 98 m and 136 m and supported by bridges linking the two towers. The north-alignment of the turbines is explained by the prevailing wind direction which comes from the Persian Gulf. The air flow through the passage, which is accelerated by the aerodynamic shape of the building, induces the wind turbines. The wind energy system is supposed to generate 1100 MWh to supply 11% of the electricity demand per year (Killa & Smith, 2008).

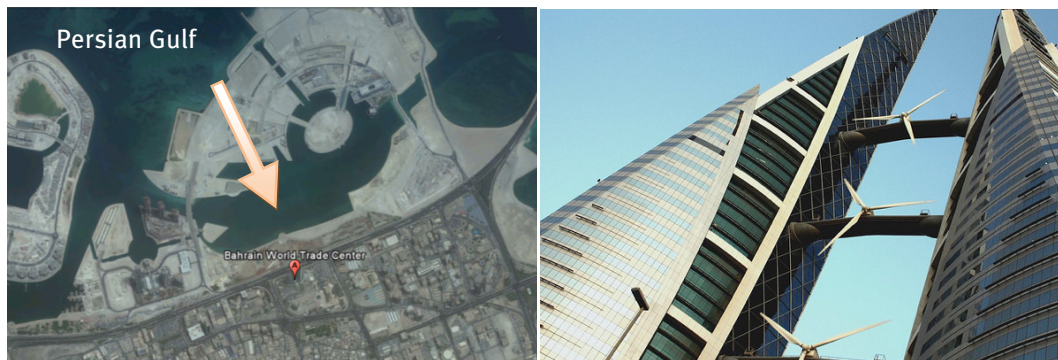


Figure 2.6 – Overview of Bahrain World Trade Centre (the arrow indicates the prevailing wind direction) (World Trade Centers Association, 2008)

Another example of wind energy building is La Strata Tower, the tallest residential building of 148 metre in London which was finished in 2010 (Figure 2.7).

It represents the first building in the world incorporating horizontal-axis wind turbines within its structure. The three nine-meter wind turbines at the top of the building are each rated at 20 kW each and are anticipated to produce 27 MWh of electricity per year which is around 4% of the electricity demand of the building. Initial calculations provided values around 45-100 MWh per annum (Rambøll Danmark A/S, 2006). The orientation of the building axis does not coincide completely with the predominant south-west wind direction due to the existing site plan.

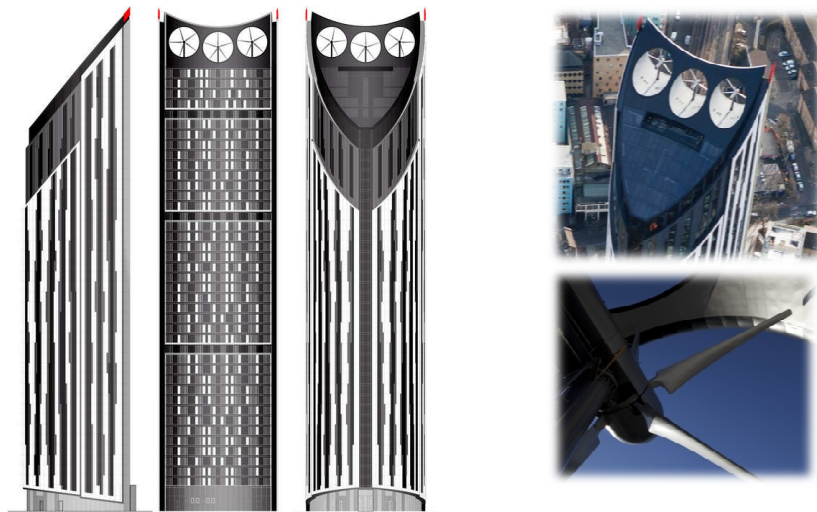


Figure 2.7 – Overview of La Strata SE1, London (Singhal, 2011; Brookfield Europe, 2011)

The most recent project incorporating wind energy turbines into the building is the 309-meter high tower in Guangzhou (China) which has been completed in 2011 (Figure 2.8).

The Pearl River Tower incorporates four large openings of approximately 6 by 6.8 m<sup>2</sup> located at the mechanical floors (level 24 and 48) that function as a type of pressure relief valve for the building and a source of wind energy. Vertical axis wind turbines with a height of 5 meters (WindSide) installed in each opening will harvest wind energy and are expected to produce 40 MWh per year which constitutes 1% of the total energy demand (Epstein, 2008). The building design will capitalise on the pressure difference between the windward and leeward sides of the structure, facilitating airflow through the openings (Figure 2.9). The facades of the structure have been designed to decrease the drag forces and optimise the wind velocity passing through these four openings. In particular, the broad sides of the structure are aligned perpendicular to the prevailing wind direction, which is most of the year from the south. This creates a positive pressure on the windward side and a negative pressure on the leeward side. From preliminary mathematical models, CFD calculations and wind tunnel testing the results showed an increase in wind velocities. By integrating the turbines within the building the coefficient of performance is expected to reach nearly 90% of extraction efficiency (Boyer, 2010).



Figure 2.8 – Overview of Pearl River Tower, Guangzhou (ScyscraperCity, 2006)

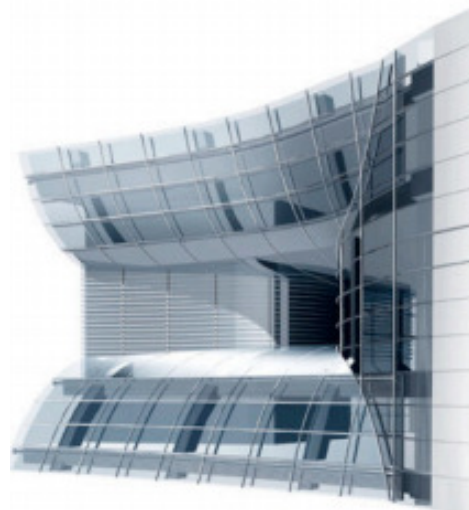
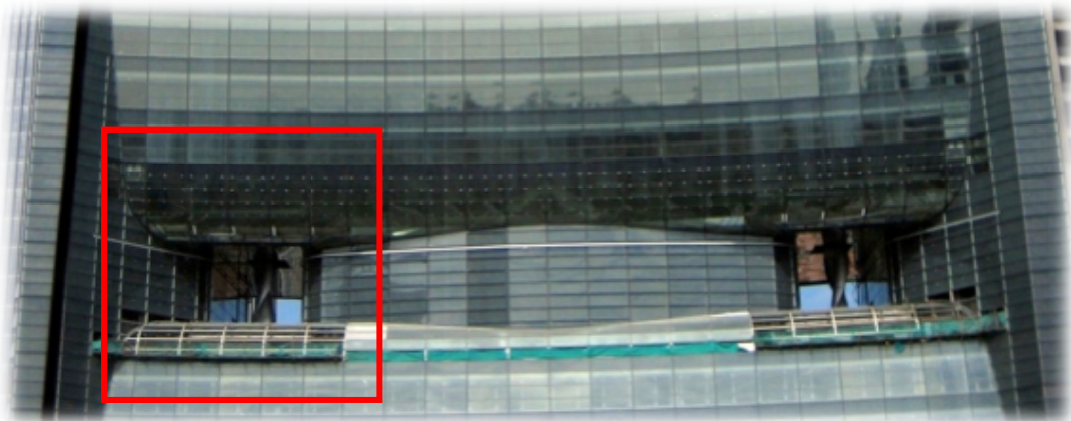


Figure 2.9 – Facade of Pearl River Tower, Guangzhou (the red square indicates the turbine location) (SOM, 2010)

The buildings mentioned in this section are illustrative examples of an integrated wind energy system design, taking into account the aerodynamic shape of the building.

#### *2.2.4 Points of attention*

Wind energy conversion systems in urban environments require specific points of attention. The most important aspect during operation covers safety of people and property in the proximity of the building with integrated wind turbines. The risk of accidents caused by the shedding of a turbine rotor blade should be evaluated (Glass & Levermore, 2011). Moreover, the probability of ice forming and a failure of the turbine suspension system should not be omitted (Campbell & Stankovic, 2001).

Other opposing aspects of wind turbines in urban environments are as follows: site aesthetics, noise and vibration pollution, flicker effect, blade-reflected light and disruption of local wildlife (Sharpe, 2010).

First, the visibility of wind turbines can considerably affect the architectural view, especially in residential or commercial areas. Second, depending on the turbine model and wind speeds it is operating at, wind turbines often generate a large amount of noise, which can be a large problem in built-up areas, especially at night when the ambient noise level is low (Moorhouse et al., 2011). The noise caused by wind turbines can have either aerodynamic or mechanical origin. The first describes the noise radiated from the blades and associated with the interaction of turbulence with the surface of the blades (Tadamasa & Zangeneh, 2011). The second is associated with the gearbox, the generator and the control equipment and can be transmitted along the structure of the turbine and radiated from the blade surfaces (Moorhouse et al., 2011). The transmittance of vibrations induced by rotation of blades to building bearing structures should be excluded by utilisation of damped bearings. Third, flicker effect as well as blade-reflected light created by the spinning blades of wind turbines may annoy people, and be dangerous for those suffering from epilepsy (Harding et al., 2008). In case of high rotation speeds of the blades the shadow might be essentially invisible.

As for wildlife, wind turbines can obstruct the flight path of birds and might injure them. Certain measures should be applied to reduce bird deaths, such as provision of additional places for birds to perch, construction of wind turbines away from migration paths, etc.

## 2.3 Principal methods to assess wind performance and energy production

Based on regional wind resource data and on an estimate of the real efficiency of actual wind turbines, one can determine the electrical power-producing potential of the wind energy. The current section describes the method of assessment used in this study which can be divided in the following steps (Manwell et al., 2009):

- meteorological potential;
- site potential;
- technical potential.

### 2.3.1 *Meteorological potential*

The available wind resource estimation can be performed using measurement data from a nearby meteorological station. Based on these records, the probability histogram indicating the number of occurrences of certain wind speed intervals can be plotted. In case a projection of measured data from one location to another is required, it is advantageous to use analytical representations for the probability distribution of the wind speed.

Several studies mention the advantage of using the Weibull distribution function of wind speed in order to assess wind energy production (Manwell et al., 2009; Mirhosseini et al., 2011; Ohunakin, 2012). The current study uses the Weibull parameters  $c$  and  $k$  to describe the wind distribution by a cumulative exceeding probability function  $P_{\theta}(U)$  mentioned by Blocken et al. (2004):

$$P_{\theta}(U) = A(\theta) \cdot \exp \left[ - \left( \frac{U}{c(\theta)} \right)^{k(\theta)} \right] \quad (2.7),$$

where  $P_{\theta}(U)$  – probability of exceeding of wind speed  $U$  at meteorological site during wind direction  $\theta$ ;  $A(\theta)$ ,  $c(\theta)$ ,  $k(\theta)$  – probability, velocity scale and shape parameters for wind direction  $\theta$ , respectively.

Weibull parameters  $c(\theta)$ ,  $k(\theta)$  are defined as follows. At first, by taking twice the logarithm of equation (2.7) one can write it in a linear form  $y = ax + b$  (parameter  $A(\theta)$  is omitted) and obtain the following dependencies described in (Jamil et al., 1995):

$$k(\theta) = a \quad (2.8),$$

$$c(\theta) = \exp \left( - \frac{b}{a} \right) \quad (2.9)$$

Secondly, by making a graph of  $y = ax + b$ , parameters  $a$  (slope of the line) and  $b$  (intersection point ordinate with  $y$ -axis) are defined and, finally, Weibull parameters for different wind directions are calculated.

### 2.3.2 *Site potential*

The principal research methods for the assessment of wind performance at a certain building site can be distinguished as follows (Mertens, 2006):

- Mathematical models;
- In-situ measurements;
- Wind tunnel measurements;
- CFD calculations.

Mathematical models are considered as difficult to use, extremely time-consuming and require a thorough knowledge of fluid dynamics. Simplified models can generally be used for elementary problems, which require an understanding of the main mechanism of the flow (Cook et al., 2005). It may not be accurate for complex flow cases and the results may not be informative (Chen, 2009). However, analytical models modified by empirical coefficients can improve the accuracy of the predictions (Foster et al., 2003).

In-situ measurements might be the most accurate tool for assessing wind flow on a particular site and certain location, especially when determining the efficiency of wind turbines before its integration into an existing building (Abohela et al., 2011). However, this tool is time-consuming, requires careful execution during experiments in order to achieve correct results and high expenses for measuring equipment.

As for wind tunnel measurements, the data obtained from these tests is recognised as reliable if the wind tunnel is an atmospheric boundary layer (ABL) tunnel which takes into account the increase of wind speed with height in the ABL and the model is accurately constructed. Nonetheless, several drawbacks of wind tunnels are mentioned such as high investment costs for tunnel, models, measuring equipment as well as highly technical operation and maintenance. Moreover, the scaling can cause Reynolds numbers (Re numbers) to drop below the threshold for fully turbulent flow, especially for the models including geometries with different special scales (van Hooff et al., 2011).

Numerical modelling with CFD might be a less time-consuming and less expensive alternative for wind tunnel experiments, depending on the type of a problem to solve. CFD simulations describe the target wind flow variables in each point of interest and provide a possibility to analyse a large amount of design configurations. However, CFD simulations have a high sensitivity to the input of the user and should preferably be performed in combination with wind tunnel or in-situ measurements for computational model validation.

For practical reasons only CFD simulations are included in the framework of the current project, but validation studies are also conducted.

### 2.3.3 *Technical potential and energy estimation*

The technical potential is calculated based on the site potential of wind resource and technical characteristics of applied wind turbines.

The following calculation algorithm is suggested:

1. The reference estimation of wind power generation  $P_w(U_{\text{turb}})$  by a single-standing turbine is determined by:

$$P_w(U_{\text{turb}}) = \frac{1}{2} \rho A C_p \eta U_{\text{turb}}^3 \quad (2.10),$$



where  $\rho$  is the air density (1.225 kg/m<sup>3</sup>),  $A$  – turbine front area,  $C_p$  – coefficient of performance,  $\eta$  – drive train efficiency (generator power/rotor power),  $U_{\text{turb}}$  – incoming wind speed.

The coefficient of performance is defined as the ratio of maximum power obtained from the wind to the total power available in the wind. According to Betz's law, the maximum theoretical value of  $C_p$ , or the maximum possible energy to be derived from engines, equals 59.3% of the total wind power (van Kuik, 2007). More specific data about the coefficient of performance and power output of a certain wind turbine depending on different wind speeds can be obtained from technical specifications provided by the manufacturer.

2. In order to express the probability of a wind speed  $U$  occurring within a certain wind speed class (between values  $U_a$  and  $U_b$ ),  $p_\theta(U)$  is defined by using the following relation (Manwell et al., 2009):

$$p_\theta(U_a \leq U \leq U_b) = \int_{U_a}^{U_b} \left[ \frac{dP_\theta(U)}{dU} \right] \quad (2.11)$$

3. The average wind turbine power  $\bar{P}_w$  can be estimated from the following equation:

$$\bar{P}_w = \int_0^\infty P_w(U_{\text{turb}}) p(U_{\text{turb}}) dU_{\text{turb}} \quad (2.12)$$

4. The energy captured from wind turbine  $\bar{E}_w$  (MWh) over period of time  $t$  (hours) equals (Manwell et al., 2009):

$$\bar{E}_w = \bar{P}_w \cdot t \quad (2.13)$$

The wind speed represents the principal factor in the current project due to its significant influence on the turbine energy yield that can be estimated from the equation (2.10). The wind speed distribution on a building site can be described by applying the conversion factor  $\gamma$  to the equation used for a meteorological site (Blocken et al., 2004):

$$P_\theta(U_{\text{turb}}) = A(\theta) \cdot \exp \left[ - \left( \frac{U_{\text{turb}}}{\gamma \cdot c(\theta)} \right)^{k(\theta)} \right] \quad (2.14),$$

$$\gamma = \frac{U_{\text{turb}}}{U} = \frac{U_{\text{turb}}}{U_{\text{ref}}} \cdot \frac{U_{\text{ref}}}{U} \quad (2.15),$$

where  $U_{\text{turb}}$  – wind speed imposed to the turbine hub,  $U_{\text{ref}}$  – reference wind speed at a certain height at the building site,  $U$  – wind speed defined at meteorological site.

## 2.4 CFD simulation guidelines

In order to obtain sufficiently accurate results the recommendations elaborated by the Architectural Institute of Japan (Tominaga et al., 2008) and the COST research cooperation (Franke et al., 2004; Franke et al., 2007) are used as guidelines throughout the study.

The following steps are suggested in order to perform CFD simulation (Franke et al., 2007):

1. Choice of target variables;
2. Choice of approximate equations describing the physics of the flow;
3. Choice of geometrical representation of the obstacles;
4. Choice of computational domain;
5. Choice of boundary conditions;
6. Choice of initial conditions;
7. Choice of computational grid;
8. Choice of time step size (for unsteady simulations);
9. Choice of numerical approximations;
10. Choice of iterative convergence criteria

### 2.4.1 *Target variables*

The target variable is the vertical distribution of wind velocities. The variable parameters intended for detailed analysis on the wind energy potential include length, width, depth and separation of the buildings. Afterwards, the Venturi-effect and wind-blocking effect, identified by Blocken & Carmeliet in 2006, should be evaluated in relation to the velocity in the middle of the passage.

### 2.4.2 *Approximate equations*

The Navier-Stokes equations needed to be solved within the obstacle layer can be replaced by simplifications. Firstly, within the lowest atmosphere layer in urban areas the assumption of non-divergent flow fields and constant density might be used (Franke et al., 2007). Secondly, the basic equations are averaged by filtering out small turbulent flow scales and substituting them by certain turbulent closure models. Thus the requirements for computational resources might be reduced without notable effect on the accuracy of the results.

Steady Reynolds-Averaged Navier-Stokes (RANS) equations of continuity and momentum lead to a statistically steady description of the turbulent flow and are used to analyse the aerodynamic performance of the different building geometries (Franke et al., 2004).

The turbulent wind flow around the building is solved by steady RANS equations in combination with the realisable  $k - \varepsilon$  turbulence model to provide closure using the commercial code ANSYS Fluent 12.1. The choice in favour of the realisable  $k - \varepsilon$  turbulence model is made due to its ability to attenuate the overproduction of turbulent kinetic energy in regions of stagnant flow without leading to worse results in the wake compared to the standard  $k - \varepsilon$  model (Franke et al., 2004).

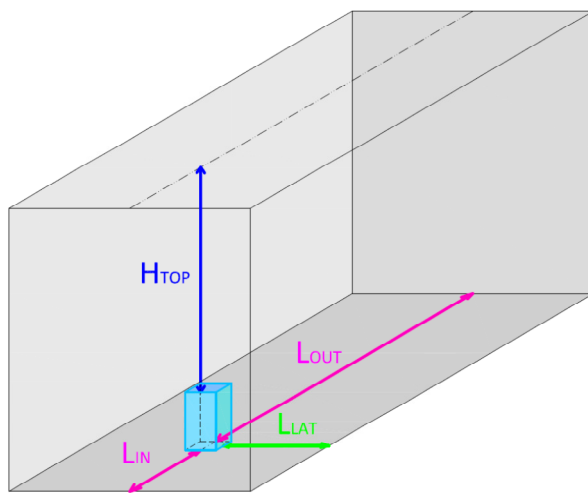
### 2.4.3 Geometrical representation of the obstacles

Within the framework of the project the aerodynamic system performance will be analysed on two buildings without explicit geometrical representation of the surroundings.

### 2.4.4 Computational domain dimensions

The general recommendations for the dimensions of the computational domain concerning a single building of height  $H_b$  are extracted from Franke et al. (2007) and are provided in Table 2.1. The size of the entire computational domain depends on the target area assigned for investigation.

Table 2.1 – Recommendations of COST guidelines (Franke et al., 2007)



Notation	Description	Value
$H_{TOP}$	Roof of the building and top of computational domain	$\geq 5H_b$
$L_{LAT}$	Lateral extension between the building's sidewalls and the lateral boundaries of the computational domain	$\geq 5H_b$
$L_{IN}$	Distance between the inflow boundary and the building	$(5 - 8)H_b$
$L_{OUT}$	Distance between the outflow boundary and the building	$\geq 15H_b$

The large distance between the roof of the building and top of the computational domain is necessary to prevent an artificial acceleration of the flow over the building, as most boundary conditions applied at the top of the computational domain do not allow fluid to leave the domain. For single buildings the top of the computational domain should be at least  $5H_b$  above the roof of the building, where  $H_b$  is the building height. Additional requirements suggest a blockage dependent distance, where the blockage is defined as the ratio of the projected area of the building in flow direction to the free cross section of the computational domain. The recommended maximum blockage value is 3% (Franke et al., 2007).

The lateral extension of the domain can be determined by the required blockage and recommended distance between the building's sidewalls and the lateral boundaries of the computational domain of  $5H_b$ .

As for longitudinal extension of the domain, the region in front of (approach flow) and the region behind (wake) the built area have to be discerned. For a single building a distance of  $5H_b - 8H_b$  between the inflow boundary and the building is recommended if the approach flow profiles are well known. The region behind the built area is terminated by the outflow boundary. In case of a single building this boundary should be positioned at least  $15H_b$  behind the building to allow for flow redevelopment behind the wake region, as fully developed flow is normally used as a boundary condition in steady RANS calculations. However, Tominaga et al. (2008) stated that the

minimum value for outflow boundary equals  $10H_b$  and the expansion of the computational domain without representation of actual surroundings can lead to unrealistic results.

#### 2.4.5 *Choice of boundary and initial conditions*

The boundary conditions represent the influence of the surroundings cut off by the domain.

The approach-flow vertical mean wind velocity profile and turbulence quantities corresponding to the estimated roughness characteristics should be assigned at the inlet of the domain.

The standard wall functions (Launder & Spalding, 1974) with the sand-grain based roughness modification (Cebeci & Bradshaw, 1977) are used for the ground and building surfaces. The wall-function modelling method economises computer time and storage, it allows the introduction of additional empirical information in special cases, as when the wall is rough. In order to correctly represent the rough fetch upstream of the model, the values of the equivalent sand-grain roughness height  $k_s$  and the roughness constant  $C_s$  should be determined for the ground surface using their relationship with  $y_0$ . For Fluent 6.3, this relationship is (Blocken et al., 2007a):

$$k_s = 9.793y_0/C_s \quad (2.16)$$

According to Blocken et al. (2007) a careful representation of the flow near the ground surface is required for ABL flow simulation. The derived requirements for upstream and downstream regions in order to achieve horizontal homogeneity of the wind speed profile include:

- horizontally homogeneous ABL flow in the upstream and downstream region of the domain which is covered by the use of wall functions;
- determination of physical roughness height  $k_s$  and corresponding aerodynamic roughness length  $y_0$ ;
- a sufficiently high mesh resolution in the vertical direction close to the bottom of the computational domain fitting the requirement of  $y_p > k_s$ , where  $y_p$  represents the distance from the centre point P of the wall-adjacent cell to the bottom of domain and  $k_s$  is a physical roughness height  $k_s$  of the terrain.

It must be mentioned, that the simulation of a horizontally homogeneous ABL over uniformly rough terrain is often required in the upstream part of a computational domain to reveal the absence of streamwise gradients in the vertical profiles of the mean wind speed and turbulence quantities. That means the vertical mean wind speed and turbulence profiles are in equilibrium with the roughness characteristics of the ground surface (Blocken et al., 2007a). Horizontal homogeneity implies that the inlet profiles, the approach flow and the incident profiles are the same. The reasons for inhomogeneity could be the lack of compatibility between the shape of the imposed inlet profiles, the type of turbulence model, the wall functions and other computational parameters. The shape of the vertical incident flow profiles influences the simulation results of flow around buildings. It is advised to assess the presence of horizontal inhomogeneity by first performing a simulation in an empty computational domain before conducting simulations with the building models present (Blocken et al., 2007b).

#### *2.4.6 Choice of computational grid*

In order to keep the truncation error small, specific attention should be devoted to the generation of a high-resolution grid. According to Franke et al. (2007) and Tominaga et al. (2008), it is important to provide a minimum of 10 cells per building side and to keep the widths of adjacent grids similar in regions of high gradients with stretching/compression ratios below  $\approx 1.3$ .

The body-fitted grids are generated by a method presented by van Hooff & Blocken (2010). By means of this technique, the geometry and the grid are created simultaneously based on translation of pre-meshed 2D cross-sections, thus avoiding generation of undesirable pyramidal or tetrahedral cells. A detailed grid-sensitivity analysis should be conducted in order to achieve grid independency for results in the following way: converged solution for three different meshes (from fine to coarse) should be compared (Franke et al., 2007). As soon as both solutions are within acceptable agreement to each other, grid-independency is achieved.

#### *2.4.7 Choice of numerical approximations*

As stated in Franke et al. (2004), first-order schemes should not be used for numerical approximations. Therefore, only second-order upwind discretisation schemes are applied to momentum, turbulent kinetic energy and turbulent dissipation rate. Standard interpolation scheme for pressure is assigned.

#### *2.4.8 Choice of iterative convergence criteria*

To keep iteration-convergence error small sufficient convergence should be achieved. The simulation can only be terminated when the residuals for continuity, momentum, turbulent kinetic energy and turbulence dissipation rate are sufficiently low and constant with increasing number of iterations (Franke et al., 2007). Absolute convergence criteria, or the residual value for which the solution of each variable will be considered converged, of at least five orders of magnitude is recommended (Franke et al., 2004).

## ***Summary***

This Chapter provides the relevant theory concerning studies in urban wind flow and illustrated some practical applications of wind turbines integrated into the built environment. The next Chapter describes the validation study conducted within the framework of the current project in order to validate the chosen computational model.

### 3 Validation study

As stated before, the results obtained from numerical simulations need to be validated. Since experimental data are not available within the framework of the current project, wind tunnel data from related studies on similar building configurations is extracted for validation. In this Chapter the validation study is described which is based on two related studies concerning pedestrian wind comfort performed by Stathopoulos & Storms (1986) and Beranek & Van Koten (1982). The validation studies are performed in the following sequence taking into account the recommendations stated in section 2.4:

1. Determination of domain extensions;
2. Determination of boundary conditions;
3. Simulation in the empty domain – in order to assess horizontal homogeneity of mean velocity profiles and turbulence quantities;
4. Grid-sensitivity analysis – in order to assess grid-independency of solutions;
5. Full-scale simulation – in order to assess Re-number independency of the results;
6. Analysis of the results.

## 3.1 Stathopoulos & Storms case

### 3.1.1 Case overview

The article describes the measurements of mean wind velocity and turbulence conditions in a passage between two rectangular buildings placed parallel to each other. Results are provided for different wind directions and for a number of geometries with varying height and passage width. Experiments are conducted at a scale of 1:400 in the atmospheric boundary layer wind tunnel at Concordia University, Montréal (Stathopoulos, 1984). The reported data contains incident flow profiles of mean velocity and turbulence intensity. The measured mean speed profile is fitted by a power-law expression with an exponent equal to 0.15. The reference wind speed measured at 5 mm height (2 m in a full scale, pedestrian level) equals 5.9 m/s. The turbulence intensity, based on the local wind speed, ranges from 20% at 5 mm to 5% at gradient height of 0.9 m (360 m in a full scale).

The experimental results contain values of the wind amplification factor  $K(n)$  at a certain point within a passage at pedestrian level height:

$$K(n) = \frac{U(n)}{U_0} \quad (3.1),$$

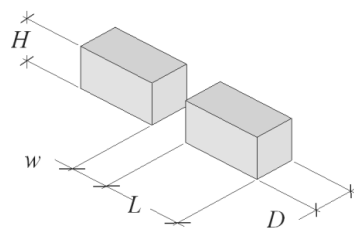
where  $U(n)$  – wind speed measured at a point  $n$  within a passage centre line,  $U_0$  – reference wind speed at the same height measured in absence of the buildings.

### 3.1.2 Validation study overview

Note that, from this point on, all the dimensions and values in this section are reported in a full scale, while the experiment and the validation study have been performed in a scale of 1:400.

One geometrical configuration with a passage width equal to 6 m is considered and described in Table 3.1.

Table 3.1 – Validation case



Parameters	Case
	#1
w [m]	6
L [m]	40
D [m]	20
H [m]	20

#### 3.1.2.1 Domain extensions

The domain dimensions are defined according to the recommendations stated in section 2.4.4 and are shown in Figure 3.1. Special emphasis is placed on the blockage ratio in the windward direction defined in section 2.4.4. In order to achieve a blockage ratio below the threshold of 3%, the domain is extended in the lateral direction (Franke et al., 2007). The measurements described in the article have been performed for a reduced scale model of 1:400. The same scale is applied for this validation study.

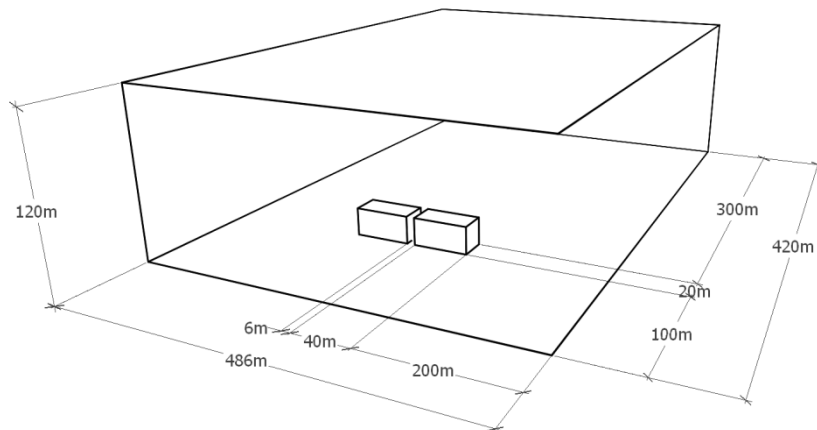


Figure 3.1 – Domain extensions (passage width  $W = 6\text{ m}$ )

### 3.1.2.2 Boundary conditions

The measured incident mean wind speed profile described in the article has been expressed by a power law with an exponent  $\alpha = 0.15$  and imposed at the inlet. The reference wind speed at a height of 2 m equals 5.9 m/s. The aerodynamic roughness length  $y_0 = 0.008\text{ m}$  is obtained by fitting the log-law profile to the experimentally determined power-law profile (Figure 3.2).

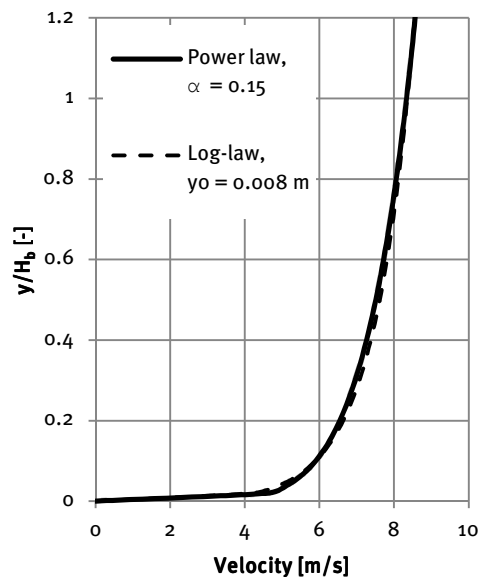


Figure 3.2 – Wind velocity profiles described by power and log laws ( $H_b$  – building height)

The approach flow turbulent kinetic energy  $k$  is calculated from the turbulence intensity  $I_u$  measured during wind tunnel experiment using  $k = (I_u U)^2$ , assuming that  $\sigma_v^2 = \sigma_w^2 \approx \sigma_u^2/2$  (Tominaga et al., 2008). The turbulence dissipation rate  $\varepsilon = (u^*)^3/\kappa(y + y_0)$ , where  $u^*$  is the friction velocity related to the logarithmic mean wind speed profile,  $\kappa$  – the von Karman constant equal to 0.42 (Richards & Hoxey, 1993),  $y$  is the height coordinate, and  $y_0$  is the aerodynamic roughness length equal to 0.008 m.

An overview of inlet profiles along the height of the domain for turbulence intensity, turbulent kinetic energy and turbulence dissipation rate can be seen in Figure 3.3.



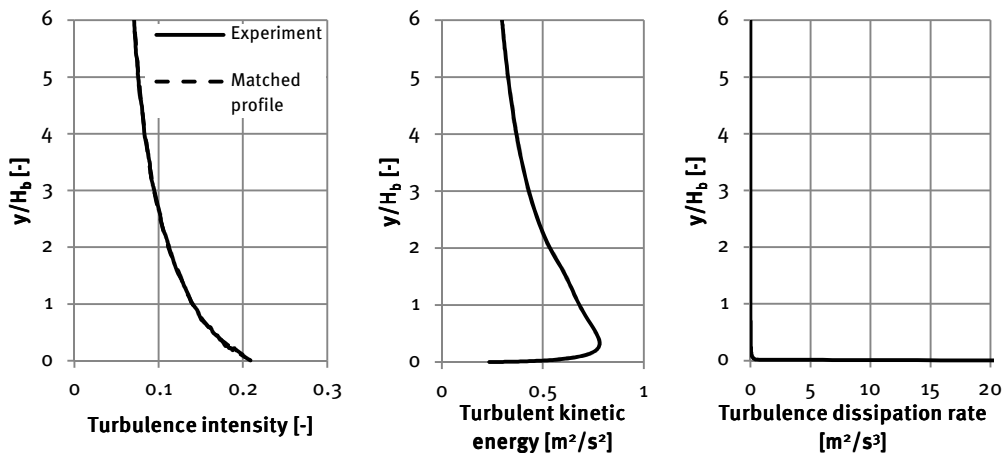


Figure 3.3 – Profiles of turbulence intensity, turbulent kinetic energy and turbulence dissipation rate imposed at the inlet

According to the requirements stated in section 2.4.5  $k_S = 9.793y_0/C_S$  and  $y_P > k_S$ ,  $C_S = 0.366$ ,  $k_S = 0.214$  m and the first cell height equals to 0.43 m for the initial grid configuration.

The building surfaces are assigned by default to be smooth with  $k_S = 0$  and  $C_S = 0.5$ . Following the recommendations of Franke et al. (2004), symmetry is prescribed to the top and lateral boundaries of the domain. Thus, they are modelled as a slip wall characterised by zero normal velocity and zero normal gradients of all variables. At the boundary behind the obstacles, a pressure outlet with zero static pressure is assigned.

### 3.1.2.3 Homogeneity analysis

The occurrence of horizontal inhomogeneity, i.e. the acceleration of the flow near the ground surface, is analysed by performing a simulation in the empty domain and comparing the profiles of wind velocity and turbulent kinetic energy along the domain.

At first, a simulation in an empty domain is performed to investigate the horizontal homogeneity of the vertical mean wind speed and turbulence quantities. The calculated profiles of mean speed and turbulent kinetic energy along the vertical lines near building level are illustrated in Figure 3.4.

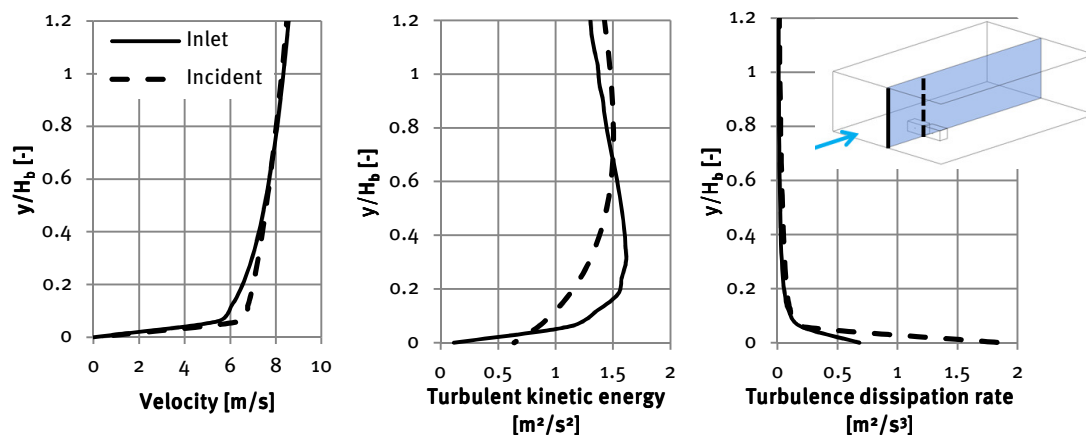


Figure 3.4 – Calculated profiles of mean wind speed, turbulent kinetic energy and turbulence dissipation rate along the vertical lines for  $k = (I_u U)^2$  ( $H_b =$  building height)

As can be seen, there is an acceleration of wind speed near the ground surface. As advised by Blocken et al. (2007), in order to improve the horizontal homogeneity the inlet profile of turbulent kinetic energy  $k = (I_u U)^2$  was replaced by  $k = 0.5(I_u U)^2$ . Figure 3.5 demonstrates that the calculated profiles suffer less from streamwise gradients along the domain, especially for the vertical wind speed profiles. Therefore, the inlet profile of turbulent kinetic energy  $k = 0.5(I_u U)^2$  will be applied in the current validation study.

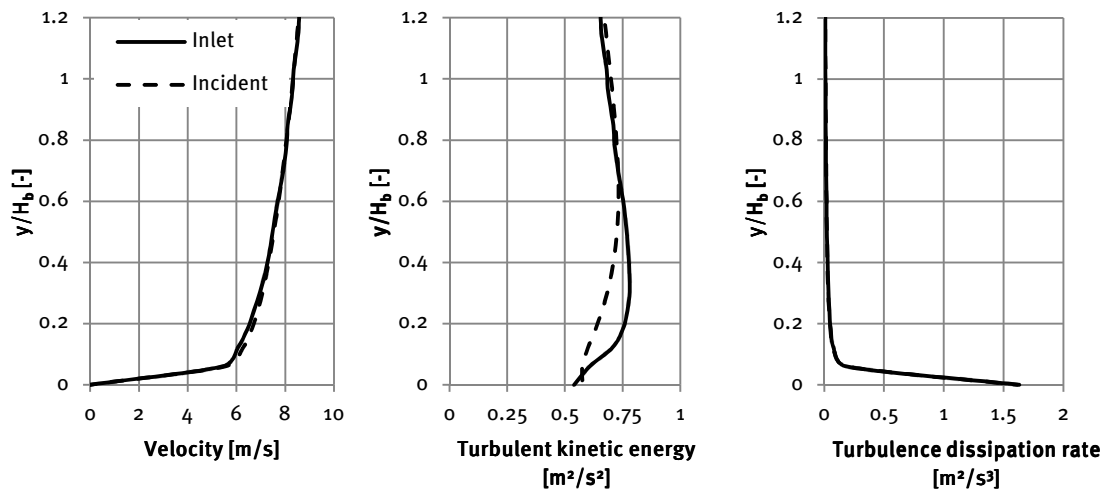


Figure 3.5 – Calculated profiles of mean wind speed, turbulent kinetic energy and turbulence dissipation rate for  $k = 0.5(I_u U)^2$ .

The positive effect of the mentioned reduction of turbulent kinetic energy is indicated in Figure 3.6. The plots illustrate turbulent kinetic energy distribution along the vertical centre plane of the domain.

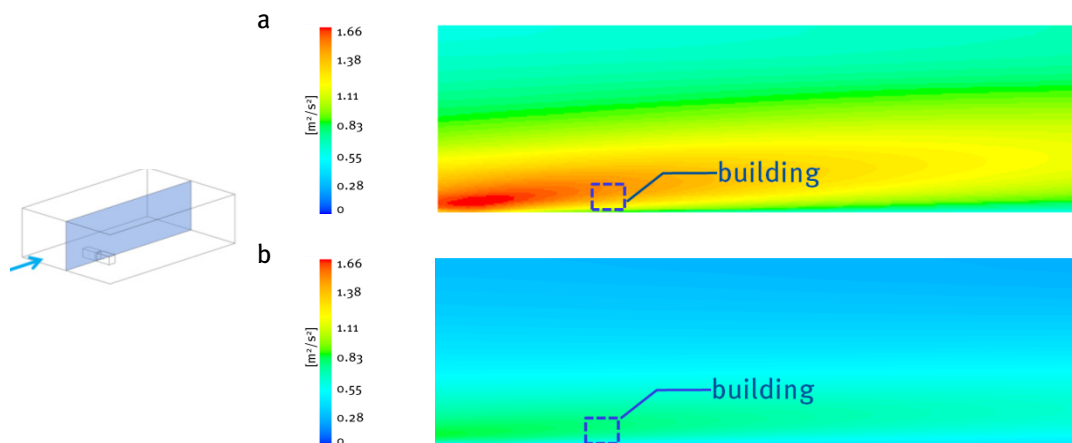


Figure 3.6 – Calculated contours of turbulent kinetic energy: a)  $k = (I_u U)^2$ ; b)  $k = 0.5(I_u U)^2$ .

### 3.1.2.4 Grid-sensitivity analysis

A grid-sensitivity analysis for case #1 is performed with the following quantities of cells: 833,216 – for coarse configuration; 2,350,240 – for medium configuration; 6,425,124 – for fine configuration (Figure 3.7). According to the requirements of  $k_S = 9.793y_0/C_S$  and  $y_P > k_S$  stated

in section 2.4.5,  $C_s = 0.53$ ,  $k_s = 0.148$  m and the first cell height varies between (0.3 – 0.6) m for the three configurations applied in the grid-sensitivity analysis.

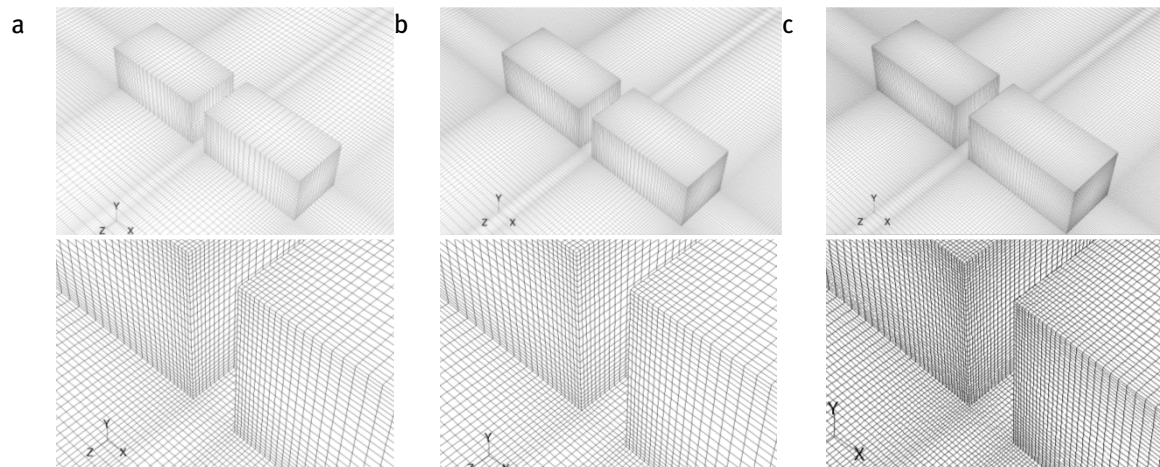


Figure 3.7 – Mesh configurations for grid-sensitivity analysis: a) coarse; b) medium; c) fine

The results of the simulations on the three different grids are compared on the lines at the passage entrance plane and at pedestrian level height (2 m), and are depicted in Figure 3.8. As indicated, the results obtained with the medium grid configuration provide a closer agreement with the fine configuration regarding the calculated values for mean wind speed and turbulent kinetic energy at the pedestrian level height (2 m). For that reason, the medium grid configuration is applied for validation case #1.

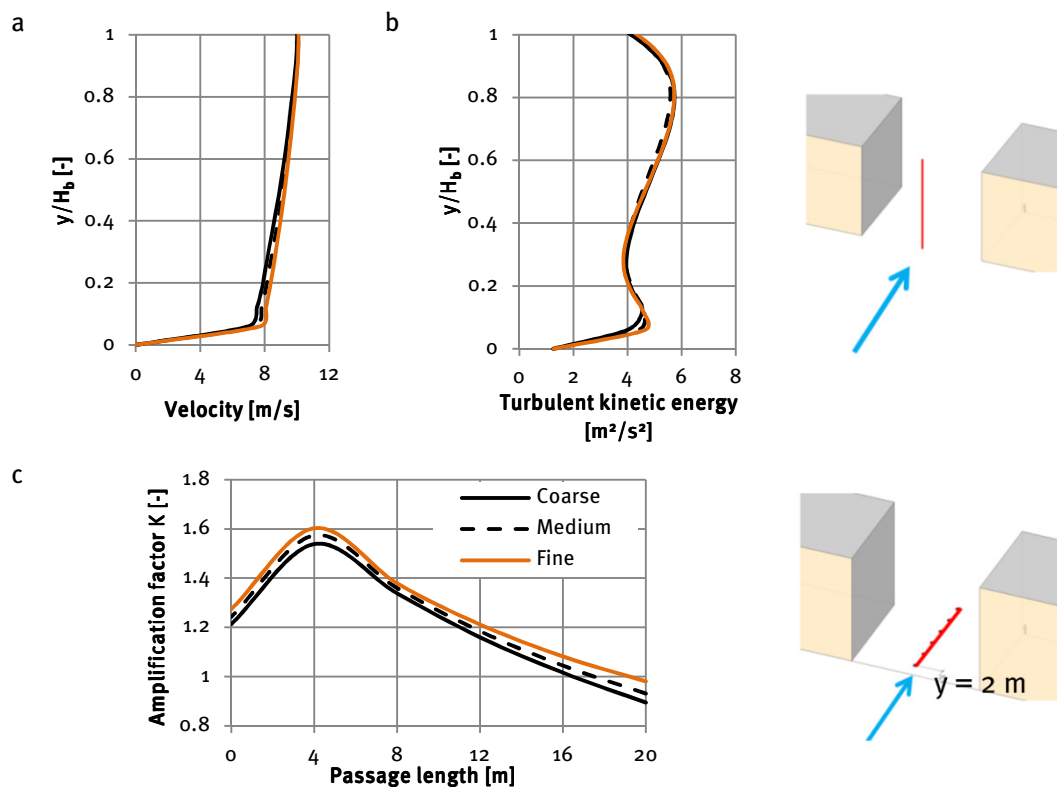


Figure 3.8 – Grid-sensitivity analysis on the passage entrance line: a) velocity; b) turbulent kinetic energy; c) velocity amplification factor along the validation line

### 3.1.2.5 Full-scale simulation

The building-related Reynolds number at a height of 20 m (building height) equals 26,699 which is above the recommended threshold value of 11,000 in order to provide Reynolds number independent flow (Snyder, 1981). However, to confirm that statement it is recommended to perform a simulation in reduced scale (1:400) as well as in a full scale and compare velocity and turbulent kinetic energy profiles as well as wind amplification factors in the target area.

A full-scale simulation was performed for the validation case #1 with the medium grid configuration. The analysis has been performed on vertical lines at the entrance of the passage and inside the passage as well as on the validation line. As shown in Figure 3.9, the differences between the values of the mean velocity, turbulent kinetic energy and velocity amplification factors in the passage are very limited. Therefore, scaled models provide sufficient degree of Reynolds number independency.

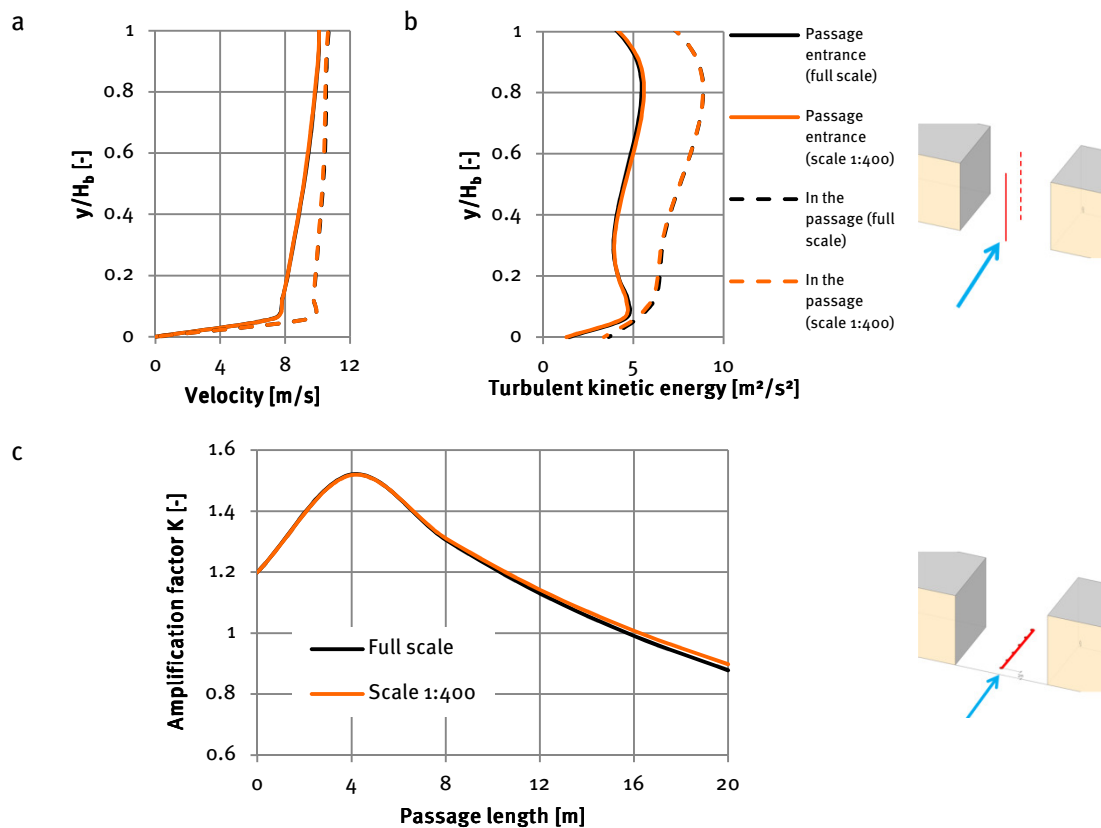


Figure 3.9 – Comparison of computed values between scaled and full-scale model: a) velocity; b) turbulent kinetic energy; c) velocity amplification factor along the validation line

### 3.1.2.6 Additional considerations

The implementation of the recommended maximum blockage value of 3% (Franke et al., 2007) was evaluated in the current study. At first, the simulation has been performed in the domain defined only by the recommended dimensions stated in Table 2.1 of the current report, resulting in a blockage ratio of 4.9%. As can be seen from Figure 3.10 (top view), the flow acceleration occurs due to an insufficient domain width and influence of the sidewalls. After that, the

additional requirement of a blockage ratio less than 3% was fulfilled by extension of the domain in lateral direction and resulted in an absence of sidewall influence on flow acceleration.

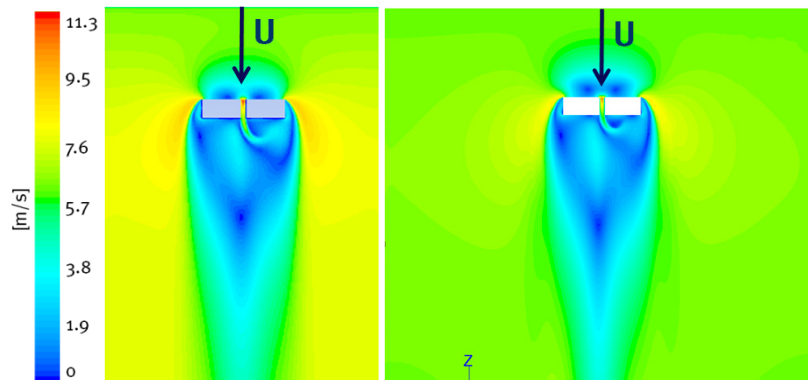


Figure 3.10 – Top view on velocity contour plots at the pedestrian level height with a blockage ratio of: a) 4.9%; b) 2.7%

Thus, the dimensions of domain should be carefully calculated considering all the recommendations stated in section 2.4.4.

Note that, the unusual curve behind the passage can be caused by the chosen numerical method (steady RANS) which provides a statistically steady description of the time-averaged turbulent flow, while in reality the flow is characterised by a fluctuating nature. To ensure the stability of the results, the character of the curve and velocity magnitude in validation points inside the passage were analysed every 100 iterations during 1000 iterations. Velocity contour plots and velocity point values provided in Appendix A confirm the steadiness of the calculation results.

### 3.1.3 Results

The results of this validation study are analysed by means of amplification factor  $K$  which is defined as the ratio of the wind speed at a certain position to the “free-field” wind speed (no buildings present) at the same position. The comparison between the results obtained from the experiments of Stathopoulos & Storms (1986) and the CFD simulations are provided in Figure 3.11. It must be mentioned that for the simulation case the “free-field” wind speed is taken at the position indicated below, where wind speed is not influenced by the presence of the buildings.

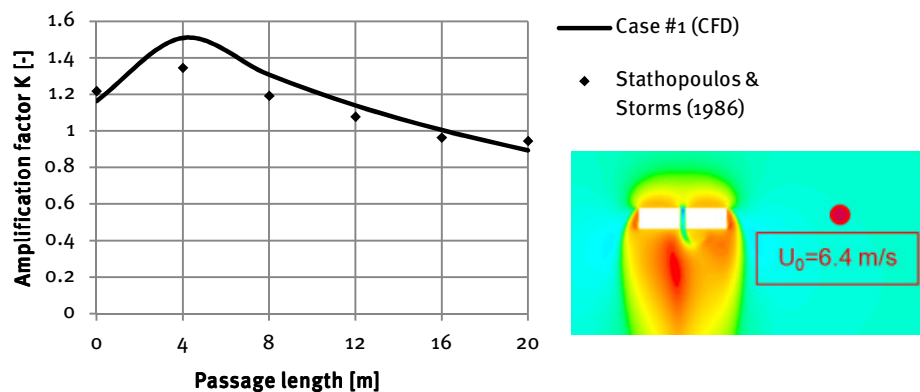


Figure 3.11 – Amplification factors  $K$  along the passage length at the pedestrian level height obtained by CFD simulation and wind tunnel measurements; indication of “free-field” wind speed

The numerical results do not completely correspond to the experimental results with a maximum deviation of 10% at the point 4 m. This might be explained by the physical modelling error in CFD and the complexity of the experiments in the wind tunnel, namely inaccuracies caused by the measurement installation (hot-wire anemometers), differences in the geometry, absence of roughness elements on the turntable, over which the IBL develops (Blocken et al., 2009). The other possible reason could be the difference in blockage ratio equal to 1% and 3% for the experiments in a wind tunnel and CFD simulation, respectively. However, the curves have the same character with maximum wind speed amplification at the point 4 m inside the passage.

## 3.2 Beranek & Van Koten case

### 3.2.1 Case overview

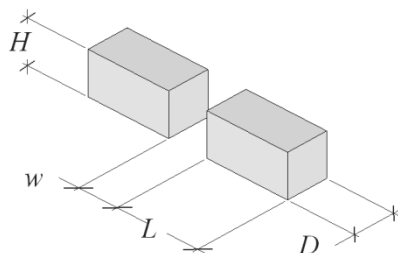
The study of Beranek & Van Koten (1982) devoted to wind comfort investigation in built-up areas provided results of wind tunnel experiments through sand erosion for different simplified building configurations. Results are provided for different wind directions and for a set of geometries in which the height, the length and the width of each building and the passage width are varying. The experiments were conducted at a scale of 1:500 with a power-law wind speed profile with an exponent  $\alpha = 0.28$ . The reported data consists of contour plots indicating the wind amplification factor at the pedestrian level height equal to 2 m. This is defined as a ratio of the local wind speed around the buildings to the approaching wind speed at the same height.

### 3.2.2 Validation study overview

Note that, from this point on, all the dimensions and values in this section are reported in a full scale, while the experiment and the validation study have been performed in a scale of 1:500.

Four geometrical configurations with different passage widths and heights are considered as described in Table 3.2.

Table 3.2 – Validation cases



Parameters	Cases			
	#2	#3	#4	#5
H [m]	25	50	25	50
w [m]	20	20	40	40
L [m]	80	80	80	80
D [m]	10	10	10	10

#### 3.2.2.1 Domain extensions

The domain dimensions are defined according to the recommendations stated in section 2.4.4 and are illustrated in Figure 3.12.

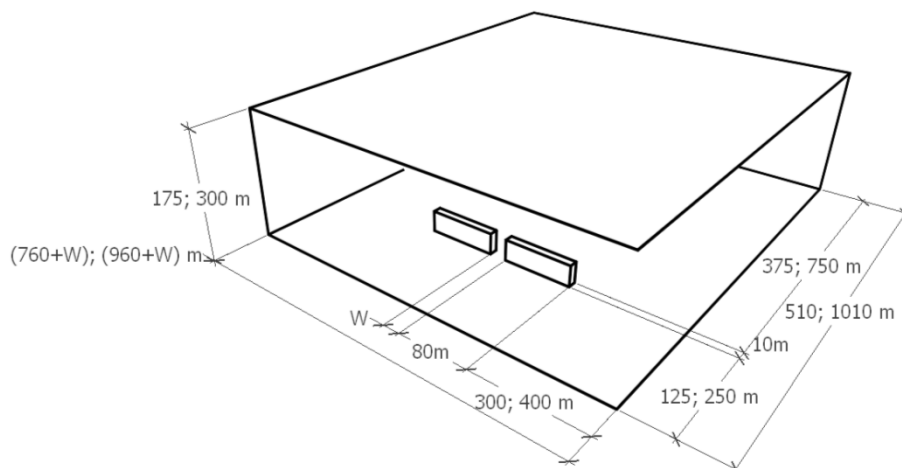


Figure 3.12 – Domain extensions (passage width  $W = [20; 40]$  m; values for building height  $H = [25; 50]$  m)

### 3.2.2.2 Boundary conditions

The measured incident mean wind speed profile has been expressed by a power law with an exponent  $\alpha = 0.28$  and is imposed at the inlet. The reference wind speed at a height of 10 m equals 5 m/s. The aerodynamic roughness length  $y_0 = 0.39$  m is obtained by fitting the log-law profile to the experimentally determined power-law profile (Figure 3.13a).

The approach flow turbulent kinetic energy  $k$  is calculated as a constant using the dependency  $k = 3.33(u^*)^2$ , the turbulence dissipation rate  $\varepsilon = (u^*)^3/\kappa(y + y_0)$ , where  $u^*$  is the friction velocity related to the logarithmic mean wind speed profile,  $\kappa$  – the von Karman constant equal to 0.42 (Richards & Hoxey, 1993),  $y$  is the height coordinate, and  $y_0$  is the aerodynamic roughness length equal to 0.39 m. The overview of inlet profile along the height of the domain for turbulence dissipation rate can be seen from Figure 3.13b.

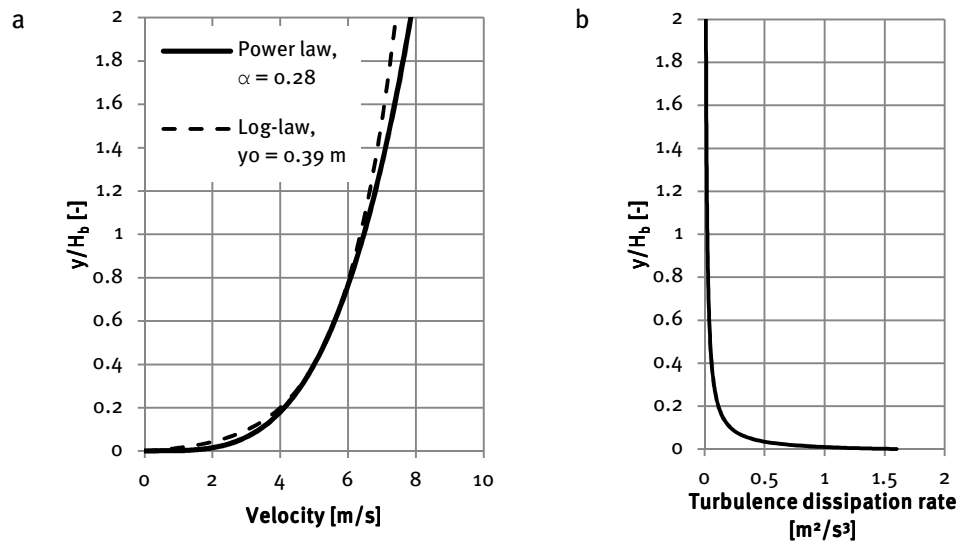


Figure 3.13 – a) Wind velocity profiles described by power and log laws; b) Profile of turbulence dissipation rate imposed at the inlet ( $H_b$  = building height)

According to the requirements stated in section 2.3.2  $k_S = 9.793y_0/C_S$  and  $y_P > k_S$ ,  $C_S = 7$ ,  $k_S = 0.545$  m and the first cell height equals to 1.1 m for the initial grid configuration.

The building surfaces are assigned by default to be smooth with  $k_S = 0$  and  $C_S = 0.5$ . Following the recommendations by Franke et al. (2004), symmetry is prescribed to the top and lateral boundaries of the domain. Thus, they are modelled as a slip wall characterised by zero normal velocity and zero normal gradients of all variables. At the boundary behind the obstacles, a pressure outlet with zero static pressure is assigned.

The building-related Reynolds number at a height of 25 m (building height) equals 22,078. However, as stated in section 3.1, simulations in reduced scale (1:500) as well as in a full scale are performed in order to compare the velocity distribution in the target area.

### 3.2.2.3 Homogeneity analysis

At first, simulation in an empty domain is performed to investigate the horizontal homogeneity of the vertical mean wind speed and turbulence quantities. The calculated profiles of mean wind



speed, turbulent kinetic energy and turbulence dissipation rate along the vertical lines near building level are illustrated in Figure 3.14.

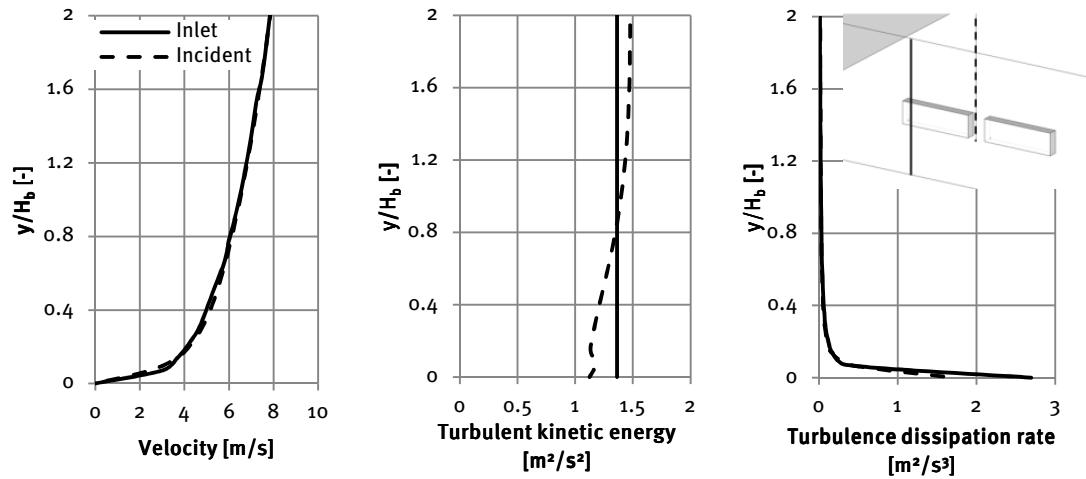


Figure 3.14 – Calculated profiles of mean wind speed, turbulent kinetic energy and turbulence dissipation rate along the vertical lines

As can be seen, there are only limited changes of the profiles near the ground surface. Therefore, the boundary conditions as mentioned before can be applied in the current validation study.

The curvature change of velocity profile at the inlet close to the ground surface occurred because of a steep increase of wind speed within  $0 - 0.1H_b$  determined by a power law. In order to analyse the influence of power law wind distribution, the simulation was performed with a log-law. The obtained wind profiles are illustrated in Figure 3.15. As can be seen, the wind profiles at the inlet and incident position correspond well to each other without the steep change observed with a power-law profile. It must be mentioned that the distribution of wind amplification factor was not changed and contour plots were the same.

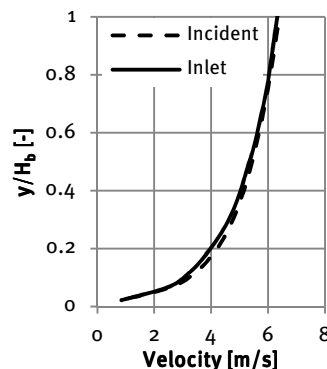


Figure 3.15 – Calculated profiles of mean wind speed described by a log-law

### 3.2.2.4 Grid-sensitivity analysis

A grid-sensitivity analysis for case #2 (Table 3.2) is performed with the following quantities of cells: 839,808 – for coarse configuration; 2,185,000 – for medium configuration; 5,391,982 – for fine configuration (Figure 3.16). According to the requirements of  $k_s = 9.793y_0/C_s$  and  $y_p > k_s$

stated in section 2.4.5,  $C_S = 7$ ,  $k_S = 0.545$  m and the first cell height varies between 0.7 – 1.4 m for the three configurations applied in the grid-sensitivity analysis.

It must be mentioned, that due to the relatively small building depth of 10 m the applied grid resolution within the passage depth is 6, 8 and 10 cells per edge for the coarse, medium and fine grid configurations, respectively.

The results of the simulations on the three different grids are compared on the lines at the passage entrance plane and are depicted in Figure 3.17. As indicated, the results obtained with the medium grid configuration provide a closer agreement with the fine configuration regarding the calculated values for mean wind speed, turbulent kinetic energy and turbulence dissipation rate. However, the fine grid is chosen for the current validation study since it fulfils the requirement of at least 10 cells per edge

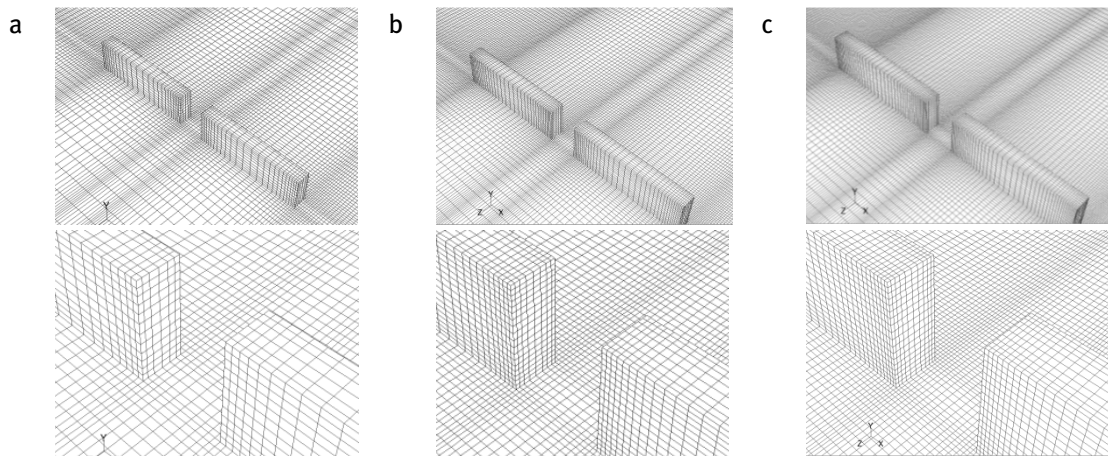


Figure 3.16 – Mesh configurations for grid-sensitivity analysis: a) coarse; b) medium; c) fine

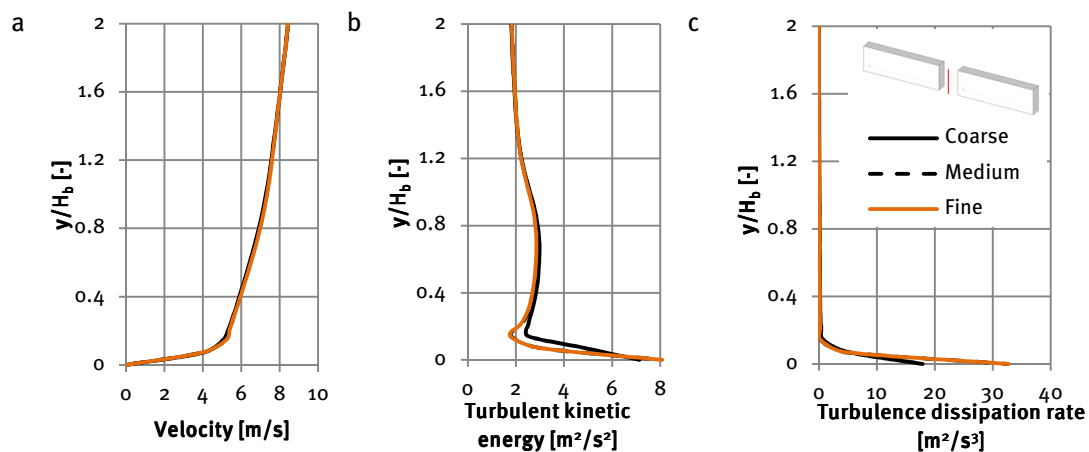


Figure 3.17 – Grid-sensitivity analysis on a passage entrance line: a) velocity; b) turbulent kinetic energy; c) turbulence dissipation rate

### 3.2.2.5 Full-scale simulation

A full-scale simulation was performed for validation case #2 with a fine grid configuration. The analysis has been performed on the vertical line at the entrance and at the end of the passage (Figure 3.18).

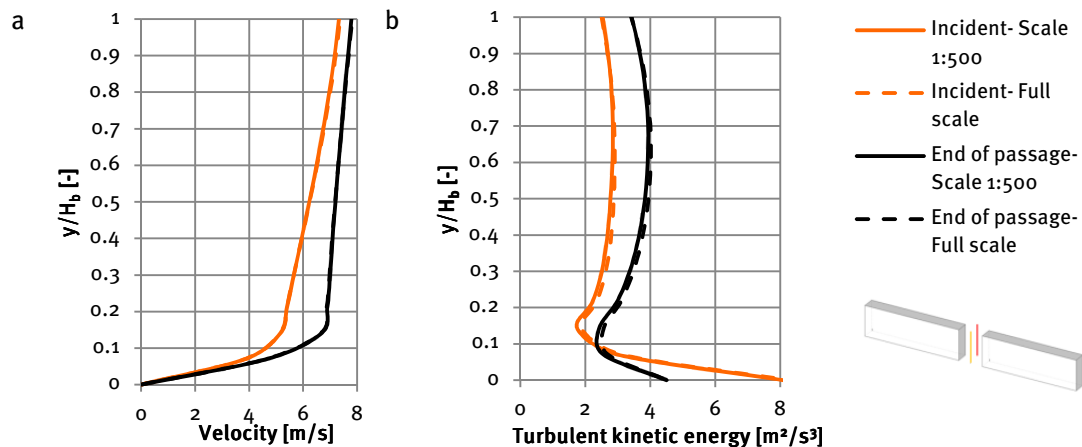


Figure 3.18 – Comparison of computed values between scaled and full-scale model: a) velocity; b) turbulent kinetic energy

As shown in Figure 3.18, the differences between the values of the mean velocity and turbulent kinetic energy are very limited. Therefore, reduced-scaled numerical modelling provides a sufficient degree of Reynolds number independency.

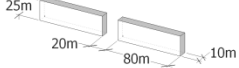
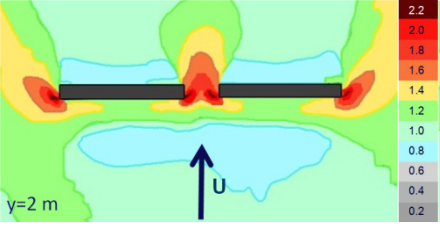
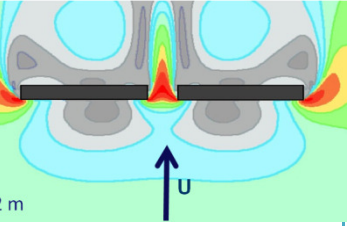
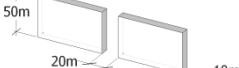
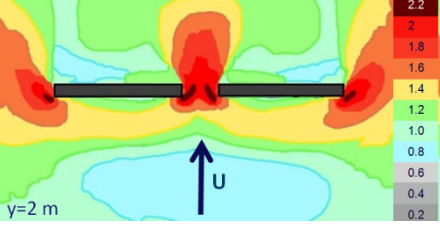
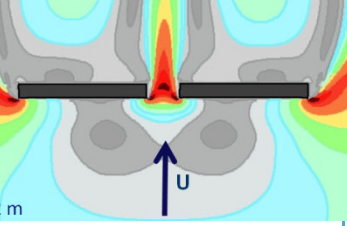
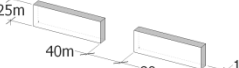
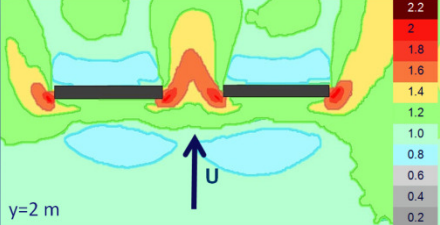
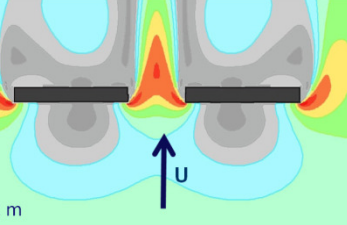

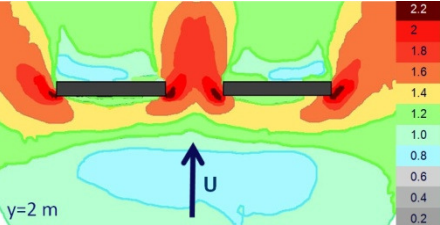
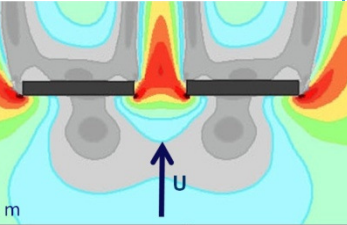
### 3.2.3 Results

The comparison between the results obtained by sand erosion experiments and CFD simulations is performed within the current validation study and is demonstrated in Table 3.3. The data provides contour plots of wind speed amplification factors at the pedestrian level height equal to 2 m.

The plots show a fair to good agreement with each other, especially in the target area within a passage.

However, there are observed differences between the sand erosion experiments and the performed CFD simulations concerning the estimation of the recirculation zone and velocities around the building corners (Figure 3.19). They might be explained by turbulence present in the flow which promotes an earlier particle motion and increases the transport. The observed initial patterns are therefore related to some measure of the instantaneous, rather than only the mean wind speed and provide a measure of both the mean and the turbulent flow field (Livesey et al., 1990; Conan et al., 2012). Moreover, sand erosion tests are carried out by changing the wind speed in the wind tunnel in discrete intervals, the size of which determines the resolution of the scour observations. Different shapes, densities and particle sizes of materials may give different results for comparisons with wind speeds measured with hot wires (Livesey et al., 1992). In regions with high turbulence levels, the sand erodes earlier for a lower mean friction-velocity due to large fluctuations around the mean that are higher than the threshold friction-velocity of the sand. Sand erosion experiments are thus overestimating the mean velocity in regions with high turbulence intensity (Conan et al., 2012).

Table 3.3 – Amplification factor plots for reference and validation studies

Case	Experiments Beranek & Van Koten (1982)	CFD Simulation
<p><b>#2</b></p> 		
<p><b>#3</b></p> 		
<p><b>#4</b></p> 		
<p><b>#5</b></p> 		

In order to evaluate the effect of turbulence on the wind amplification factor a simulation for one of the validation cases was performed with a lower turbulent kinetic energy profile  $k = 1.5u^{*2}$ . The plots presented in Figure 3.19c reveal only a light underestimation of a standing vortex in the upstream region compared to the case with higher turbulent kinetic energy (Figure 3.19b). Therefore, it can be concluded that slight discrepancies revealed in the front of the buildings between the results obtained by sand erosion experiments of Beranek & van Koten (1982) and the CFD simulations (Table 3.3) are caused by earlier sand particle motions due to the turbulence in the flow.

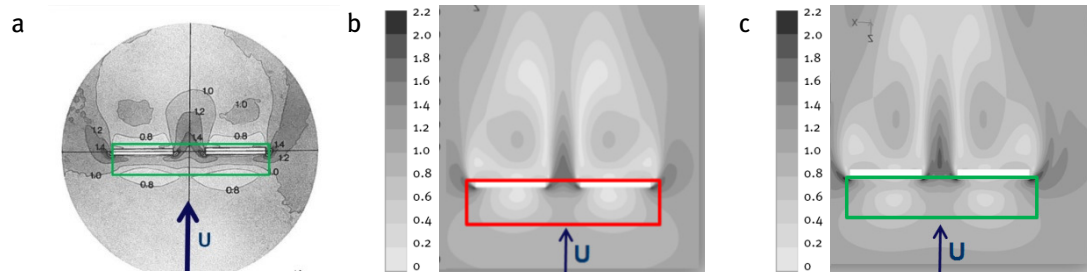


Figure 3.19 – Wind speed amplification factors at pedestrian level height determined by: a) experiments (Beranek & Van Koten, 1982); b) CFD simulation,  $k = 3.33u^*$ ; c) CFD simulation,  $k = 1.5u^*$

## Summary

The current Chapter provides the results of the validation study conducted in order to validate the chosen computational model. The results confirm the acceptable compliance between the results extracted from previous studies and performed CFD simulations. Therefore, the turbulence model and the boundary conditions for the parametric study are chosen according to the computational parameters of the validation study. The parametric study conducted by means of CFD in order to investigate the influence of building geometries on the wind speed distribution within the building passages as well as the computational parameters are described in the following Chapter.

## 4 Parametric study

The Chapter describes the parametric study that was performed in order to investigate the influence of geometrical parameters of the building on the wind speed distribution in the middle of the passage between two buildings. The parametric study was conducted by means of CFD.

### 4.1 Study outline

#### 4.1.1 Studied configurations

The proposed set-up represents two parallel rectangular building blocks. The variable parameters of the building blocks intended for detailed analysis of the wind performance are assigned as follows (Figure 4.1):

- Height of the building,  $H$ ;
- Length of the building,  $L$ ;
- Depth of the building,  $D$ ;
- Width of the passage,  $w$ .

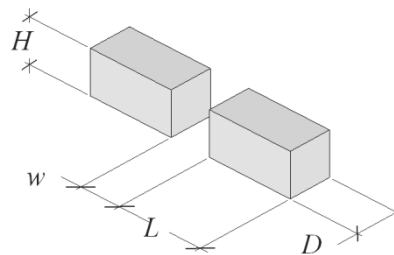


Figure 4.1 – Geometry overview

In order to categorise the buildings and arrange the data the building influence scale factor  $S$  is used which is defined by Wilson et al. (1989):

$$S = (B_L B_S^2)^{\frac{1}{3}} \quad (4.1),$$

where  $B_L$  is the larger and  $B_S$  is the smaller dimension of the windward facade.

Furthermore, the ratio  $w/S$  is considered which was mentioned by Stathopoulos et al. (1992) in their study on pedestrian wind comfort.

All studied configurations are presented in Table 4.1. It must be mentioned that configurations within the range of  $0.125 \leq w/S < 1.25$  were chosen as they are defined to be advantageous in terms of wind amplification factor (Blocken et al., 2007b).

Table 4.1 – Configuration overview

L [m]	H [m]	D [m]	w [m]	S [m]	w/S [-]
45	60	30	20	49.53	0.40
		45	40	49.53	0.81
		60	60	49.53	1.21
	90	30	20	56.70	0.35
		45	40	56.70	0.71
		60	60	56.70	1.06
	120	30	20	62.40	0.32
		45	40	62.40	0.64
		60	60	62.40	0.96
70	60	30	20	63.16	0.32
		45	40	63.16	0.63
		60	60	63.16	0.95
	90	30	20	76.12	0.26
		45	40	76.12	0.53
		60	60	76.12	0.79
	120	30	20	83.78	0.24
		45	40	83.78	0.48
		60	60	83.78	0.72

#### 4.1.2 Numerical simulation parameters

The parametric study was conducted by means of CFD, using pre-processor Gambit 2.4.6 and commercial code ANSYS Fluent 12.1 (ANSYS, Inc., 2009). Note that, from this point on, all the dimensions and values in this section are reported in a full scale.

##### 4.1.2.1 Computational geometry and grid

The domain extensions for all studied configurations are defined according to the recommendations stated in section 2.4.4. The domain dimensions are varied depending on the building configuration within  $L \times D \times H = [710 - 1400] \text{ m} \times [1230 - 2460] \text{ m} \times [360 - 720] \text{ m}$ . Simulations were performed in a scale of 1:500.

High-resolution structured computational grids providing at least 10 cells between adjacent surfaces were generated according to the recommendations stated in section 2.4.6. The number of cells for every configuration lies between about 0.2 and 2.7 million cells. A high-resolution mesh is applied in the target area – i.e. in the passage between two buildings (Figure 4.2). A detailed grid-sensitivity analysis has been performed on the building configuration  $L \times H \times D = 45 \text{ m} \times 90 \text{ m} \times 45 \text{ m}$  with a passage width of 20 m. The configuration with the narrowest passage width is chosen due to higher velocity gradients expected within the passage in comparison to the gradients within passages with larger widths.

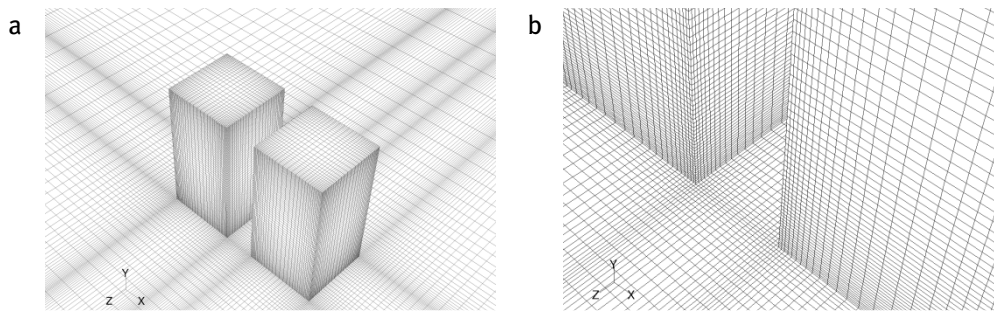


Figure 4.2 – Computational grid for configuration  $L \times H \times D = 45 \text{ m} \times 90 \text{ m} \times 45 \text{ m}$ : a) Overview of the buildings; b) Passage view

#### 4.1.2.2 Boundary conditions

At the inlet of the domain a mean speed profile defined by the log-law is imposed. In order to investigate the influence of the surface roughness of the terrain on the wind speed distribution two aerodynamic roughness lengths were studied:  $y_0 = 0.03 \text{ m}$  and  $y_0 = 1 \text{ m}$ . Turbulent kinetic energy  $k$  is calculated using the relation  $k = 3.33(u^*)^2$ , the turbulence dissipation rate  $\varepsilon = (u^*)^3 / \kappa(y + y_0)$ . Figure 4.3 shows profiles of approach-flow mean wind speed, turbulent kinetic energy and turbulence dissipation rate along the height of the domain imposed at the inlet for different values of  $y_0$ . The wind direction at this stage is chosen to be parallel to the passage.

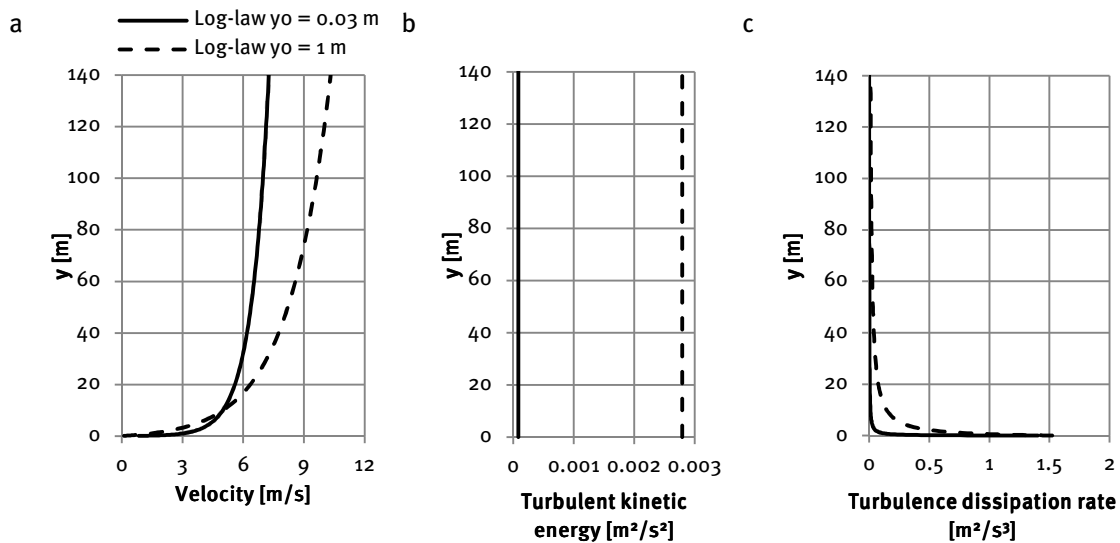


Figure 4.3 – Profiles imposed at the inlet for  $y_0 = 0.03 \text{ m}$ ;  $y_0 = 1 \text{ m}$ : a) velocity; b) turbulent kinetic energy; c) turbulence dissipation rate

Regarding the requirements stated in section 2.4.5 the combinations  $C_s = 7$ ,  $k_s = 0.042 \text{ m}$  and  $C_s = 7$ ,  $k_s = 1.4 \text{ m}$  are selected for  $y_0 = 0.03 \text{ m}$  and  $y_0 = 1 \text{ m}$ , respectively. The building surfaces are assumed to be smooth  $C_s = 0.5$ ,  $k_s = 0 \text{ m}$ . Zero static pressure is imposed at the outlet of the domain and the top of the domain is modelled as a slip wall (zero normal velocity and zero normal gradients of all variables).

In order to investigate the influence of wind direction on the wind speed distribution within a passage, one additional wind direction angle of  $30^\circ$  is studied for several configurations. This auxiliary study is performed for the aerodynamic roughness length  $y_0 = 1 \text{ m}$  due to the coarser grid configuration which saves computation time.



#### 4.1.2.3 Solver settings

The 3D steady RANS equations are solved in combination with the realisable  $k - \varepsilon$  turbulence model (Shih et al., 1995). Pressure-velocity coupling is solved by the SIMPLE algorithm, pressure interpolation is standard and second-order discretisation schemes are used for both the convection terms and the viscous terms of the governing equations. Iterations have been terminated when all scaled residuals showed no further reduction for at least 1000 iterations meaning that the solution has been converged. The scaled residuals were:  $10^{-5}$  for continuity,  $10^{-7}$  for velocities,  $10^{-7}$  for turbulent kinetic energy and  $10^{-5}$  for turbulent dissipation rate.

#### 4.1.2.4 Grid-sensitivity analysis

A grid-sensitivity analysis is performed for the case with dimensions  $L \times H \times D = 45 \text{ m} \times 90 \text{ m} \times 45 \text{ m}$  with a passage width of 20 m (Figure 4.4). Three configurations varying by an overall linear factor of  $\sqrt{2}$  are considered with the following quantities of cells for  $y_0 = 0.03 \text{ m}$ : 708,540 – for coarse configuration; 2,526,000 – for medium configuration; 5,427,840 – for fine configuration. The amount of cells for  $y_0 = 1 \text{ m}$  for coarse, medium and fine configurations equals to 193,956; 544,760; 1,070,888, respectively. The first cell height varies within 0.20 – 0.40 m and 1.45 – 2.25 m for  $y_0 = 0.03 \text{ m}$  and  $y_0 = 1 \text{ m}$ , respectively.

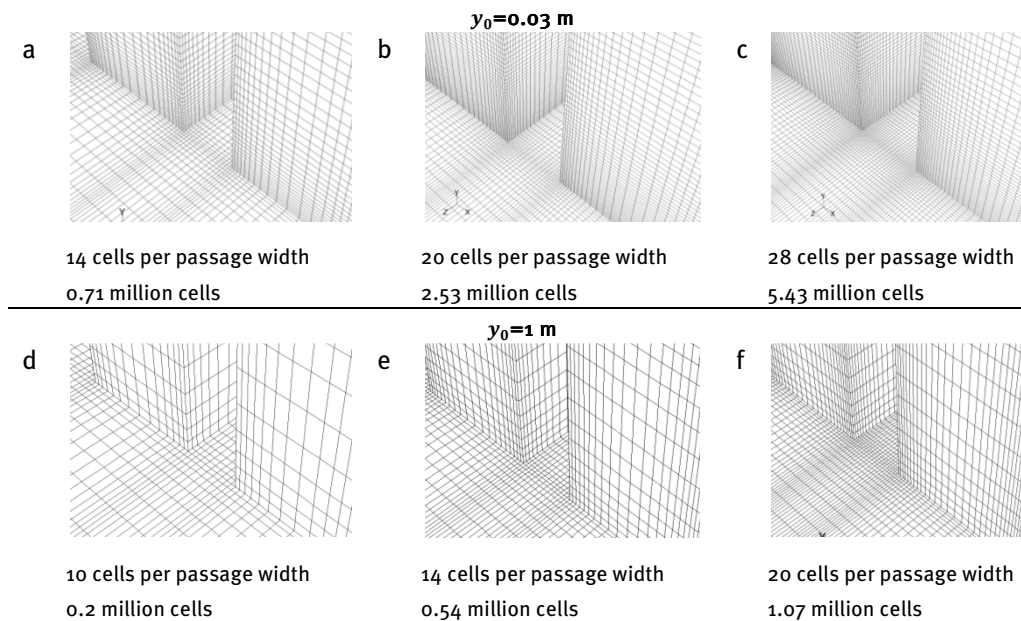


Figure 4.4 – Mesh configurations for grid-sensitivity analysis:  $y_0 = 0.03 \text{ m}$  a) coarse; b) medium; c) fine;  $y_0 = 1 \text{ m}$  d) coarse; e) medium; f) fine

The vertical lines for the grid-sensitivity analysis are taken at the passage entrance plane and are depicted in Figure 4.5. As indicated, the medium and fine grid configurations provide a close agreement between each other regarding the calculated values for mean wind speed, turbulent kinetic energy and turbulence dissipation rate for the two aerodynamic roughness lengths. The medium grid configuration is chosen for both cases. The grid resolution for larger passage widths is determined by providing a minimum of 20 cells per passage width and keeping the stretching/compression ratios between adjacent cells below 1.3. The second requirement is followed to define the amount of cells for the building edges.

#### 4.1.2.5 Area of interest

As stated before, the wind performance within a passage is the primary interest of the current project. To be more specific, the wind amplification due to the contraction of the flow area caused by the presence of the buildings should be evaluated.

The wind amplification through central vertical cross-section of the passage (Figure 4.6) is analysed in order to estimate the location of the maximum amplification point for all of the studied configurations. This wind amplification is quantified by means of the wind amplification factor which has two different definitions within the framework of the current study (Table 4.2).

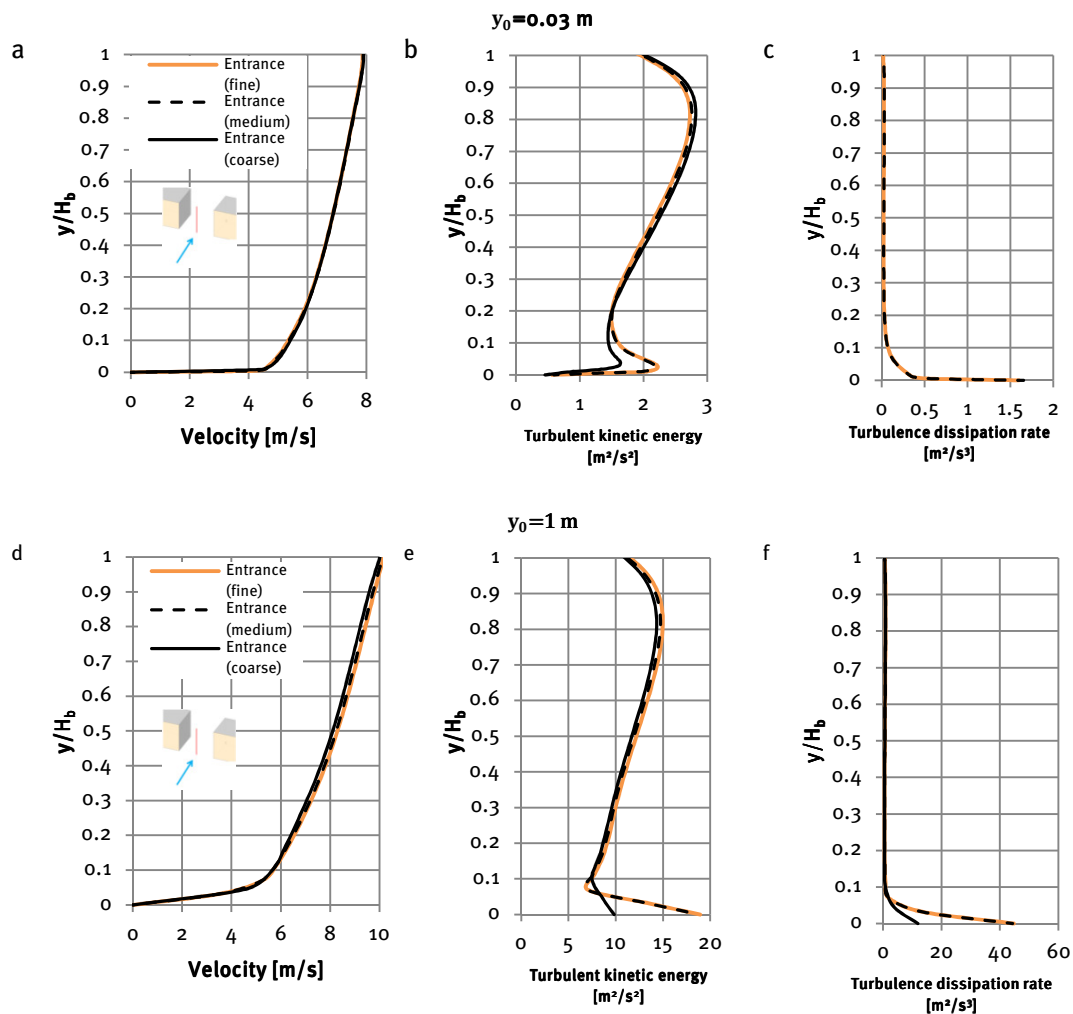


Figure 4.5 – Grid-sensitivity analysis on a passage entrance line: a, d) velocity; b, e) turbulent kinetic energy; c, f) turbulence dissipation rate

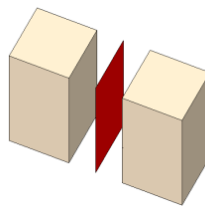


Figure 4.6 – Indication of the plain for wind performance analysis

Table 4.2 – Wind amplification factors

Wind amplification factor	Explanation
$K = \frac{U_{\max}}{U_0}$	$U_{\max}$ – maximum wind speed occurred within a passage centre plane at any height; $U_0$ – incident wind speed with no buildings present at the height of observed $U_{\max}$
$K_{60} = \frac{U_{\max}}{U_{60}}$	$U_{\max}$ – maximum wind speed occurred within a passage centre plane at any height; $U_0$ – incident wind speed with no buildings present at the height equal to 60 m

The analysis of wind amplification factors has been performed on vertical and horizontal lines through the vertical centre plane of the passage and using contour plots.

## 4.2 Calculation results

This section describes the distribution of the two amplification factors as defined in Table 4.2 depending on different building geometries and roughness conditions of the terrain. The values of wind amplification factors  $K$ ,  $K_{60}$  are calculated based on the results obtained by the CFD simulations. The results for all the building configurations and both aerodynamic roughness lengths for two wind directions are depicted in graphs below.

### 4.2.1 Wind amplification factor $K$

Figure 4.7 illustrates the values of  $K = \frac{U_{\max}}{U_0}$  as a function of  $w/S$  for different building geometries through the vertical centre plane of the passage. The values are sorted by two aerodynamic roughness lengths of the terrain. The values of  $K$  range within 1.123 – 1.3 for  $y_0 = 0.03$  m and 1.05 – 1.3 for  $y_0 = 1$  m. The deviation of the amplification factors for the buildings with the same value of  $w/S$  reaches 5%. However, it is possible to define a characteristic curve describing the distribution. The values of  $K$  reach their maximum around  $w/S = 0.32$  for  $y_0 = 0.03$  m and around  $w/S = 0.64$  for  $y_0 = 1$  m.

The influence of roughness conditions on the amplification factor is discussed in section 4.2.4.

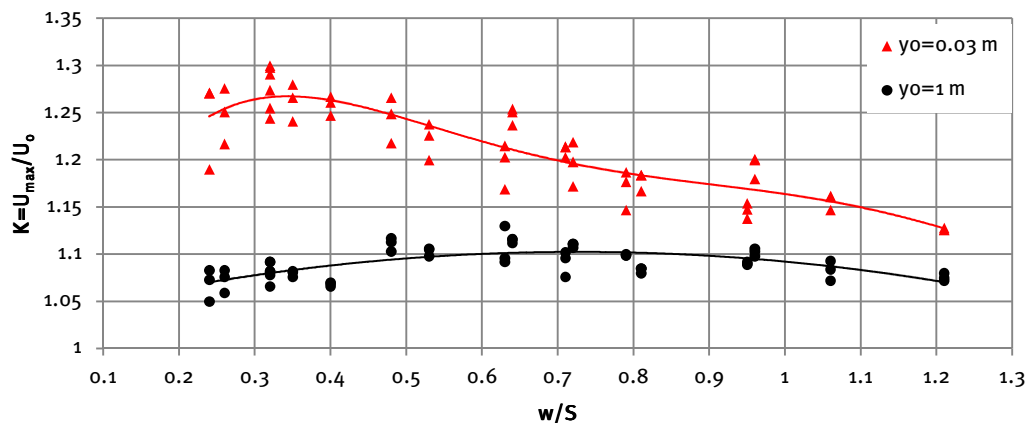


Figure 4.7 – Overview of calculated amplification factors  $K$

In order to reveal more robust relations, a comparison is conducted regarding one parameter at a time:

- Height of the building,  $H$ ;
- Length of the building,  $L$ ;
- Depth of the building,  $D$ ;
- Width of the passage,  $w$ .

#### 4.2.1.1 Influence of the building height $H$

The values of the amplification factors  $K$  as a function of  $w/S$  sorted by building heights are presented in Figure 4.8, while Figure 3.9 illustrates distribution of  $K$  as a function of the building height.

Concerning the results obtained for the aerodynamic roughness length  $y_0 = 1$  m, the maximum values of amplification factor  $K$  have a tendency, in general, to occur for the higher building height  $H = 120$  m. Regarding the results with  $y_0 = 0.03$  m, the buildings with  $H = 120$  m demonstrate the highest values of  $K$  within  $0.25 < w/S < 0.6$  and the buildings with  $H = 60$  m in general have lower values of  $K$  compared to the ones with  $H = 90$  m,  $120$  m. This difference is more pronounced for  $w/S > 0.5$ . However, distinct trendlines of the amplification factors for this roughness length defined for  $H = 90$  m,  $120$  m can barely be determined.

It can be concluded, that in contrast to the effect on the wind speed distribution, there is no strongly pronounced influence of the single building heights on the amplification factor  $K$ .

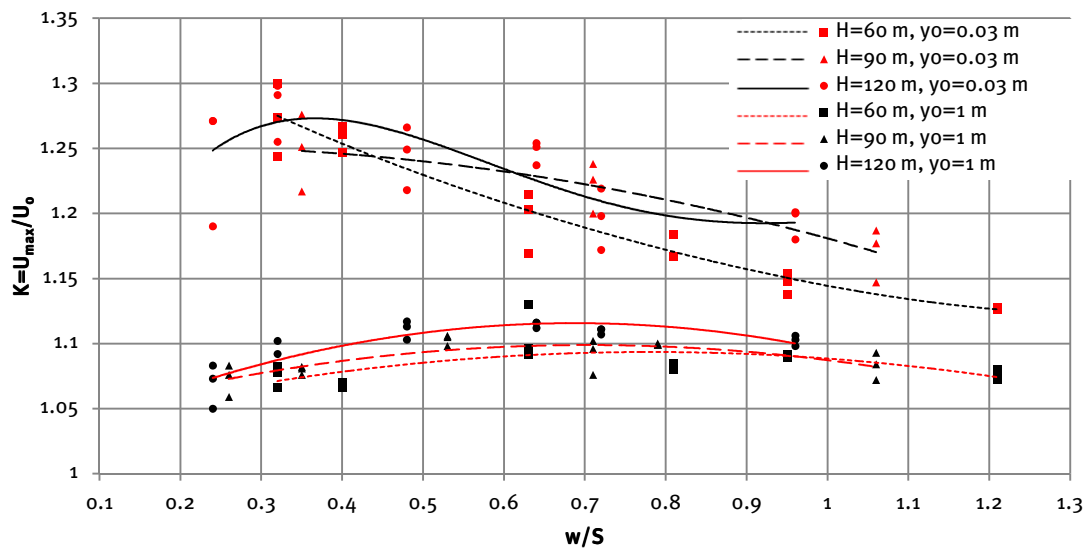


Figure 4.8 – Dependency of amplification factor  $K$  on the ratio  $w/S$  sorted by building heights

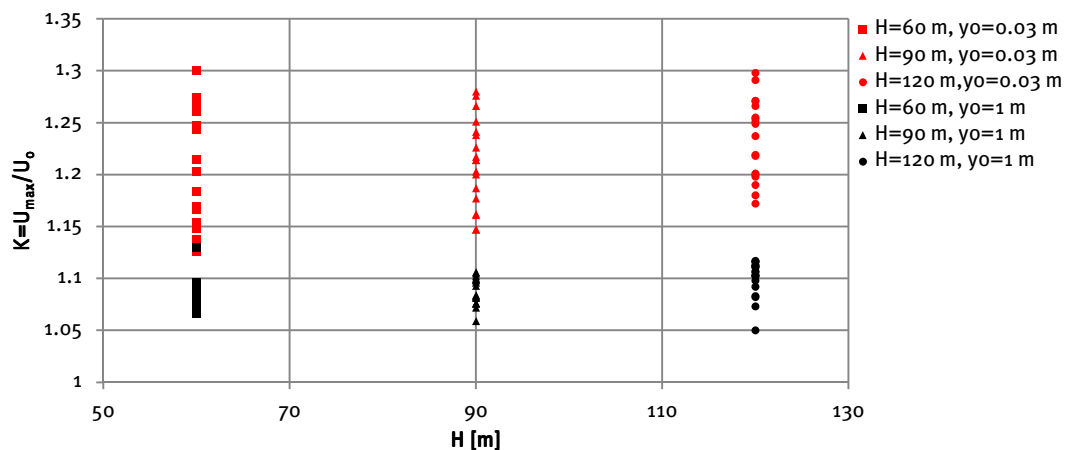


Figure 4.9 – Dependency of amplification factor  $K$  on the building height  $H$

#### 4.2.1.2 Influence of the building length $L$

The values of the amplification factors  $K$  as a function of  $w/S$  sorted by building lengths are presented in Figure 4.10. The single dependency of  $K$  on the building length is depicted in Figure 4.11.

The amplification factors  $K$  defined for  $y_0 = 0.03$  m with a ratio  $w/S > 1$  have the tendency to be higher for the buildings with  $L = 45$  m than the ones with  $L = 70$  m. The distribution of values of  $K$  for  $y_0 = 1$  m demonstrate no dependencies on building length  $L$ .

As can be seen from Figure 4.11, the values of  $K$  defined for the same aerodynamic roughness lengths are within the similar range. Therefore, it is hardly possible to draw any conclusion about the single dependency of the wind amplification factor on the building length.

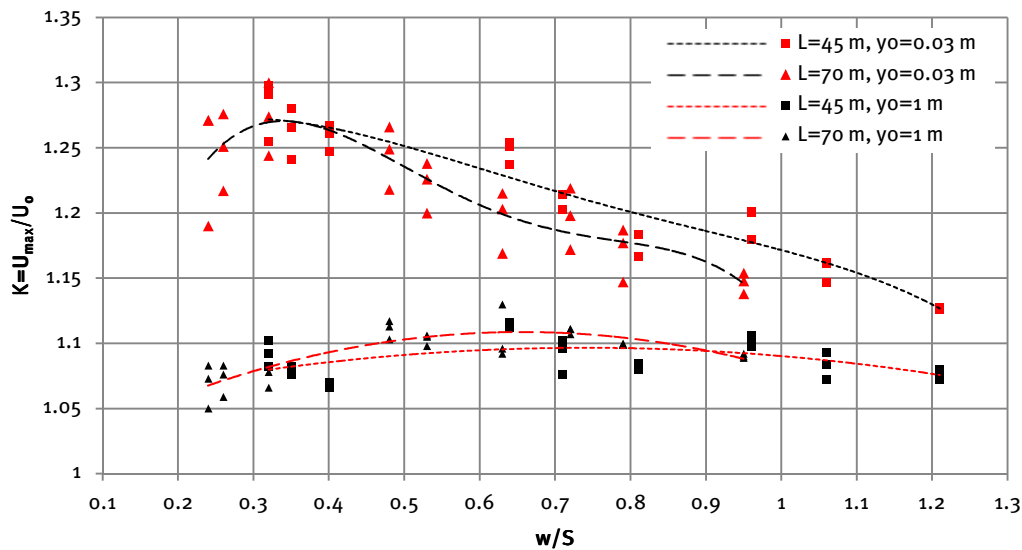


Figure 4.10 – Dependency of amplification factor  $K$  on the ratio  $w/S$  sorted by building lengths

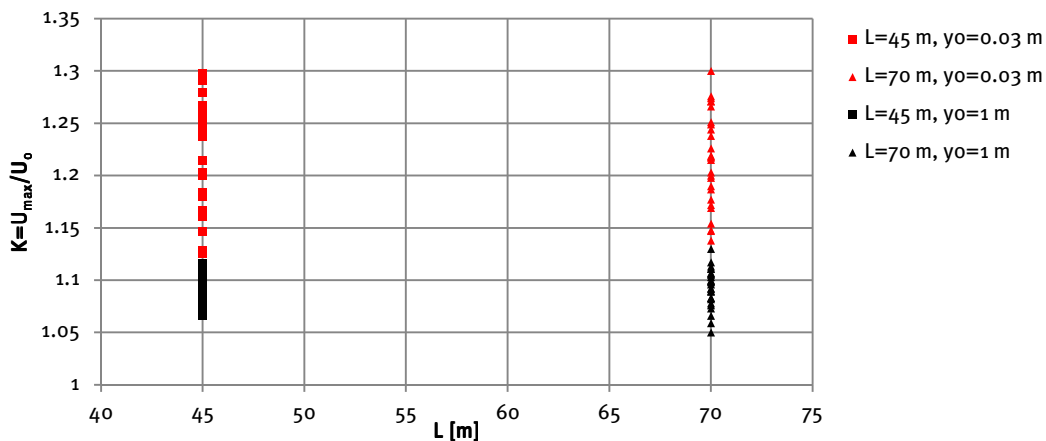


Figure 4.11 – Dependency of amplification factor  $K$  on the building length  $L$

#### 4.2.1.3 Influence of the building depth $D$

The values of the amplification factor sorted by the building depths are presented in Figure 4.12, while Figure 3.13 illustrates distribution of  $K$  as a function of the building depth.

Regarding  $y_0 = 0.03$  m, it can be concluded that buildings with depths  $D = 45$  m,  $60$  m are, in general, more beneficial than the ones with  $D = 30$  m. It must be mentioned, that the amplification factors defined for the buildings with  $D = 60$  m just slightly exceed the values

defined for the buildings with  $D = 45$  m (Figure 4.12). Again, no clear dependencies can be distinguished for  $y_0 = 1$  m.

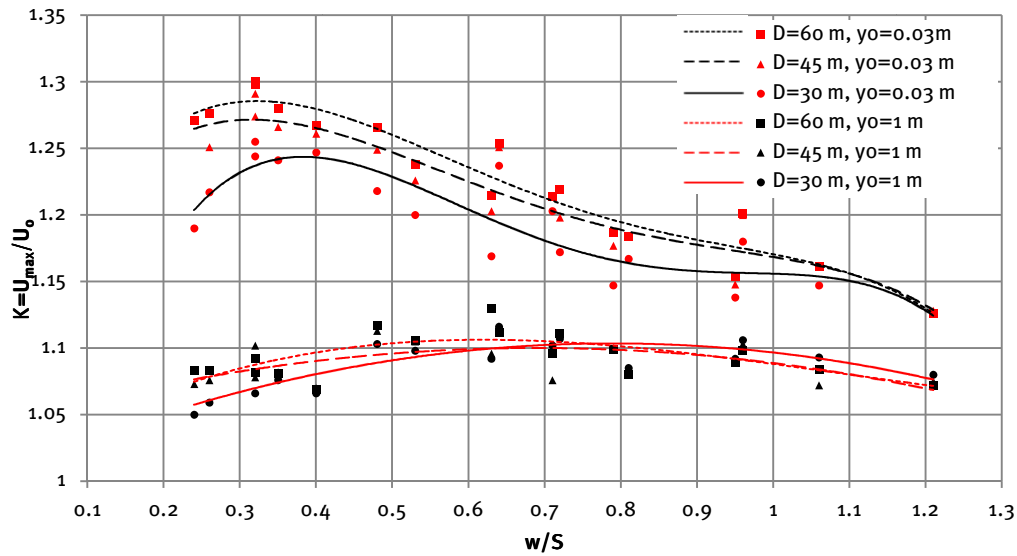


Figure 4.12 – Dependency of amplification factor  $K$  on the ratio  $w/S$  sorted by building depths

Figure 4.13 indicates a slight increment of amplification factors with increasing building depths, especially for  $y_0 = 0.03$  m. Thus, it can be suggested that passages with larger depths are more advantageous in terms of wind amplification.

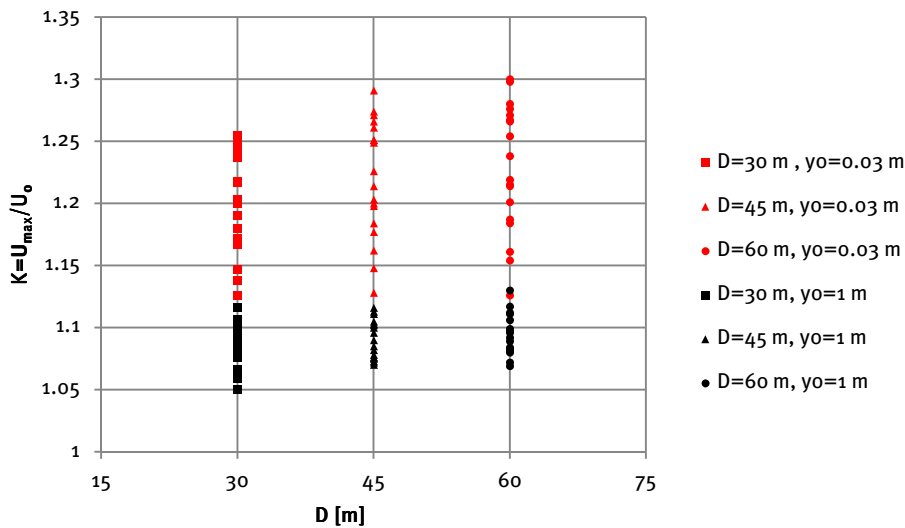


Figure 4.13 – Dependency of amplification factor  $K$  on the building depth  $D$

#### 4.2.1.4 Influence of the passage width $w$

The values of the amplification factors sorted by passage widths are presented in Figure 4.14 and the values of the amplification factors as a function of the width of the passage are presented in Figure 4.15.

It appears that for  $y_0 = 0.03$  m a narrow passage width of  $w = 20$  m is more advantageous than a width of  $w = 60$  m in terms of the flow amplification. As for  $y_0 = 1$  m, the maximum amplification factors are occurred for larger passage width  $w = 40$  m and  $w = 60$  m.

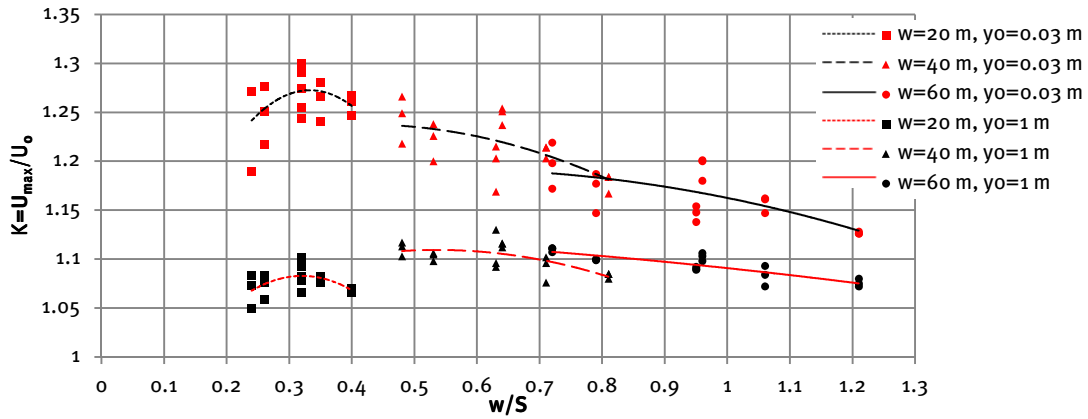


Figure 4.14 – Dependency of amplification factor  $K$  on the ratio  $w/S$  sorted by passage widths

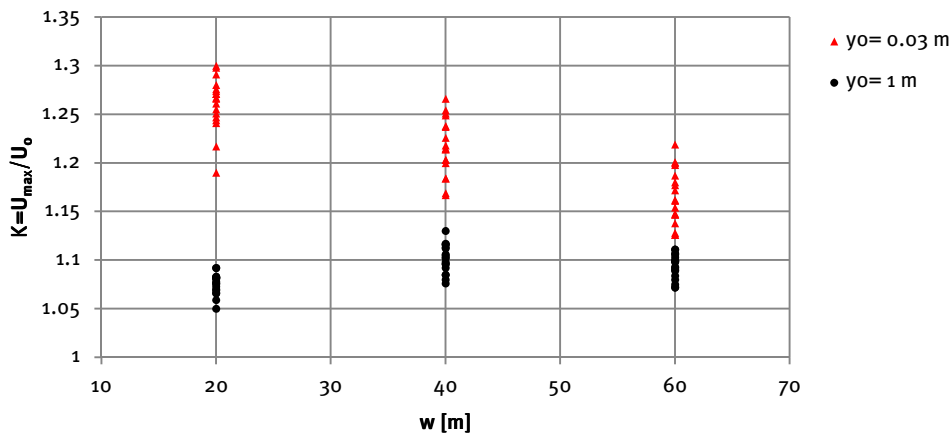


Figure 4.15 – Dependency of amplification factor  $K$  on the passage width  $w$

#### 4.2.2 Analysis of amplification factor $K$ on a certain building geometry

The following building geometries were chosen in order to demonstrate the influence of one parameter at a time on the amplification factor (Table 4.3).

Table 4.3 – Building configurations

Variable parameter	H [m]	L [m]	D [m]	w [m]
Building height, H	60; 90; 120	45	60	20
Building length, L	120	45; 70	60	20
Building depth, D	120	45	30; 45; 60	20
Passage width, w	120	45	60	20; 40; 60

The results of this comparison are presented in Figure 4.16.



The following observations can be highlighted for the considered geometries:

- Amplification factor  $K$  is increasing by increasing the building height  $H$  for both aerodynamic roughness lengths;
- Amplification factor  $K$  is decreasing by increasing the building lengths  $L$  for the both aerodynamic roughness lengths;
- Amplification factor  $K$  is increasing by increasing the building depth  $D$  for the aerodynamic roughness length  $y_0 = 0.03$  m, while for  $y_0 = 1$  m the dependency is ambiguous with a maximum amplification factor  $K$  revealed for the building with  $D = 45$  m;
- Amplification factor  $K$  is decreasing by increasing the passage width  $w$  for the aerodynamic roughness length  $y_0 = 0.03$  m, while for  $y_0 = 1$  m the dependency is ambiguous with a maximum amplification factor  $K$  revealed for the building with  $w = 40$  m.

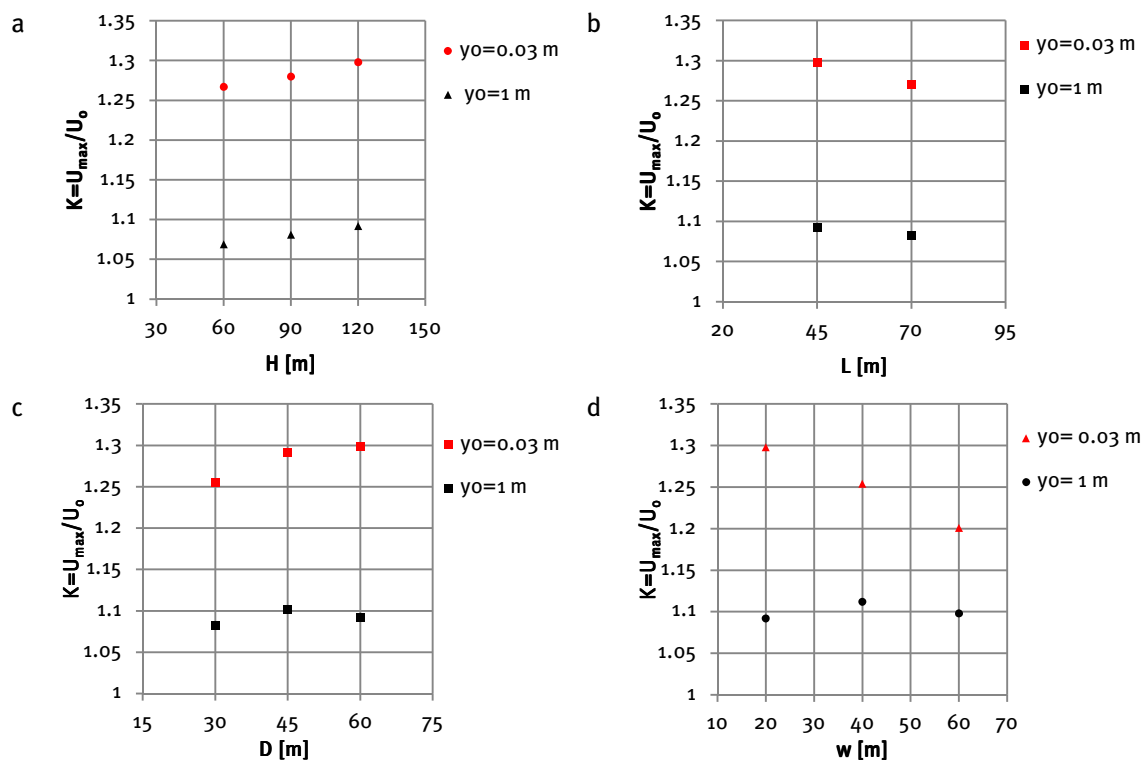


Figure 4.16 – Dependency of amplification factor  $K$  on: a) the building height; b) the building length; c) the building depth; d) the passage width

### 4.2.3 Amplification factor $K_{60}$

The graph for  $K_{60} = \frac{U_{\max}}{U_{60}}$  demonstrates a chaotic distribution of the amplification factor  $K_{60}$  along  $w/S$  (Figure 4.17). Therefore, barely any dependencies can be described. However, the values of  $K_{60}$  will be applied during the estimation of wind energy potential.

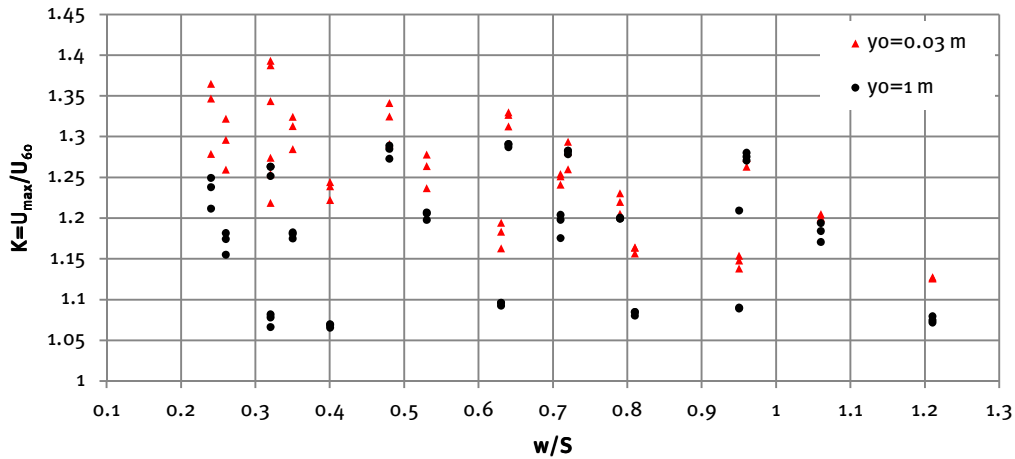


Figure 4.17 – Overview of calculated amplification factors  $K_{60}$

#### 4.2.4 Influence of terrain roughness

The values of  $K$  presented in section 4.2.1 demonstrate a significant difference between wind amplification factor distributions for different aerodynamic roughness lengths. The values for  $y_0 = 0.03$  m generally exceed the values defined for  $y_0 = 1$  m.

To examine this occurrence, a number of contour and vector plots were analysed for the case  $L \times H \times D = 45$  m  $\times$  120 m  $\times$  60 m with a passage width of 60 m which are presented in Figure 4.18. It can be seen, that the difference between velocities within the passage and around a building corner for  $y_0 = 0.03$  m is more pronounced in contrast to the case with  $y_0 = 1$  m. The higher velocities for  $y_0 = 1$  m in comparison to  $y_0 = 0.03$  m are caused by higher gradients of wind speed along the height determined by a log-law distribution (Figure 4.19).

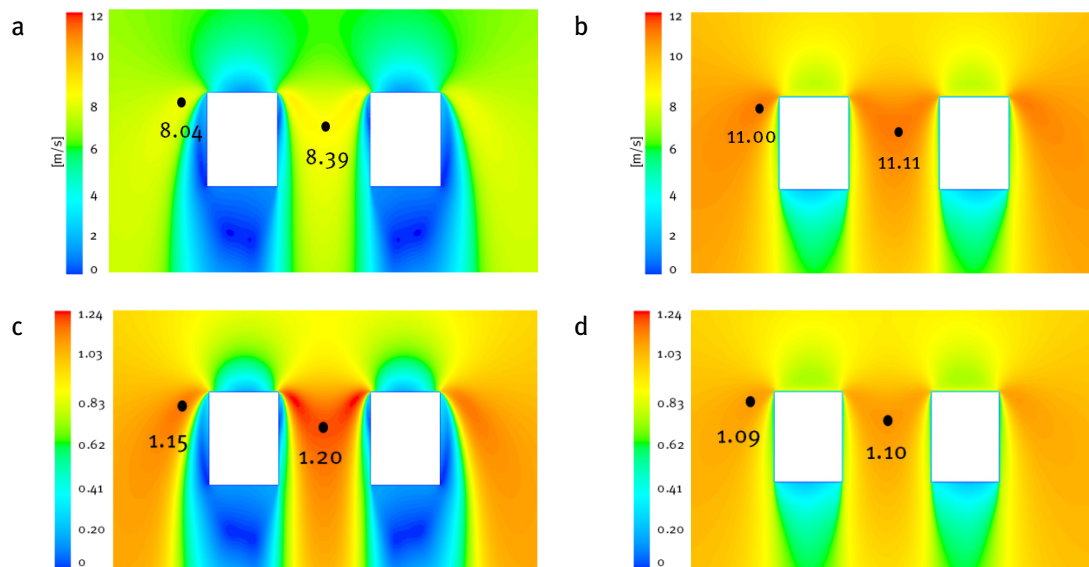


Figure 4.18 – (a, b) Velocity contour plots at the determined height of the maximum wind speed, top view: a)  $y_0 = 0.03$  m ( $H = 97$  m); b)  $y_0 = 1$  m ( $H = 120$  m); (c, d) Velocity amplification factors  $K = \frac{U_{\max}}{U_0}$  at the height of the maximum wind speed, top view: c)  $y_0 = 0.03$  m ( $H = 97$  m); d)  $y_0 = 1$  m ( $H = 120$  m)

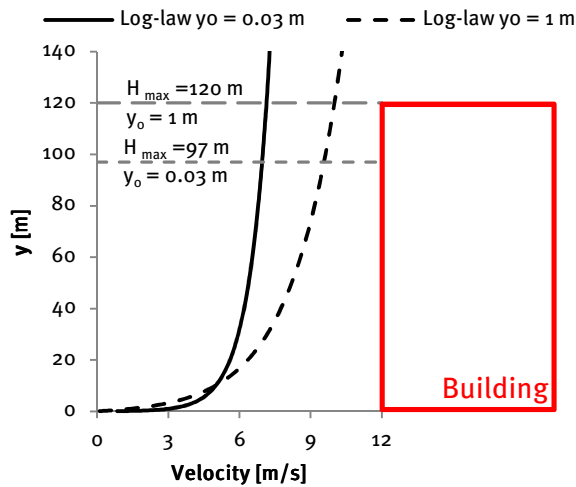


Figure 4.19 – Velocity distribution for  $y_0 = 0.03$  m and  $y_0 = 1$  m with indication of heights of maximum wind speed in the passage

The direction of velocity vectors has been analysed at the vertical centre passage plane for the both cases and no any difference, except the values of wind speed, has been observed. The distribution of velocity vectors is depicted in Figure 4.20.

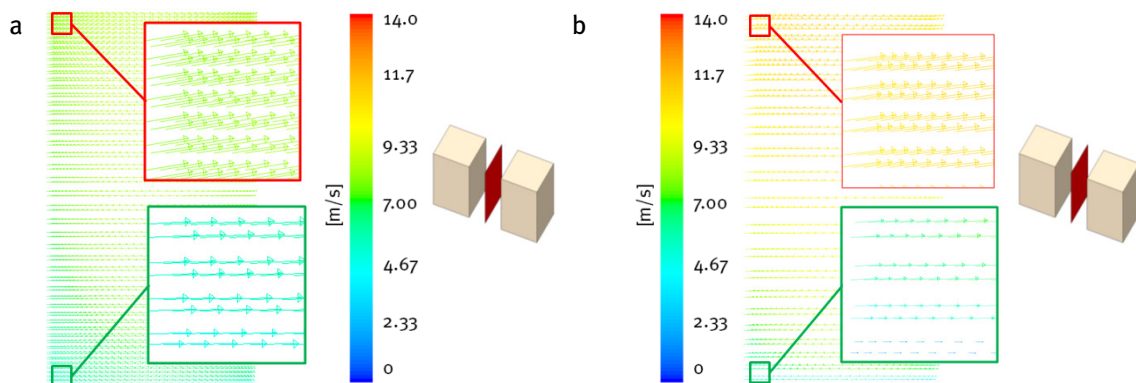


Figure 4.20 – Velocity vectors through the vertical centre passage plane: a)  $y_0 = 0.03$  m; b)  $y_0 = 1$  m

Furthermore, the pressure distribution on the windward facades has been examined (Figure 4.21). In addition to higher pressure values for  $y_0 = 1$  m due to higher wind velocities in comparison to  $y_0 = 0.03$  m, the location of the stagnation point is  $0.8H_b$  and  $0.9H_b$  for  $y_0 = 1$  m and  $y_0 = 0.03$  m, respectively ( $H_b$  – building height).

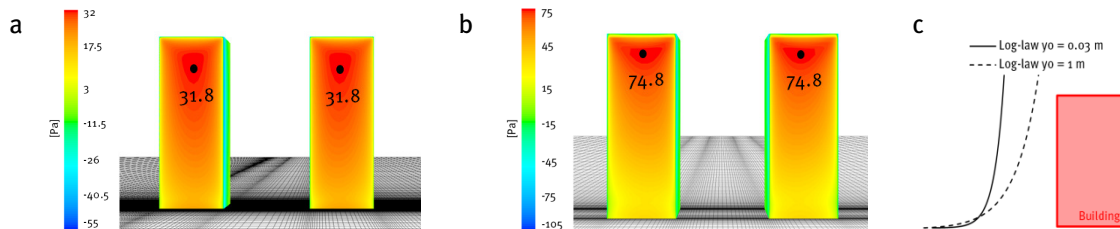


Figure 4.21 – Pressure distribution on the windward facades: a)  $y_0 = 0.03$  m; b)  $y_0 = 1$  m; c) log-law distribution of the wind speed

It can be suggested that lower amplification factors for aerodynamic roughness length  $y_0 = 1$  m are caused by faster development of wind velocity along the height in comparison to  $y_0 = 0.03$  m (Figure 4.19).

Further research is recommended in order to define the influence of aerodynamic roughness length on wind speed distribution.

### 4.2.5 Influence of wind direction

The values of maximum amplification factors  $K$  for 18 cases ( $y_0 = 1 \text{ m}$ ) are calculated at the vertical centre plane of the passage for a wind direction with an incident angle of  $30^\circ$  and are summarised in Figure 4.22. The values of  $K$  are lying in the range of 0.98 – 1.02 meaning minimum effect on the flow amplification.

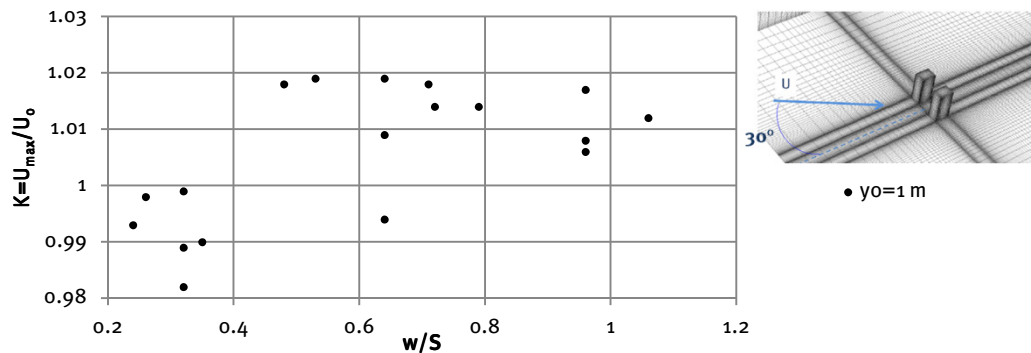


Figure 4.22 – Amplification factors  $K$  calculated for  $30^\circ$  wind direction

Comparing the amplification factors defined for parallel and angular wind directions, it can be concluded that amplification factors are generally decreased by 6% in the second case (Figure 4.23).

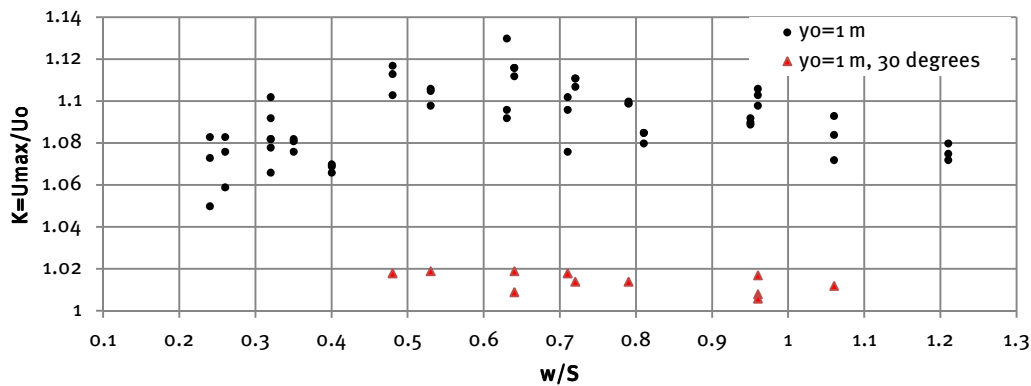


Figure 4.23 – Amplification factors  $K$  calculated for parallel wind direction (black dots) and  $30^\circ$  wind direction

Regarding the dependency of the wind amplification factors on the building parameters for a wind direction with an incident angle of  $30^\circ$ , it can only be revealed for variation of the building depth: amplification factors for  $D = 60 \text{ m}$  are slightly higher than the ones for  $D = 30 \text{ m}$ ,  $45 \text{ m}$  (Figure 4.24).

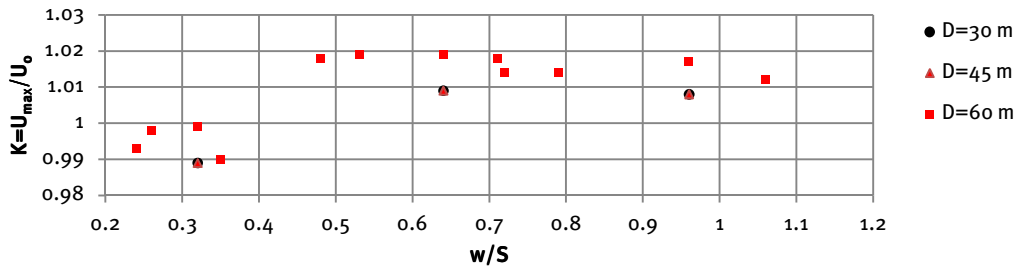


Figure 4.24– Dependency of amplification factor  $K$  on the ratio  $w/S$  sorted by building depths

The wind speed distribution within the passage is analysed for the case  $L \times H \times D = 45 \text{ m} \times 120 \text{ m} \times 60 \text{ m}$  with a passage width of 60 m, which is characterised by high amplification factors. The distribution of the amplification factor  $K = \frac{U_{\max}}{U_0}$  through the frontal and vertical centre planes of the passage as well as through a horizontal cross section at building roof height is described in Figures 4.25, 4.26, where  $U_0$  equals to the incident wind speed at the height of 120 m. The illustrated graphs indicate a considerable impact of wind direction on the velocity distribution within a passage. By inclination of the wind the maximum value of the wind speed at the vertical centre plane of the passage is decreased by approximately 6% and the maximum amplification point drifts away from the centre of the passage. This shift will affect the performance of the building-integrated wind turbine. However, the maximum point remains located within the upstream part of the passage.

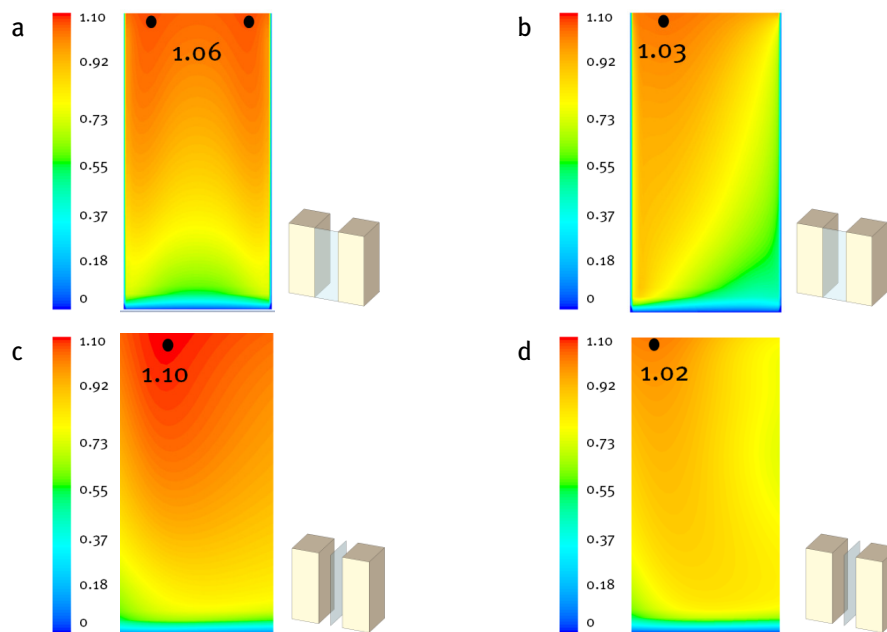


Figure 4.25 – Contour plots of the wind amplification factor  $K = \frac{U_{\max}}{U_0}$  for  $y_0 = 1 \text{ m}$  ( $U_0$  is the incident wind speed at the height of 120 m): (a, c) parallel wind direction: a) frontal plane; c) passage centre plane; (b, d)  $30^\circ$  wind direction: b) frontal plane; d) passage centre plane

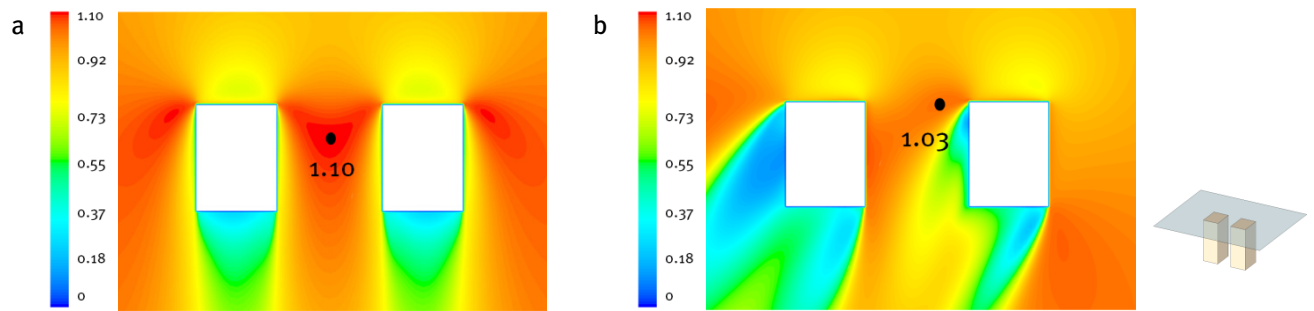


Figure 4.26 – Contour plots of the wind amplification factor  $K = \frac{U_{max}}{U_0}$  through the building top plane for  $y_0 = 1$  m ( $U_0$  is the incident wind speed at the height of 120 m): a) parallel wind direction; b)  $30^\circ$  wind direction

## Summary

This Chapter illustrates the results of the parametric study conducted in order to investigate the influence of building geometries on the wind speed distribution within the building passages. The significant influence of the wind direction and the terrain roughness on wind distribution within the building passages is revealed and analysed. It must be noted, that it is hardly possible to determine clear dependencies of the wind amplification factors on the ratio of the passage width  $w$  to the building influence scale factor  $S$ . However, it can be concluded that the configurations with  $w/S = 0.32$  for  $y_0 = 0.03$  m and around  $w/S = 0.64$  for  $y_0 = 1$  m are the most advantageous in terms of wind amplification. The following Chapter describes the estimation of a wind energy potential for the geometry  $L \times H \times D = 45$  m  $\times$  120 m  $\times$  60 m with different passage widths characterised by the highest amplification factors equal up to 1.3.

## 5 Estimation of the wind energy potential

This Chapter describes the estimation of a wind energy potential for the geometry with the highest revealed amplification factors.

### 5.1 Estimation outline

#### 5.1.1 *Geometry of the buildings*

The optimal building geometry (Figure 5.1) is chosen based on the highest amplification factors  $K$  equal up to 1.3, which are defined during the parametric study. The passage width varies between  $w = 20, 40, 60$  m.

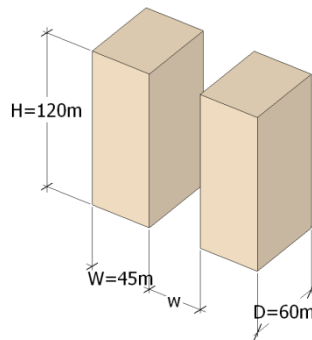


Figure 5.1 – Geometry

#### 5.1.2 *Meteorological data*

It is assumed that the buildings are placed in Eindhoven (The Netherlands).

The data for the Netherlands, provided by the Dutch Meteorological Institute (KNMI), covers a period of 30 years (1971-2000) and provides averaged values and an occurrence frequency of potential wind velocities. Wind is measured at a height of 10 m at a meteorological station with an aerodynamic roughness length equal to  $y_0 = 0.03$  m. Within the framework of the current project the aerodynamic roughness length for the building site is assumed to be equal to  $y_0 = 0.03$  m. The wind data provided by KNMI is carefully analysed and Weibull parameters  $c(\theta), k(\theta)$  are defined for every wind direction (Appendix B).

Since the buildings are likely to be oriented to the prevalent wind direction, the wind distribution defined by the angle span of  $200^\circ - 250^\circ$  is taken into account (Figure 5.2).

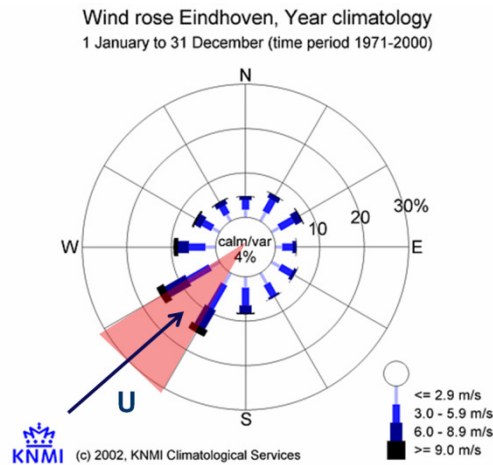


Figure 5.2 – Annual wind rose for Eindhoven indicating the variation of the wind speed direction during the period from 1971-2000 (KNMI)

### 5.1.3 Applied wind turbines

Based on the building dimensions and passage widths, three suitable HAWTs are chosen for annual power estimation (Table 5.1). The indication of the heights at which the turbines are placed is provided as well. The hub height is determined by positioning the wind turbine at the highest possible point within a passage centre plane on condition that blades are not beyond the building height (Figure 5.3). The detailed technical specifications of the turbines are provided in Appendix C.

Table 5.1 – Overview of applied wind turbines

Passage width [m]	Turbine	Rotor diameter [m]	Hub height [m]	Rated power [kW]	Manufacturer
20	WES18	18	111	80	Wind energy solutions BV <a href="http://www.windenergysolutions.nl">www.windenergysolutions.nl</a>
40	E33	33.4	103	330	ENERCON GmbH <a href="http://www.enercon.de">www.enercon.de</a>
60	E33	52.9	93	800	ENERCON GmbH <a href="http://www.enercon.de">www.enercon.de</a>

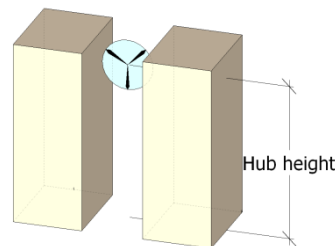


Figure 5.3 – Hub height



## 5.2 Calculation

This section provides the calculation and the results of the annual energy output estimation.

### 5.2.1 Calculation for the prevalent wind direction

In order to describe the wind speed distribution at a building site the conversion factor  $\gamma$  described by equation (2.15) in section 2.3.2 should be defined.

The first term  $\left(\frac{U_{\text{turb}}}{U_{\text{ref}}}\right)$  represents the design related contribution and is obtained by the numerical simulations for  $y_0 = 0.03$  m. It is calculated by taking the ratio of the wind speed at the prospective turbine location within a passage (point value) to an incident wind speed at the reference height of 60 m. The value of the incident wind speed is taken at a sidewall of the domain. The locations of the points are indicated in Figure 5.4.

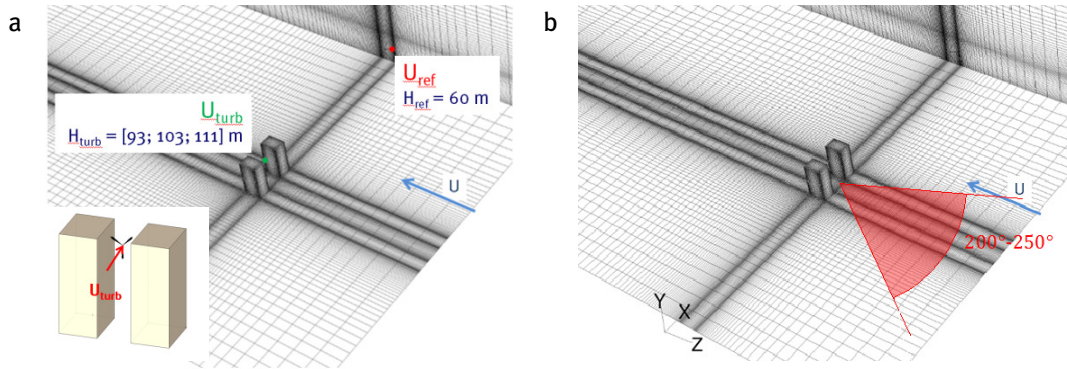


Figure 5.4 – a) Indication of reference wind speed points b) Indication of considered wind direction

The second term  $\left(\frac{U_{\text{ref}}}{U}\right)$  indicates the terrain related contribution and can be derived from the log-law wind speed distribution (2.2), the reference height  $y_{\text{ref}} = 60$  m. It is assumed, that there is no difference in terrain roughness between the meteorological site and the building site characterised by  $y_0 = 0.03$  m. Therefore:

$$\frac{U_{\text{ref}}}{U} = \frac{\ln\left(\frac{y_{\text{ref}}+y_0}{y_0}\right)}{\ln\left(\frac{y_{10}+y_0}{y_0}\right)} = \frac{\ln\left(\frac{60+0.03}{0.03}\right)}{\ln\left(\frac{10+0.03}{0.03}\right)} \quad (5.1)$$

Calculation is performed on the angle span  $200^\circ - 250^\circ$ , the design related contribution  $\left(\frac{U_{\text{turb}}}{U_{\text{ref}}}\right)$  defined for one wind direction (perpendicular to facade) is assumed to be constant within this angle span.

The defined values are summarised in Table 5.2

Table 5.2 – Values of conversion factor  $\gamma$

Passage width [m]	$\left(\frac{U_{\text{turb}}}{U_{\text{ref}}}\right)$	$\left(\frac{U_{\text{ref}}}{U}\right)$	$\gamma$
20	1.39	1.31	1.82
40	1.33	1.31	1.74
60	1.27	1.31	1.66

With the use of the parameters stated in Appendix B, Weibull probability density functions (2.11) modified by the conversion factor  $\gamma$  are defined for each case and are presented in Figure 5.5. The graphs indicate the increase in the mean speed value in the passage caused by the presence of the buildings, which is desirable in terms of wind energy generation.

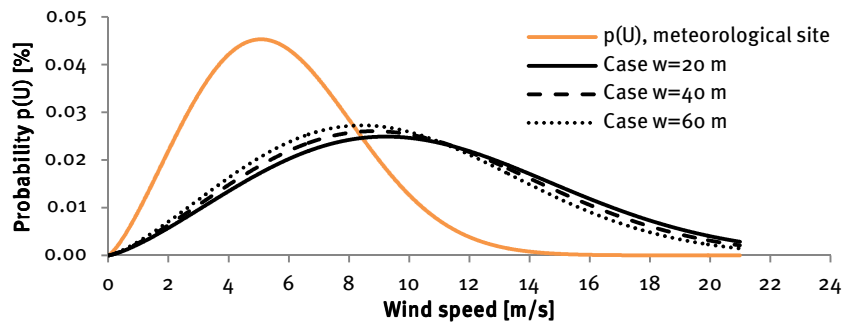


Figure 5.5 – Wind probability density function

Based on the defined distribution and wind power generation by a certain turbine  $P_w$  determined by (2.10), the annual energy captured from the wind turbine  $\bar{E}_w$  (2.13) is calculated assuming 8760 hours per year. The results of the estimation are provided in Figure 5.6. As can be seen, by applying the wind turbine with larger diameter and thus higher rated power the annual captured energy can be significantly increased.

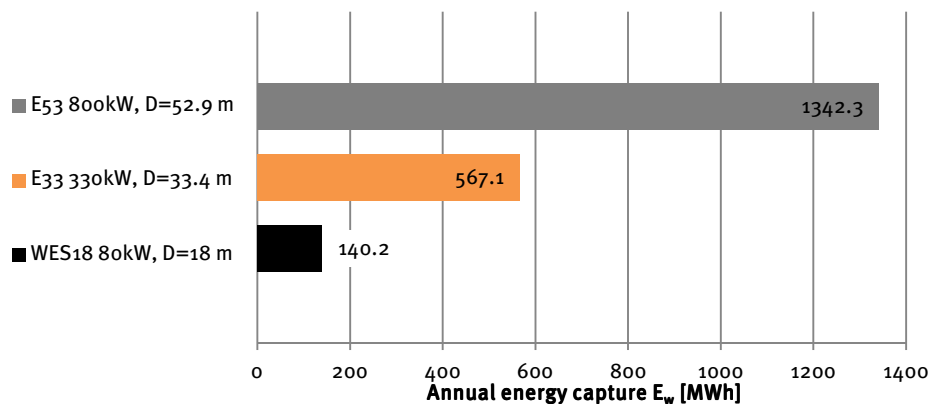


Figure 5.6 – Annual energy estimation produced by wind turbines from prevalent wind direction

### 5.2.2 Calculation for $30^\circ$ wind direction

The similar energy calculation was performed for another wind direction in order to estimate its relevance on power output. The conversion factor has been defined based on results obtained from numerical simulation for a wind direction of  $30^\circ$  from the perpendicular line to the building facades and using the probability density function for wind of angle span  $170^\circ - 190^\circ$  (Figure 5.7). The efficiency of the wind turbine is assumed to be independent of the angle of attack.

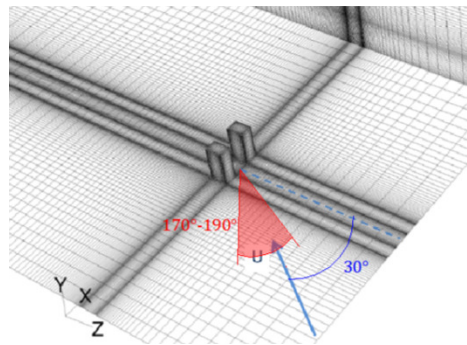


Figure 5.7 – Indication of considered wind direction

The defined values for the conversion factor  $\gamma$  are summarised in Table 5.3.

Table 5.3 – Values of conversion factor  $\gamma$

Passage width [m]	$\left(\frac{U_{\text{turb}}}{U_{\text{ref}}}\right)$	$\left(\frac{U_{\text{ref}}}{U}\right)$	$\gamma$
20	1.17	1.31	1.53
40	1.16	1.31	1.52
60	1.15	1.31	1.51

Figure 5.8 represents the Weibull probability density functions defined for the three passage widths for a wind direction of  $30^\circ$ . The reference wind distribution on the meteorological site (not affected by the presence of the buildings) is provided as well. Again, the graphs indicate the increase in the mean speed value in the passage compared to the reference values. The value of the mean speed for this case is lower than for a parallel wind direction due to the lower probability of this wind direction and lower wind amplification factors in the passage due to the inclination of the wind direction.

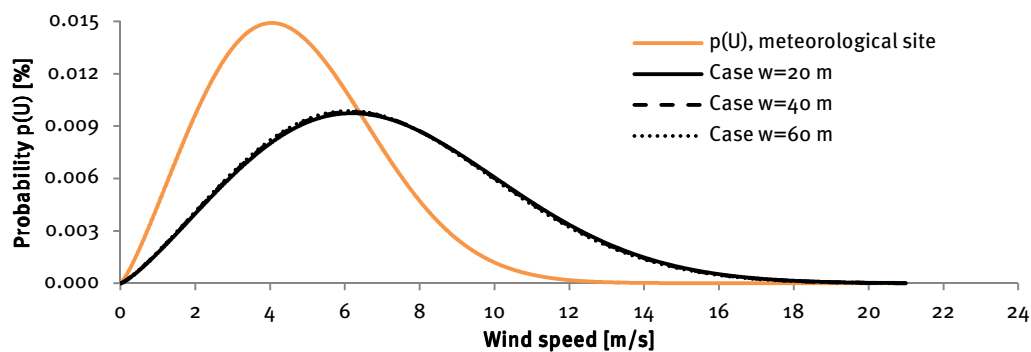


Figure 5.8 – Wind probability density function

Figures 5.9 represent the annual energy output from the turbines. The efficiency of the wind turbine is assumed to be constant for the considered wind directions. As can be seen, the annual power output of wind turbines is decreased by 83% in average compared to the parallel wind direction due to the dependency on the mean wind speed and amplification factor values.

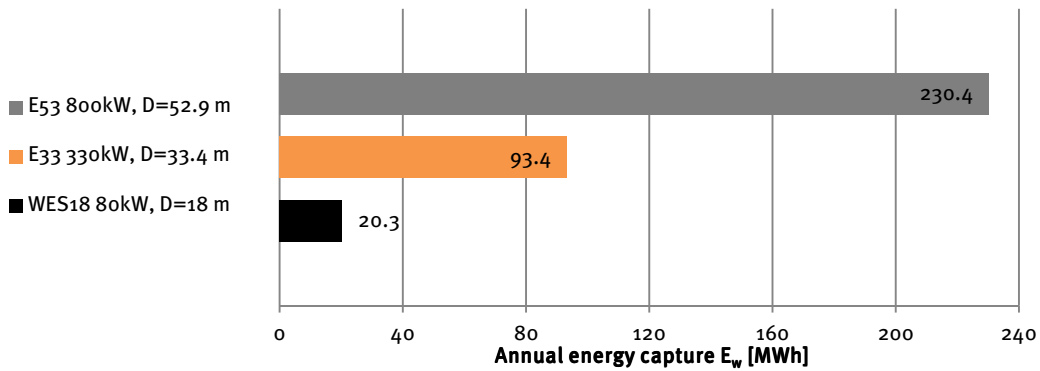


Figure 5.9– Annual energy estimation produced by wind turbines from 30° wind direction

### 5.2.3 Calculation for [-30°] wind direction

The similar energy calculation is performed for another wind direction in order to estimate its relevance on power output. The conversion factor has been defined based on results obtained from numerical simulation for a wind direction of (-30°) from the perpendicular line to the building facades and using the probability density function for wind of angle span 260° – 280° (Figure 5.10). The efficiency of the wind turbine is assumed to be independent on the angle of attack.

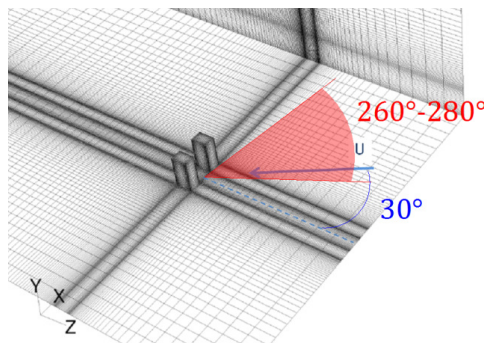


Figure 5.10 – Indication of considered wind direction

The values for the conversion factor  $\gamma$  remain equal to the ones defined for 30° (Table 5.3). Figures 5.11 and 5.12 represent Weibull probability density functions and the annual energy output from turbines, respectively. The mean wind speed is increased compared to 30° wind direction due to higher probability of this wind angle.

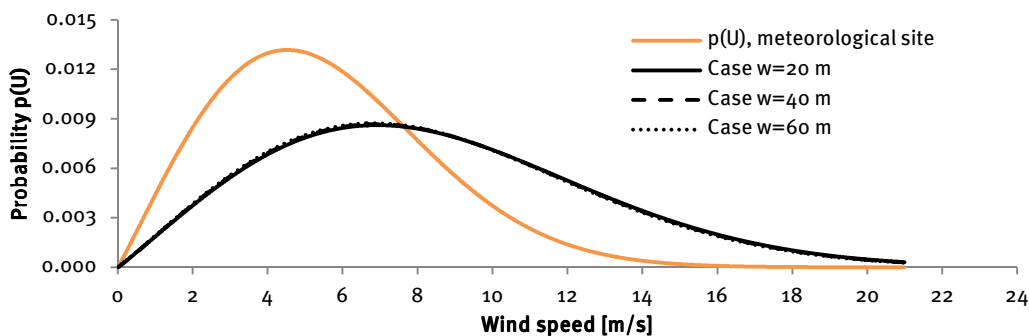


Figure 5.11 – Wind probability density function

Due to the higher probability of the examined wind direction compared to the wind direction of  $30^\circ$ , the annual power output is increased by 33% in average.

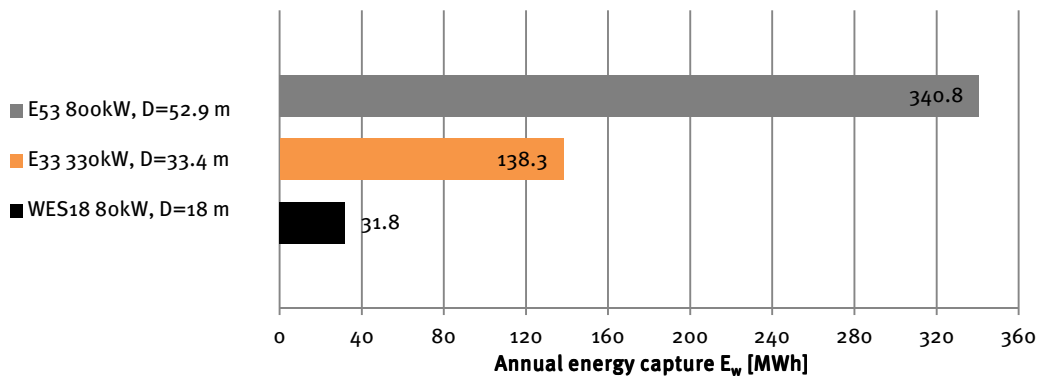


Figure 5.12– Annual energy estimation produced by wind turbines from  $[-30^\circ]$  wind direction

#### 5.2.4 The annual power generation

Based on the data presented in sections 5.2.1 – 5.2.3, the annual power generation of the considered building-integrated wind turbines is calculated. In addition, the annual energy output is defined for a reference case, which represents wind turbines installed at the same location, with the same meteorological conditions, except the presence of the buildings. The results are summarised in Figure 5.13. It must be mentioned, that the angle span of  $170^\circ - 280^\circ$  is taken into account. As can be seen, the annual power generated by the large-scale wind turbine E53 with rotor diameter equal to 52.9 m integrated into the passage with the width of 60 m can reach 1913.5 MWh, while for the smallest wind turbine WES18 the annual power output equals to 192.3 MWh. Based on the obtained results, it can be stated, that the power output of the wind turbines integrated in between free-standing buildings can be increased in average by 35% due to the amplification of the wind speed in the passage.

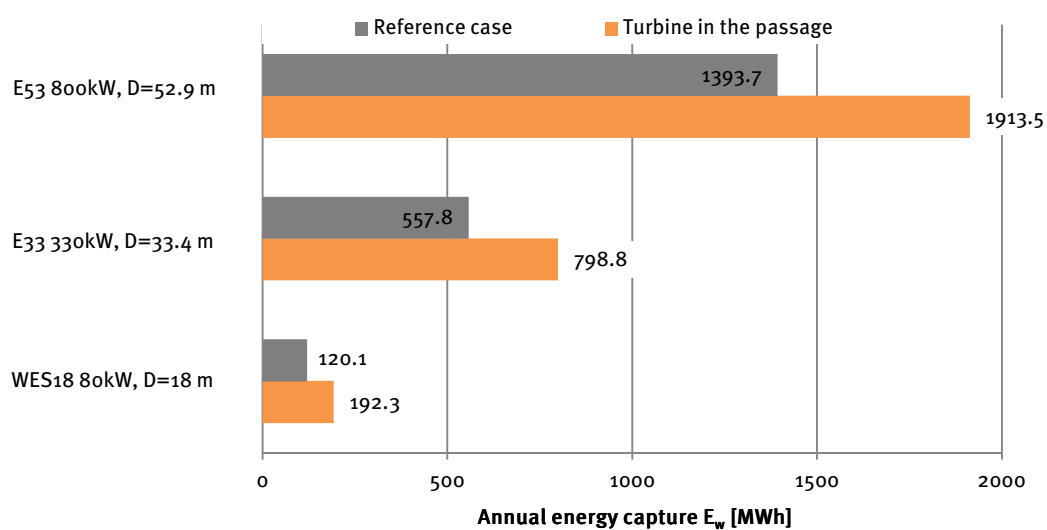


Figure 5.13– Annual energy estimation produced by wind turbines from the angle span of wind  $[170^\circ - 280^\circ]$

## *Summary*

This Chapter provides the evaluation of a wind energy potential defined for the building geometry  $L \times H \times D = 45 \text{ m} \times 120 \text{ m} \times 60 \text{ m}$  with passage widths of 20, 40 and 60 m. Three wind turbines are chosen according to available area for a rotor within a passage with the following values of rated power: 80, 330 and 800 kW. The annual power generation is defined by consideration of the wind angle span of  $170^\circ - 280^\circ$ . The following Chapter provides the discussion on the following questions: influence of the building geometry, terrain roughness and wind direction on the wind amplification within a passage; feasibility of integrating wind turbines into the built environment. The limitations of the current study and recommendations for further research are analysed as well. The conclusions are summarised in Chapter 7.

## 6 Discussion

This Chapter provides the discussion of the obtained results regarding the research objectives mentioned in section 1.2.

### 6.1 Influence of building geometry on the wind amplification in the passage

First, the results obtained for the aerodynamic roughness length  $y_0 = 0.03$  m are discussed.

While considering the influence of geometrical parameters on the wind speed distribution in between buildings, it can be concluded that the highest buildings with narrow passage widths and low values of characteristic ratio  $w/S < 0.6$  are more advantageous for wind flow amplification. Nonetheless, Blocken et al. (2007b) proposed that the condition  $w/S > 0.125$  should be fulfilled in order to avoid the so-called wind-blocking effect resulting in decrease of the wind flow through the passage. In addition, narrow passage widths are only suitable for wind turbines with small rotor diameters and thus result in a low rated power. The higher wind amplification factors with an increment of around 4% are revealed for the buildings with large depths. It is observed that generally there is no pronounced influence of the building length on the wind amplification. However, while considering only one building configuration (section 4.2.2), the maximum amplification factor  $K$  in the passage has been decreased by 2% by increasing the building length from 45 m to 70 m. This occurrence can be also referred to wind-blocking effect of the present buildings.

As for the values of  $K$  defined for  $y_0 = 1$  m, the highest buildings with a passage width of 40 m are observed to be the most advantageous. The configurations within  $0.5 < w/S < 0.7$  are mainly characterised by highest values of  $K$ . Again, while generally no clear trend has been observed for all the building geometries, examining one building configuration (section 4.2.2) showed the influence of building length and depth on wind amplification in the passage. A building geometry with a depth  $D$  of 45 m and a length  $L$  of 45 m demonstrated higher values of the wind amplification factor  $K$ .

Regarding general trends that can be summarised, the maximum amplification factors  $K$  have been defined for building geometries fitting the condition  $w/S = 0.32$  for  $y_0 = 0.03$  m and  $w/S = 0.64$  for  $y_0 = 1$  m. The values of  $K$  demonstrate a stable decrease for  $w/S > 0.32$  and  $w/S > 0.64$  for  $y_0 = 0.03$  m and  $y_0 = 1$  m, respectively. Based on these observations, decisions about the most desirable building configuration can be made during the design process.

## 6.2 Influence of terrain roughness on the wind distribution in the passage

As mentioned in section 4.2.4, there is a significant difference in distribution of the values of wind amplification factor  $K$  for  $y_0 = 0.03$  m and  $y_0 = 1$  m. The difference reaches a maximum of 18% for  $w/S = 0.32$ . Further research is required on that matter, while it can be suggested that the wind speed profile determined by the log-law dependency and imposed at the inlet in the numerical simulation is responsible for velocity and turbulent kinetic energy distribution throughout the domain. It must be mentioned, that the extent of friction velocity characterising velocity fluctuations in the turbulent boundary layer is also defined depending on the value of  $y_0$  and a log-law.

## 6.3 Influence of wind direction on the amplification

The wind angle span of  $(-30^\circ) - 30^\circ$  has been considered as it provides the highest wind amplification factors in the building passages (Stathopoulos & Storms, 1986). Moreover, by taking into account the performance of wind turbines at different wind incident angles, this span appears to be more advantageous and determinative for the energy generation.

As revealed in section 4.2.5, by changing the incident wind direction from angle of  $0^\circ$  to  $30^\circ$  the wind amplification within a passage centre plane can be decreased up to 6%. The position of the maximum wind velocity point is drifted away from the centre plane to the passage sidewalls, but still remains in the upstream part of the passage.

## 6.4 Feasibility of wind turbines in built environment

While assessing the feasibility to integrate wind turbines in a building passage, it is sensible to define the energy demand for the proposed buildings. The building geometry  $L \times H \times D = 45$  m  $\times$  120 m  $\times$  60 m with a passage width  $w$  equal to 20 m has been examined. The choice in favour of the lowest value of  $w$  is made based on the following aspects:

- Highest wind amplification factors;
- Application of a wind turbine with the smallest rotor diameter, since large-scale wind turbines are characterised by: 1) high weight and thus significant loads on the bearing structure of buildings; 2) high level of noise and vibration during operation; 3) effect on site aesthetics and human perception.

First, the energy demand for the specified buildings is estimated. The buildings are assumed to function as office blocks in Eindhoven. According to the U.S. Department of Energy (2012), the average estimated annual energy consumption for newly built office buildings is equal to 277 kWh/m<sup>2</sup>. Assuming 55,000 m<sup>2</sup> of office space per building, the estimated annual electricity load for two buildings amounts to 24,970 MWh. The annual generation for an appropriate wind turbine WES18 as calculated in section 5.2.4 equals to 192.3 MWh. Thus, the wind turbine is likely to reduce the total electricity demand by 0.8%. Transferring that to the money equivalent for the



Netherlands equal to 0.13 €/kWh (Eurostat, 2012), the annual reduction of the electricity bill can reach € 25,000. In case of the passage width of 60 m and applied wind turbine E53, the annual power output can supply up to 8% of the annual electricity demand which equal to € 248.755 in the money equivalent. It must be noted, that the estimation of the annual percentage of power supply is comparable to the values defined for existing projects mentioned in section 2.2.3.

The simplified estimation of the investment costs based on the data determined for the single-standing wind turbine (Sol-Vent Energy Ltd., 2010; Renewables First Ltd., 2011) is indicated in Figure 6.1. The investment costs comprise the costs of turbine itself, supporting tower, transformers, shipping and transportation of components, equipment hire, civil and electrical work. The costs of structures supporting wind turbine and necessary for building reinforcement are assumed to be equal to the tower cost. It must be mentioned, that the value of investment costs is highly dependent on the geographical location, site characteristics and applied wind turbine and it should be defined by using explicit data of a project (Krohn et al., 2009).

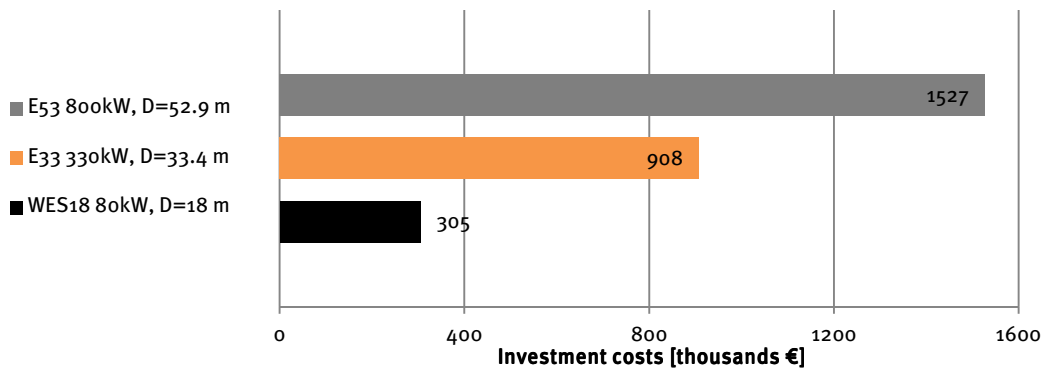


Figure 6.1 – Estimated investment costs

Operation and maintenance costs for onshore wind energy include expenses for insurance, regular maintenance and repair, spare parts and administration, and are generally estimated to be around 1.5 c€ per kWh of wind power produced over the total lifetime of a turbine (Krohn et al., 2009). Considering the annual maintenance costs and annual energy generation, the payback time can be estimated (Table 6.1). As can be seen from the results, the payback time of considered cases is shorter for large-scale wind turbines and still it constitutes a long time span. The thorough economical evaluation should be conducted in order to make a decision of integrating wind turbine into the building and its feasibility.

Table 6.1 – Estimation of payback time

Wind turbine	WES18	E33	E53
Investment costs [thousands €]	305	908	1527
Annual maintenance costs [thousands €]	2.88	11.98	28.70
Annual energy generation [thousands €]	25.0	103.8	248.8
Payback [years]	13.8	9.9	6.9

In order to determine the most preferable location of the wind turbines, the distribution of the wind amplification factor  $K_{60}$  through the vertical passage centre plane is examined for all the building geometries and the two wind directions. It is revealed that the maximum values of  $K_{60}$  tend to occur closer to the entrance of the passage within  $0.85H_b - 1H_b$ , where  $H_b$  – building height. Therefore, wind turbines are preferably to be installed within the top upstream part of the passage. The distribution of the wind amplification factor  $K_{60}$  for a building geometry considered within this section for wind directions of  $0^\circ$  and  $30^\circ$  is illustrated in Figure 6.2.

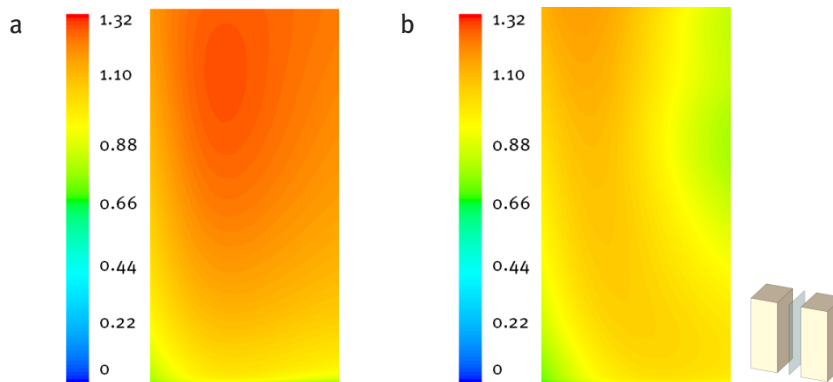


Figure 6.2 – Contour plots of amplification factor  $K_{60}$  defined for the buildings  $L \times H \times D = 45 \text{ m} \times 120 \text{ m} \times 60 \text{ m}$  with a passage width  $w = 20 \text{ m}$  ( $y_0 = 0.03 \text{ m}$ ) through the vertical passage centre plane:  
 a) parallel wind direction; b)  $30^\circ$  wind direction

## 6.5 Current limitations of the study

Before stating the conclusions, the limitations of the current project should be mentioned, which can be summarised as follows:

- This study is limited to buildings with simplified geometries (building blocks);
- During the calculation of the annual energy output of the proposed wind turbines the aerodynamic roughness length for the building site is assumed to be equal to the one of the meteorological site  $y_0 = 0.03 \text{ m}$ , which does not represent the roughness of the urban terrain;
- No explicit surroundings are represented around the building set-up and the influence of urban environment on the wind flow is taken into account by applying two different aerodynamic roughness lengths;
- The efficiency of wind turbines is assumed to be constant and independent on the wind angle of attack. However, in reality off-axis winds, which direction is not perpendicular to the plane of the rotor, due to yaw error or vertical wind components result in a skewed wake in the downside of the rotor and affect the performance of a wind energy system (Manwell et al., 2009);
- Only HAWTs are considered for integration within building passages;
- The objective of the current project is to achieve the wind amplification within the passage, which causes the occurrence of high wind speeds at pedestrian level height. The question of pedestrian wind comfort has not been addressed within the framework of the study.

It should be noted that all the limitations are caused by time constraints.

Despite of the limitations, the following crucial aspects are considered within the study:

- Two aerodynamic roughness lengths have been considered and amplification factors have been defined for all the geometries;
- The study examined a wide range of geometries;
- The orientation of the buildings is based on the prevailing wind direction according to the meteorological data for Eindhoven;
- An extensive data analysis of the wind distribution, influenced by the presence of the buildings, is performed.

## 6.6 Recommendations for further research

Recommendations for further research comprise:

- Conduct the extensive study on the influence of terrain roughness on wind speed distribution within building passages;
- Perform the study with a extensive representation of surroundings for the specific location and validate the results by experiments;
- Investigate different building shapes, which are more aerodynamic and thus advantageous for wind amplification;
- Assess the performance of VAWTs;
- Consider the influence of the wind direction on a power output of a wind turbine;
- Suggest measures to guarantee pedestrian wind comfort around the buildings.

## 7 Conclusions

The following conclusions can be made based on this study:

- The building configurations which are the most advantageous in terms of wind amplification are characterised by the ratio  $w/S = 0.32$  for  $y_0 = 0.03$  m and  $w/S = 0.64$  for  $y_0 = 1$  m;
- Considering  $y_0 = 0.03$  m, the highest buildings with narrow passage widths and low values of characteristic ratio  $0.125 < w/S < 0.6$  are more advantageous for a wind flow amplification within the passage;
- Considering  $y_0 = 1$  m, the highest buildings with medium passage widths within  $0.5 < w/S < 0.7$  are more advantageous for a wind flow amplification within the passage;
- The most preferable location of wind turbines is defined as the top upstream part of the passage;
- Significant influence of the aerodynamic roughness length and wind direction on wind speed distribution within passages is revealed;
- Unfortunately, the distribution of the wind amplification factors  $K = \frac{U_{\max}}{U_0}$ ;  $K_{60} = \frac{U_{\max}}{U_{60}}$  can hardly be described as a function of the universal ratio of  $w/S$ ;
- Considering the annual electricity power produced by wind turbines, it can supply up to 8% of the annual energy demand for the two office buildings ( $H = 120$  m) with a total office space area of 110,000 m<sup>2</sup>. The power output is highly dependent on the type of the wind turbine, which should be carefully determined depending on the geometrical and structural parameters of the buildings, taking into account the aspects mentioned in section 2.2.4. The energy demand is dependent on the functioning of the building and its dimensions. Integration of a wind turbine can reduce the electricity costs for the owners to a certain extent which can be evaluated at the design stage. Moreover, it helps to decrease the reliance on scarce and expensive fossil fuels which are responsible for a significant amount of CO<sub>2</sub> emissions.

## References

- Abohela, I., Hamza, N. & Dudek, S., 2011a. Effect of Roof Shape on Energy Yield and Positioning of Roof Mounted Wind Turbines. In Soebarto, V., ed. *12th Conference of International Building Performance Simulation Association*. Sydney, 2011a. IBPSA Australasia and AIRAH.
- Abohela, I., Hamza, N. & Dudek, S., 2011. Urban Wind Turbines Integration in the Built Form and Environment. *FORUM Ejournal*, 10, pp.23-29.
- Alnaser, W.E. & Al-Karaghoul, A., 2000. Wind availability and its power utility for electricity production in Bahrain. *Renewable Energy*, 21, pp.247-54.
- Anderson, J.D., 1984. *Fundamentals of Aerodynamics*. McGraw-Hill.
- ANSYS, Inc., 2009. *ANSYS FLUENT 12.0 User's Guide*.
- Ayhan, D. & Saglam, S., 2012. A technical review of building-mounted wind power systems and a sample simulation model. *Renewable and Sustainable Energy Reviews*, 16, pp.1040-49.
- Balduzzi, F., Bianchini, A., Carnevale, E.A., Ferrari, L. & Magnani, S., 2011. Feasibility analysis of a Darrieus vertical-axis wind turbine installation in the rooftop of a building. *Applied Energy*, In Press, p.9.
- Bell, J.H. & Mehta, R.D., 1984. *Contraction design for small low-speed wind tunnels*. Stranford: Stranford University. Department of Aeronautics and Astronautics.
- Beranek, W.J. & Van Koten, H., 1982. Beperken van windhinder om gebouwen. In *Deel 2, Stichting Bouwresearch no. 90*. Deventer: Kluwer Technische Boeken BV. p.149.
- Blocken, B., 2011. *CFD in Building Engineering: Fundamentals and applications in urban physics and wind engineering. Coursebook*. Eindhoven.
- Blocken, B., Carmeliet, J. & Stathopoulos, T., 2007b. CFD evaluation of wind speed conditions in passages between parallel buildings - effect of wall-function roughness modifications for atmospheric boundary layer flow. *Journal of Wind Engineering and Industrial Aerodynamics*, 95, pp.941-62.
- Blocken, B., Defraeye, T., Derome, D. & Carmeliet, J., 2009. High-resolution CFD simulations for forced convective heat transfer coefficients at the facade of a low-rise building. *Building and Environment*, 44, pp.2396-412.
- Blocken, B., Roels, S. & Carmeliet, J., 2004. Modification of pedestrian wind comfort in the Silvertop Tower passages by an automatic control system. *Journal of Wind Engineering and Industrial Aerodynamics*, 92(10), pp.849-73.
- Blocken, B., Stathopoulos, T. & Carmeliet, J., 2008. Wind Environmental Conditions in Passages between Two Long Narrow Perpendicular Buildings. *Journal of Aerospace Engineering*, 21(4), pp.280-87.
- Blocken, B., Stathopoulos, T. & Carmeliet, J., 2007a. CFD simulation of the atmospheric boundary layer: wall function problems. *Atmospheric Environment*, 41(2), p.238-252.
- Blocken, B., Stathopoulos, T., Carmeliet, J. & Hensen, J., 2011. Application of CFD in building performance simulation for the outdoor environment: an overview. *Journal of Building Performance Simulation*, 4(2), pp.157-84.
- Boyer, J.L., 2010. *Can skyscrapers power our cities?* [Online] Available at: [http://www.thevitruvianomission.com/The\\_Vitruvian\\_Omission/Pearl\\_River.html](http://www.thevitruvianomission.com/The_Vitruvian_Omission/Pearl_River.html) [Accessed October 2011].

Brookfield Europe, 2011. *Strata - a landmark for urban living*. [Online] Available at: <http://www.stratalondon.com/tower> [Accessed 21 September 2011].

Cace, J., Horst, E. T., Syngellakis, K., Niel, M., Clement, P., Heppener, R. & Peirano, E., 2007. *Urban Wind Turbines, Guidelines for Small Wind Turbines in the Built Environment*. [Online] Cace, J., Horst, E. t., Syngellakis, K., Niel, M., Clement, P., Heppener, R., et al. (2007). Urban Wind Turbines, Guide Lines for Small Wind Turbines in the Built Environment. Retrieved on 25-01-2010, from: Intelligent Energy Europe Available at: [http://www.urbanwind.net/pdf/SMALL\\_WIND\\_TURBINES\\_GUIDE\\_final.pdf](http://www.urbanwind.net/pdf/SMALL_WIND_TURBINES_GUIDE_final.pdf) [Accessed October 2011].

Campbell, N.S. & Stankovic, S., 2001. *Assessment of Wind Energy Utilisation Potential in Moderately Windy Built-up Areas*. London: Wind energy for the built environment (WEB).

Campbell, N.S. & Stankovic, S., 2001. *Wind Energy for the Built Environment (Project WEB). Assessment of Wind Energy Utilisation Potential in Moderately Windy Built-up Areas*. London: BDSP Partnership.

Cebeci, T. & Bradshaw, P., 1977. *Momentum Transfer in Boundary Layers*. New York: Hemisphere Publishing Corporation.

Chen, Q., 2009. Ventilation performance prediction for buildings: A method overview and recent applications. *Building and Environment*, 44(4), pp.848-58.

Conan, B., van Beeck, J. & Aubrun, S., 2012. Sand erosion technique applied to wind resource assessment. *Journal of Wind Engineering & Industrial Aerodynamics*, In Press.

Cook, M., Ji, Y. & Hunt, G., 2005. CFD modelling of buoyancy-driven natural ventilation. In *Ninth International IBPSA Conference on Building Simulation*. Montréal, 2005.

Denoon, R., Cochran, B., Banks, D. & Wood, G., 2008. Harvesting Wind Power from Tall Buildings. In *CTBUH 8th World Congress*. Dubai, 2008.

Dutton, A.G., Halliday, J.A. & Blanch, M.J., 2005. *The Feasibility of Building Mounted/Integrated Wind Turbines (BUWTs): Achieving their potential for carbon emission reductions*. Final report. London: Energy Research Unit, CCLRC.

EEA, 2010. *European Environment Agency. Europe's onshore and offshore wind energy potential. An assessment of environmental and economic constraints*. Luxembourg: Office for Official Publications of the European Communities.

Epstein, K., 2008. How Far Can You Go? Case study: Pearl River Tower. *High performing buildings*.

European Commission, 2011. *Renewables make the difference*. Information report. Luxembourg: Publications Office of the European Union European Union.

Eurostat, 2011a. *European Commission. Energy, transport and environment indicators*. Luxembourg: Publications Office of the European Union.

Eurostat, 2011b. *European Commission. Key figures on Europe*. Luxembourg: Publications Office of the European Union.

Eurostat, 2012. *Electricity prices by type of user*. [Online] Available at: [http://epp.eurostat.ec.europa.eu/tgm/table.do?tab=table&plugin=1&language=en&pcode=tsie\\_r040](http://epp.eurostat.ec.europa.eu/tgm/table.do?tab=table&plugin=1&language=en&pcode=tsie_r040) [Accessed 22 May 2012].

EWEA, 2011. *European Wind Energy Association. Pure Power: Wind energy targets for 2020 and 2030*. Kampenhout: Artoos.

- Foster, A.M., Swain, M.J., Barrett, R. & James, S.J., 2003. Experimental verification of analytical and CFD predictions of infiltration through cold store entrances. *International Journal of Refrigeration*, 26(8), pp.918-25.
- Franke, J., Hellsten, A., Schlünzen, H. & Carissimo, B., 2007. *Best Practice Guideline for the CFD Simulation of Flows in the Urban Environment*. Brussels: COST Office.
- Franke, J. et al., 2004. Recommendations on the use of CFD in wind engineering. In van Beeck, J.P.A.J., ed. *International Conference on Urban Wind Engineering and Building Aerodynamics: COST Action 14 - Impact of Wind and Storm on City Life and Built Environment*. Sint-Genesius-Rode, 2004. Von Karman Institute.
- Glass, A. & Levermore, G., 2011. Micro wind turbine performance under real weather conditions in urban environment. *Building Services Engineering Research and Technology*.
- Glass, A. & Levermore, G., 2011. Micro wind turbine performance under real weather conditions in urban environment. *Building Services Engineering Research and Technology*, 32(3), pp.245-62.
- Harding, G., Harding, P. & Wilkins, A., 2008. Wind turbines, flicker, and photosensitive epilepsy: Characterizing the flashing that may precipitate seizures and optimizing guidelines to prevent them. *Epilepsia*, 49(6), pp.1095-98.
- IEA Wind, 2011. *2010 Annual Report*. Information report. New York: PWT Communications, LLC Executive Committee of the Implementing Agreement for Co-operation in the Research, Development, and Deployment of Wind Energy Systems of the International Energy Agency.
- IEA, 2011. *International Energy Agency: Renewable Energy*. [Online] Available at: [http://www.iea.org/subjectqueries/keyresult.asp?keyword\\_id=4116](http://www.iea.org/subjectqueries/keyresult.asp?keyword_id=4116) [Accessed 10 November 2011].
- Jamil, M., Parsa, S. & Majidi, M., 1995. Wind power statistics and an evaluation of wind energy density. *Renewable Energy*, 6(5-6), pp.623-28.
- Jensen, N.O., Petersen, L.E. & Troen, I., 1984. *Extrapolation of Mean Wind Statistics with Special Regard to Wind Energy Applications*. WMO. World Climate Programme Report No. WCP-86.
- Killa, S. & Smith, R.F., 2008. Harnessing Energy in Tall Buildings: Bahrain World Trade Center and Beyond. In *CTBUH 8th World Congress 2008*. Dubai, 2008.
- Krohn, S., Morthorst, P.-E. & Awerbuch, S., 2009. *The Economics of Wind Energy. A report by the European Wind Energy Association*. Annual report. EWEA.
- Launder, B.E. & Spalding, D.B., 1974. The numerical computation of turbulent flows. *Computer Methods in Applied Mechanics and Engineering*, 3, p.269–289.
- Letherman, S.B., Cotton, M.A., Stansby, P.K., Chen, C. & Chen, D., 2000. An assessment of k- $\epsilon$ s and k-l turbulence models for a wide range of oscillatory rough bed flows. *Journal of Hydroinformatics*, 2, pp.221-34.
- Livesey, F., Inculet, D., Isyumov, N. & Davenport, A.G., 1990. A scour technique for the evaluation of pedestrian winds. *Journal of Wind Engineering and Industrial Aerodynamics*, 36, pp.779-89.
- Livesey, F., Morrish, D., Mikitiuk, M. & Isyumov, N., 1992. Enhanced scour tests to evaluate pedestrian level winds. *Journal of Wind Engineering and Industrial Aerodynamics*, 41-44, pp.2265-76.
- Lu, L. & Ip, K.Y., 2009. Investigation on the feasibility and enhancement methods of wind power utilization in high-rise buildings of Hong Kong. *Renewable and Sustainable Energy Reviews*, 13, pp.450-61.

Manwell, J.F., McGowan, J.G. & Rogers, A.L., 2009. *Wind Energy Explained: Theory, Design and Application*. 2nd ed. Chichester, UK: John Wiley & Sons, LTD.

Mertens, S., 2006. *Wind Energy in the built environment : concentrator effects of buildings*. Essex: Multiscience Publishing.

Mirhosseini, M., Sharifi, F. & Sedaghat, A., 2011. Assessing the wind energy potential locations in province of Semnan in Iran. *Renewable and Sustainable Energy REviews*, 15, pp.449-59.

Mochida, A. & Lun, Y.F., 2006. Prediction of wind environment and thermal comfort at pedestrian level in urban area. In *The Fourth International Symposium on Computational Wind Engineering*. Yokohama, 2006.

Moorhouse, A., Elliott, A., Eastwick, G., Evans, T., Ryan, A., Hunerbein, S. von, Bescond, V. le & Waddington, D., 2011. Structure-borne sound and vibration from building-mounted wind turbines. *Environmental Research Letters*, p.9.

Müller, G., Jentsch, M.F. & Stoddart, E., 2009. Vertical axis resistance type wind turbines for use in buildings. *Renewable Energy*, pp.1407-12.

Murakami, S., 1990. Computational Wind Engineering. *Journal of Wind Engineering and Industrial Aerodynamics*, 36, pp.517-38.

Ohunakin, O.S..A.O.O., 2012. Assessment of wind energy potential and the economics of wind power generation in Jos, Plateau State, Nigeria. *Energy for Sustainable Development*, 16, pp.78-83.

Petersen, E.L. et al., 1998. Wind Power Meteorology. Part I: Climate and Turbulence. *Wind energy*.

Rambøll Danmark A/S, 2006. *Castle House - Wind Turbine Project. Feasibility study*. Virum.

Renewables First Ltd., 2011. *Introduction to Farm Wind Turbines / Medium-wind Turbines*. [Online] Renewables First Ltd. (2.1) Available at: [http://www.google.nl/url?sa=t&rct=j&q=introduction%20to%20farm%20wind%20turbines%20%2F%20medium-wind%20turbines&source=web&cd=1&ved=oCFwQFjAA&url=http%3A%2F%2Fwww.renewablesfirst.co.uk%2Fdownloads.html%3Ffile%3Dtl\\_files%2Frenewables\\_first%2Fimages%2Fpage%](http://www.google.nl/url?sa=t&rct=j&q=introduction%20to%20farm%20wind%20turbines%20%2F%20medium-wind%20turbines&source=web&cd=1&ved=oCFwQFjAA&url=http%3A%2F%2Fwww.renewablesfirst.co.uk%2Fdownloads.html%3Ffile%3Dtl_files%2Frenewables_first%2Fimages%2Fpage%20) [Accessed 2 June 2012].

Richards, P.J. & Hoxey, R.P., 1993. Appropriate boundary conditions for computational wind engineering models using the k- $\epsilon$  turbulence model. *Journal of Wind Engineering and Industrial Aerodynamics*, 46&47, pp.145-53.

ScyscraperCity, 2006. *China skyscraper plan will generate energy*. [Online] Available at: <http://www.skyscrapercity.com/showthread.php?t=410543&langid=5> [Accessed 21 September 2011].

Sharpe, T., 2010. The Role of Aesthetics, Visual and Physical Integration in Building Mounted Wind Turbines - an Alternative Approach. *Paths to Sustainable Energy*, pp.279-300.

Shih, T.H., Liou, W.W., Shabbir, A. & Zhu, J., 1995. A new k-[epsilon] eddy-viscosity model for high Reynolds number turbulent flows - model development and validation. *Comput. Fluids*, 24(3), pp.227-38.

Singhal, S., 2011. *Strata SE1 Tower in UK by BFLS Architects designed using MicroStation*. [Online] Available at: <http://www10.aecafe.com/blogs/arch-showcase/2011/04/15/strata-se1-in-elephant-castle-uk-by-bfls-architects/> [Accessed 21 September 2011].



Snyder, W.H., 1981. *Guideline for Fluid Modeling of Atmospheric Diffusion*. No. EPA-600/8-81-009. Chicago: Environmental Sciences Research Laboratory United States Environmental Protection Agency.

Sol-Vent Energy Ltd., 2010. *WES18 & WES30 (Wind Energy Solutions)*. [Online] Available at: <http://sol-ventenergy.co.uk/wind-turbines/enercon-e-33-a-e-53/42-wind-energy-solutions.html> [Accessed 1 June 2012].

SOM, 2010. *Pearl River Tower*. [Online] Available at: [http://www.som.com/content.cfm/pearl\\_river\\_tower](http://www.som.com/content.cfm/pearl_river_tower) [Accessed 21 September 2011].

Stankovic, S., Campbell, N. & Harries, A., 2009. *Urban Wind Energy*. 1st ed. London: Earthscan.

Stathopoulos, T., 1984. Design and fabrication of a wind tunnel for building aerodynamics. *Journal of Wind Engineering and Industrial Aerodynamics*, 16, pp.361-76.

Stathopoulos, T. & Storms, R., 1986. Wind environmental conditions in passages between buildings. *Journal of Wind Engineering and Industrial Aerodynamics*, 24, pp.19-31.

Stathopoulos, T., Wu, H. & Bédard, C., 1992. Wind environment around buildings: A knowledge-based approach. *Journal of Wind Engineering and Industrial Aerodynamics*, 41-44, pp.2377-88.

Tadamasa, A. & Zangeneh, M., 2011. Numerical prediction of windturbinenoise. *Renewable Energy*, 36(7), p.1902-1912.

Tominaga, Y., Mochida, A., Yoshie, R., Kataoka, H., Nozu, T., Yoshikawa, M. & Shirasawa, T., 2008. AIJ guidelines for practical applications of CFD to pedestrian wind environment around buildings. *Journal of Wind Engineering and Industrial Aerodynamics*, 96, pp.1749-61.

U.S. Department of Energy, 2012. *Buildings Energy Data Book. Office Building Markets and Companies*. [Online] Available at: <http://buildingsdatabook.eere.energy.gov/TableView.aspx?table=3.6.1> [Accessed 15 May 2012].

UNFCCC, 2011. *Kyoto Protocol*. [Online] Available at: [http://unfccc.int/kyoto\\_protocol/items/2830.php](http://unfccc.int/kyoto_protocol/items/2830.php) [Accessed October 2011].

van Hooff, T. & Blocken, B., 2010. Coupled urban wind flow and indoor natural ventilation modelling on a high-resolution grid: A case study for the Amsterdam ArenA stadium. *Environmental Modelling & Software*, pp.51-65.

van Hooff, T.A.J., Blocken, B.J.E., Aanen, L. & Bronsema, B., 2011. A venturi-shaped roof for wind-induced natural ventilation of buildings: wind tunnel and CFD evaluation of different design configurations. *Building and Environment*, pp.1797-807.

van Kuik, G.A.M., 2007. The Lanchester–Betz–Joukowsky Limit. *Wind Energy*, 10, pp.289-91.

Veerman, H.P.J., Ganzevles, F.L.A. & Pengel, K., 2004. Wake vortex investigations by means of stereoscopic PIV and 5-hole probe. In Stanislas, M., Westerweel, J. & Kompenhans, J., eds. *Particle image velocimetry: recent improvements. Proceedings of the EUROPIV 2 Workshop held in Zaragoza, Spain, March 31-April 1, 2003.*, 2004. Springer.

Verkaik, J.W., 2006. *On wind and roughness over land*. Wageningen : Wageningen Universiteit.

Wallace, J.M. & Hobbs, P., 2006. *Atmospheric Science: An Introductory Survey*. 2nd ed. Elsevier Inc.

Wieringa, J., 1992. Updating the Davenport Terrain Roughness Classification. *Journal of Wind Engineering and Industrial Aerodynamics*.

Wieringa, J., 1993. Representative roughness parameters for homogeneous terrain. *Boundary-layer meteorology*.

Wilson, D.J., 1989. Airflow around buildings. In *ASHRAE Handbook of Fundamentals*. pp.14.1-14.18.

World Trade Centers Association, 2008. *Bahrain World Trade Center*. [Online] Available at: <http://www.bahrainwtc.com/> [Accessed 21 September 2011].

Zhai, Z., Zhang, Z., Zhang, W. & Chen, Q., 2007. Evaluation of Various Turbulence Models in Predicting Airflow and Turbulence in Enclosed Environments by CFD: Part-1: Summary of Prevalent Turbulence Models. *HVAC&R Research*, 13(6), pp.853-70.

Zhang, Z., Zhang, W., Zhai, Z. & Chen, Q., 2007. Evaluation of Various Turbulence Models in Predicting Airflow and Turbulence in Enclosed Environments by CFD: Part-2: Comparison with Experimental Data from Literature. *HVAC&R Research*, 13(6), pp.871-86

## Appendices

## Appendix A – Tracking iterations

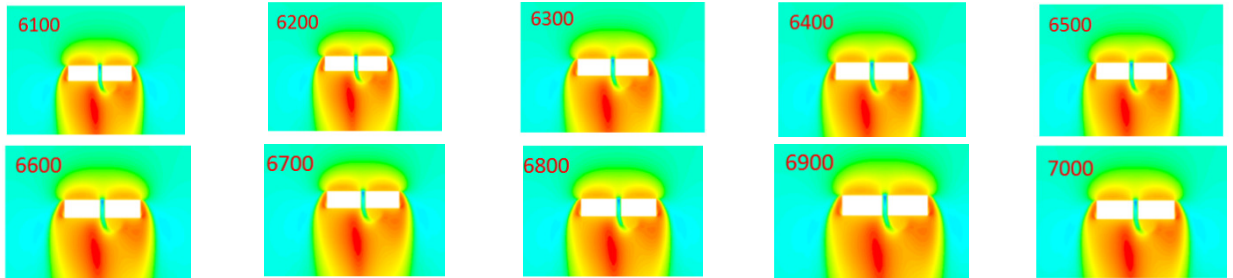


Figure A.1 – Velocity contour plots at pedestrian level height (2 m – full scale), top view

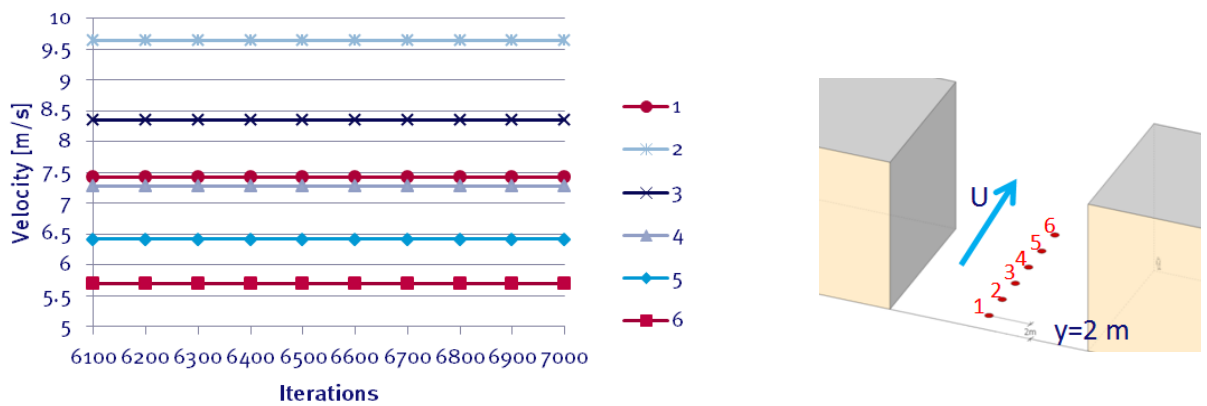


Figure A.2 – Point measurements of velocity at pedestrian level height (2 m – full scale)

## Appendix B – Weibull parameters

*Table B.1 – Calculated Weibull parameters*

<b>Direction (<math>\theta</math>), degrees</b>	<b>350-10</b>	<b>20-40</b>	<b>50-70</b>	<b>80-100</b>
<b>A(<math>\theta</math>), probability [%]</b>	4.77	6.72	7.4	4.76
<b>k(<math>\theta</math>)</b>	2.0928	2.4282	2.572	2.4744
<b>c(<math>\theta</math>)</b>	4.7380	4.6979	5.2279	4.7772
<b>Direction (<math>\theta</math>), degrees</b>	<b>110-130</b>	<b>140-160</b>	<b>170-190</b>	<b>200-220</b>
<b>A(<math>\theta</math>), probability [%]</b>	5.95	6.3	8.46	15.51
<b>k(<math>\theta</math>)</b>	2.4189	2.2141	2.2406	2.3211
<b>c(<math>\theta</math>)</b>	4.5028	4.0856	5.2661	6.3559
<b>Direction (<math>\theta</math>), degrees</b>	<b>230-250</b>	<b>260- 280</b>	<b>290-310</b>	<b>320-340</b>
<b>A(<math>\theta</math>), probability [%]</b>	15.31	9.47	6.19	5.04
<b>k(<math>\theta</math>)</b>	2.3167	2.0507	1.9488	2.0151
<b>c(<math>\theta</math>)</b>	6.6075	6.2669	5.5904	4.9573

## Appendix C – Technical specifications of wind turbines

Table C.1 – Technical specifications

Wind turbine	WES18 (Wind Energy Systems)	E33 (Enercon)	E53 (Enercon)
Rated power [kW]	80	330	800
Rotor diameter [m]	18	33.4	52.9
Swept area [m <sup>2</sup> ]	254	876	2198
Power coefficients Cp for wind speeds [m/s]:			
1	0	0.00	0
2	0	0.00	0.19
3	0.19	0.35	0.39
4	0.29	0.40	0.44
5	0.31	0.47	0.46
6	0.33	0.50	0.48
7	0.33	0.50	0.49
8	0.35	0.50	0.49
9	0.35	0.47	0.49
10	0.33	0.47	0.48
11	0.31	0.41	0.42
12	0.28	0.35	0.34
13	0.23	0.28	0.27
14	0.19	0.23	0.22
15	0.16	0.18	0.18
16	0.14	0.15	0.15
17	0.12	0.13	0.12
18	0.10	0.11	0.10
19	0.08	0.11	0.09
20	0.06	0.09	0.08
21	0.04	0.08	0.06
22	0.03	0.07	0.06